An Investigation into the Feasibility of a Sea Water and Ice Based Acoustic UHE Neutrino Telescope

Simon Bevan

University College London

Submitted to University College London in fulfilment
of the requirements for the award of the
degree of Doctor of Philosophy.

October 2008

Declaration

I, Simon Bevan, confirm that the work presented in this thesis is my own. Where information has been derived from other sources, I confirm that this has been indicated in the thesis.

Abstract

Using acoustic techniques, it is hoped that a new type of telescope can be developed to search for ultra-high energy (UHE) ($> 10^{20}$ eV) neutrinos. Using an 8 hydrophone array, ACoRNE is investigating the practicality of such an acoustic telescope. This thesis reports on the progress of this investigation, focusing on data analysis and event reconstruction, with the aim of reducing the acoustic background at Rona. The sensitivity of the Rona array is presented, and a limit placed on the flux of UHE neutrinos. The feasibility of acoustic detection in ice is also investigated.

Acknowledgements

I would like to thank my supervisors - David Waters and Mark Lancaster, for all of their patience, knowledge, and support. I would also like to thank Mum, Dad, Luke, and Nicky, for more than can be expressed here. For everyone who has made me smile, this is for you. One big final thanks must go to tea, the true drink of champions.

Contents

List of Figures

List of Tables

Chapter 1

Overview

Due to the finite 50 Mpc inelastic collision length of UHE protons in the cosmic microwave background radiation there is a maximum energy of protons of cosmological origin. The highest energy protons interact via photo-production reactions and produce a flux of high energy neutrinos. This produces the 'guaranteed' flux of so-called GZK neutrinos.

Many experiments have made excellent progress over recent years in the detection of (U)HE neutrinos. Using optical, air shower, radio, and acoustic detectors these experiments have published many important results. The optical experiments include AMANDA, IceCube, ANTARES, NEMO, and Lake Baikal, with AMANDA publishing a significant null-result for point sources, and making a leading limit for the diffuse flux. The most successful air shower detector is the Pierre-Auger observatory. The Pierre-Auger observatory has tentatively linked UHE cosmic rays to local AGN, seen evidence of the GZK suppression, and placed a limit on the flux of UHE neutrinos. Radio experiments include RICE, ANITA, GLUE and FORTE. All have progressed the field and published competitive limits on the neutrino flux. ANITA flew in late 2008 and is the most promising experiment to make a first detection of UHE neutrinos. The least developed UHE neutrino detectors are the acoustic experiments. This is still an emerging field, but substantial progress in the understanding of the methods needed to make this a viable technique has been achieved through the SAUND and ACoRNE experiments.

Using data from the ACoRNE detector this thesis sets out to discuss the possibility

of using acoustic techniques as a viable detection method. Much work was done by the ACoRNE collaboration in developing a UHE neutrino shower model and in data reduction and analysis of raw data from the Rona array. Using a specifically designed set of 9 match filters, optimised over 0 to 5000 m, and at angles of -3 to 3 , the data was reduced to a set of possible neutrino pulse candidates. This was reduced further by finding coincidences between these candidates on sets of 4 or more hydrophones. Cross correlation was then performed on each set of pulse coincidences, aligning all trigger times, and removing any pulse from the coincidence that appeared not to have originated from the same event. Any repeated events and events with coincidences of less than four hydrophones are removed.

Further reduction was then performed using an artificial neural network. Each pulse was classified using the dominant frequency, the number of peaks greater than two standard deviations, the Kurtosis, Skewness, and the output of further match filters. Using a noise data set, created from 3000 pulses from the reduced Rona data, and a signal data set, created from 3000 simulated signals over distance and angle superimposed on background noise from the Rona array, a neural network was trained using the 7 pulse classifications. Further work was done in optimising the neural network over 0 to 4000 m, and at angles of -2 to 2 . Any pulses that failed the neural network cut were removed from the coincidence, and events with coincidences of less than four hydrophones after this were removed. Final energy and fiducial volume cuts were made. The efficiency of the data reduction and analysis was tested, and was found to be 100% efficient for energies $> 10^{21.5}$ eV, 43% efficient at 10^{21} eV, and 0% efficient at 10^{20} eV.

To test the reduction and analysis code, data from a Rona field trip was analysed. From the 6th-8th August 2007 a field trip was made to the Rona array. Bi-polar, sinusoidal, and step pulses were placed into the water at varying voltages. From this data, a small section was analysed, containing bi-polar pulses at 25 V. 25 out of 100 of these pulses were successfully identified. To identify these pulses, a new match filter was used corresponding to the shape of the pulse after detection at the hydrophones.

These 25 pulses were then reconstructed. The vertices of the reconstructed pulses reconstructed to the expected position of the boat and aligned with the boat's trajectory. The events also reconstructed at a depth of 12.5 m, the depth that the pulses were injected. Optimisation of the hydrophone positions was then tried. The results of this

were not successful, with the events reconstructing to a depth of 60 m, and the wrong side of the array to where the signals were injected.

The final test on the field trip data was to look at the energy loss over distance. Using the 25 reconstructed events and the four closest hydrophones, the energy of the detected pulse was plotted against distance. Plotting on a log scale, the gradient of the line was found to be -2.1 $\pm$ 0.23. With an expected fall of $1/r^2$, this proved a successful test on the field trip data of the reduction and analysis code.

The Rona data (290 days) was reduced to two coincident neutrino like events. To investigate the array efficiency of the detector a detailed Monte Carlo was created including pulse generation and detection at the Rona array. The number of events detected was calculated for varying degrees of coincidence and the efficiencies of the Rona array calculated. Combining this with the efficiency of the data reduction and analysis, a UHE neutrino flux limit has been calculated, and is presented in two different ways. The systematic errors of the analysis were discussed, and the limit curve updated to reflect this.

Possible extensions of the analysis performed in this thesis have been briefly discussed.

Finally, acoustic detection in ice has been examined. In ice, the velocity profile changes with depth, and acoustic pulses refract strongly as they propagate. The Monte Carlo was extended to incorporate refraction, reflection, and the pulse properties in ice. Arrays based on the Arianna and IceRay design were investigated and sensitivities were calculated. It was shown that an Arianna-type array detecting single pulses would be the most sensitive.

Chapter 2

Ultra-High Energy Neutrino Astronomy

2.1 Introduction

Until the early twentieth century our knowledge of the universe was limited to studying only the visible part of the electromagnetic spectrum. As time has progressed techniques have been developed to exploit the entire range of the electromagnetic spectrum (radio, infrared, visible, ultraviolet, X-ray, and most recently gamma rays), but studying only the electromagnetic spectrum has limitations. There are optically dense places in the universe where electromagnetic radiation cannot escape and, at high energies, the range of photons is limited due to the interaction with background photons, as discussed further in section 2.5. However, exploiting the electromagnetic spectrum is not the only way to study the universe. The universe can also be studied by looking at particles that arrive at Earth - astro-particle physics.

Astro-particle physics was pioneered by Viktor Hess in the early 20th century [1]. For many years scientists had been unable to explain the source of an ionising background radiation in the atmosphere that penetrated electroscopes sent aloft in balloons. It was assumed that the radiation must have its source on Earth. In a series of balloon ascents in 1911-13, Hess found that the radiation increased rapidly with altitude, and suggested it had extraterrestrial origins.

Astro-particle physics is a growing field with new techniques constantly being devel-

oped. One such method is to study the universe via the detection of ultra-high energy neutrinos. This method is still in its infancy, but if the new techniques prove to be successful, unanswered questions in particle and astro-physics could be answered (see section 2.4.1).

2.2 The Standard Model of Particle Physics

The standard model of particle physics (SM) [2, 3, 4][1] has been very successful in describing the interactions and properties of the fundamental particles of nature for many years, and has stood up to very rigorous testing by many different experiments.

The SM is a SU(3) $\otimes$ SU(2) $\otimes$ U(1) gauge theory, and assumes that all interactions between fermions and gauge bosons take place via the exchange of force carrying particles. This will be discussed further in the following sections. All masses and lifetimes in the following sections will be taken from [5].

2.2.1 Fermions

Fermions have half integer spin, and can be sub-divided into leptons and quarks (tables 2.1 and 2.2 respectively). Each group can then be subdivided into 3 generations, with each generation containing two particles separated by a unit charge. Each fermion also has its corresponding antiparticle, giving a total of 24 fermions.

The heavier flavours of charged leptons can decay to the lighter flavours and the τ is heavy enough to decay to quarks. Leptons do not feel the strong force. Quarks, unlike leptons, feel all three forces. They carry the colour charge of the strong force (red, green, or blue), and are never seen in isolation. When in a bound state the colour must be neutral. Quarks bind in two ways, in a meson (a quark and anti-quark with of the same colour and anti-colour), and a baryon (3 quarks all of different colours). Collectively the bound states are known as hadrons.

Flavour	Charge (Proton Charge)	Mass (MeV)	Lifetime (s)
e	-1	0.51	$> 4.6 \times 10^{26}$
ν_e	0	$< 2 \times 10^{-6}$	> 300
μ	-1	105.66	2.2×10^{-6}
ν_μ	0	< 0.19	> 15.4
τ	-1	1776.99	290.6×10^{-15}
ν_τ	0	< 18.2	no data

Table 2.1: *Properties of the standard model leptons.*

Flavour	Charge (Proton Charge)	Mass (MeV)
u	$2/3$	1.5-3.0
d	$-1/3$	3-7
s	$2/3$	95 ± 25
c	$-1/3$	1250 ± 90
b	$2/3$	4200 ± 70
t	$-1/3$	$(172.6 \pm 1.4) \times 10^3$

Table 2.2: *Properties of the SM quarks. Note - the top mass is the latest result from the Tevatron [6], and not that quoted in [5].*

Mediator	Charge (Proton Charge)	Mass (GeV)
gluon	0	0
photon	0	0
$W^\pm$	± 1	80.403 ± 0.029
Z^0	0	91.1876 ± 0.0021

Table 2.3: *The gauge bosons in the standard model.*

2.2.2 Bosons

Forces in the SM model are described in terms of the exchange of the gauge bosons (table 2.3). The electromagnetic force is described by the exchange of the photon. The photon couples proportionally to the charge of particles, and only charged particles feel the electromagnetic force. The photon is massless, and thus the EM force has an infinite range.

The strong force is mediated by 8 gluons which couple to the colour of the quarks and gluons. The gluon is massless, but the range of the strong force is not infinite, it is of the order of a few fempto-metres. The reason for the non-infinite range is because of the colour charge of the gluons. As a quark is separated from its 'partner quarks', the strong force remains constant in strength and it becomes energetically favourable for a quark/anti-quark pair to spontaneously appear out of the vacuum than for the quark to be separated further.

The weak force is mediated by the $W^{\pm}$ and Z^0. It is felt by all particles carrying weak isospin. The Z^0 also couples to the electromagnetic charge. Because of the high masses of the W and Z^0, weak interactions are suppressed at low energies.

2.2.3 The Neutrino

The idea of the neutrino first arose in 1930 when there appeared to be a problem in the energies measured in nuclear beta decay (a nucleus A is transformed into a lighter nucleus B with the emission of an electron). It is convenient in two-body decays for the outgoing energies to be determined in the centre of mass frame. In this frame, A is at rest, so that B and the electron recoil with equal and opposite momenta, then the conservation of energy dictates that the electron energy is:

$$E = \frac{m_A^2 - m_B^2 + m_e^2}{2m_A} \quad c^2 \tag{2.1}$$

If the masses of A and B are known, the electron energy E would always be fixed, but this was not the case. When experiments were performed it was found that the energy of the electron varied considerably, with equation 2.1 only giving the maximum energy.

[1]Natural units are assumed: $\hbar = \mathrm{c} = 1$

This was a problem, as seemingly the conservation laws were broken. However, Pauli suggested that along with nucleus B and the electron there was another, electrically neutral particle emitted. For the electron to achieve the energies that were found in the study beta decay, this particle had to be extremely light or massless. It was later that Fermi named this particle the neutrino [2].

Until the mid-1950s there was compelling theoretical evidence for the neutrino, but no direct experimental evidence: it left no tracks, it did not decay, it just proved a handy book-keeping tool for the conservation laws. In 1953 Cowen and Reines finally detected this elusive particle at the Savannah River nuclear reactor in South Carolina looking at inverse beta decays. These results provided unambiguous conformation of the neutrino's existence [2].

The detailed properties of the neutrino remained mysterious. It is known to be electrically neutral, but does it have mass or have the same flavours as the other leptons? Also is the neutrino its own anti-neutrino? The photon is its own antiparticle, as is the neutral pion. This question was first addressed in the late 1950s by Davis and Harmer [7] by studying the reactions:

$$\nu + n \rightarrow p^+ + e^- \tag{2.2a}$$

$$\bar{\nu} + n \rightarrow p^+ + e^-, \tag{2.2b}$$

using reactor neutrinos. Reaction 2.2a was observed but 2.2b was never observed. This was thought to establish that the neutrino and anti-neutrino were two unique particles. But this was not quite true. The neutrino could still be its own anti-neutrino but just exist in two helicity states, and hence reaction 2.2b was looking at the wrong helicity state[2] state. This theory is known as the Majorana theory [8]. The advantage of the Majorana theory is that it more naturally gives the neutrino a very small mass, whereas

[2]Helicity describes the projection of the spin vector onto the momentum vector and is defined as:

$$H = \frac{\dot{\mathbb{S}} \cdot \dot{\mathbb{P}}}{|\dot{\mathbb{S}}||\dot{\mathbb{P}}|}, \tag{2.3}$$

where $\dot{\mathbb{S}}$ is the spin vector and $\dot{\mathbb{P}}$ the momentum vector. Particles are named Right-handed when the spin is in the direction of the momentum, and left-handed when the spin and momentum are in opposite directions.

the Dirac theory doesn't explain the mass. If the neutrino follows Dirac or Majorana physics is still unanswered [9].

Experimentally, the decay:

$$\mu^- \rightarrow e^- + \gamma, \tag{2.4}$$

is never observed. But reactions such as:

$$\mu^- \rightarrow e^- + \nu + \bar{\nu}, \tag{2.5}$$

are observed. A possible solution to this observation is to have a neutrino associated with the muon, and a neutrino associated with the electron, and a conservation law requiring a conservation of lepton flavour. Lederman, Schwartz and Steinberg successfully distinguished both neutrinos in 1962 [10]. The tau neutrino was eventually added to the list in 2000 [11].

The final property of the neutrino still under investigation is neutrino mass oscillations between different flavours. A problem first arose in 1968 in the Homestake Mine experiment [12]. Here it was noticed that there was a deficit in solar electron neutrinos being detected in comparison to that predicted from the standard solar model. There were two suggested solutions to the problem. Firstly that the standard solar model (SSM) needed modifying, or that there was an error in the experiment. Experiments were designed, notably SAGE [13], Kamiokande, and Super-Kamiokande [14], to try and repeat the results of Homestake Mine using different methods. All found a similar deficit in solar neutrinos leaving the conclusion that the SSM was wrong. But there seemed to be no sensible modification of the SSM that would agree with the experimental data.

In 1964 oscillations were observed in the Kaon sector [15]. The question was then raised as to whether the neutrino can oscillate, which requires the neutrino to have a non-zero mass. Both neutrino mass and oscillation are widely studied fields in modern neutrino physics and will be discussed in detail in the next section.

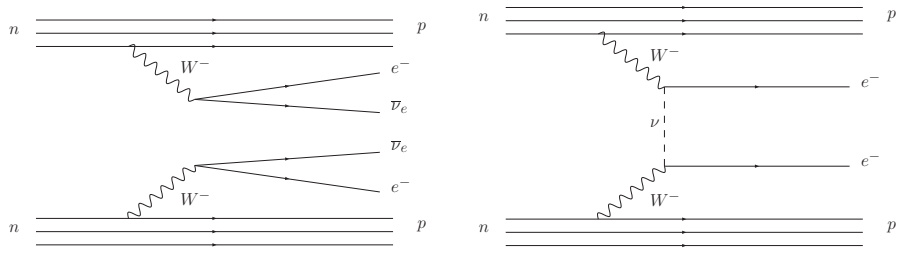

(a) **(b)**

Figure 2.1: *Double beta decay. Diagram (a) shows double beta decay where neutrinos are produced, and diagram (b) shows neutrinoless double beta decay. Neutrinoless double beta decay would show that the neutrino is its own anti-particle, and hence a Majorana particle.*

2.3 Review of Current Neutrino Physics

2.3.1 Dirac and Majorana Mass

Appendix 11.1 describes how mass in the SM is described. This is known as the Dirac mass, and assumes that the particle and anti-particle are fundamentally different. But in the standard model, as there is no right-handed neutrino, the neutrino is left with a zero mass. A alternative way to allow the neutrino to have mass is to define a Majorana mass term [16, 17]. This assumes that the neutrino is the same particle as the anti-neutrino.

Whether the neutrino is a Dirac or Majorana particle is therefore one of the most important questions in neutrino physics today, which is being investigated by many experiments, for example the (Super-)NEMO experiment [9].

If the neutrino is not its own anti-particle, neutrinoless double beta decay, depicted in diagram (b) in figure 2.1, would never happen. However, if the neutrino is a Majorana particle, neutrinoless double beta decay is possible. Therefore by searching for neutrinoless double beta decay, the fundamental nature of the neutrino can be studied. To date no conclusive evidence for neutrinoless double beta decay has been found.

2.3.2 Neutrino Oscillations

If the neutrino has mass, neutrino mass eigenstates can be defined. Neutrinos are produced and observed as weak eigenstates, but they propagate through space as mass eigenstates, leading to the possibility of oscillation. This can be considered as analogous to weak mixing in the quark sector. The weak quark eigenstates are related to the mass eigenstates by the 3×3 CKM matrix [2]. Similarly the weak neutrino eigenstates are related to the neutrino mass eigenstates by a unitary matrix U. This unitary matrix is known as the PMNS (Pontecorvo-Maki-Nakagawa-Sakata) matrix [18]. The relationship between the neutrino mass eigenstates is given by:

$$|\nu_\alpha \rangle = \sum_i U^*_{\alpha i} |\nu_i\rangle \tag{2.6}$$

$$|\nu_i \rangle = \sum_\alpha U_{\alpha i} |\nu_\alpha\rangle \ , \tag{2.7}$$

where $\nu_\alpha = (\nu_e, \nu_\mu, \nu_\tau)$ represents the flavour states, and $\nu_i = (\nu_1, \nu_2, \nu_3)$ represents the mass eigenstates. U represents the PMNS mixing matrix:

$$U = \begin{pmatrix} U_{e1} & U_{e2} & U_{e3} \\ U_{\mu 1} & U_{\mu 2} & U_{\mu 3} \\ U_{\tau 1} & U_{\tau 2} & U_{\tau 3} \end{pmatrix} \tag{2.8}$$

which can be parameterised by:

$$U = \begin{pmatrix} c_{13}c_{12} & c_{13}s_{12} & s_{13}e^{-i\delta} \\ -c_{23}s_{12} - s_{13}c_{12}s_{23}e^{+i\delta} & c_{23}c_{12} - s_{13}s_{12}s_{23}e^{+i\delta} & c_{13}s_{23} \\ s_{23}s_{12} - s_{13}c_{12}c_{23}e^{+i\delta} & -s_{23}c_{12} - s_{13}s_{12}c_{23}e^{+i\delta} & c_{13}c_{23} \end{pmatrix} \times \begin{pmatrix} 1 & 0 & 0 \\ 0 & e^{i\alpha} & 0 \\ 0 & 0 & e^{i\beta} \end{pmatrix} \tag{2.9}$$

where $s_{ij} = \sin\theta_{ij}$ and $c_{ij} = \cos\theta_{ij}$. In the factorised form the PMNS [19] matrix becomes:

$$U = \begin{pmatrix} 1 & 0 & 0 \\ 0 & c_{23} & s_{23} \\ 0 & -s_{23} & c_{23} \end{pmatrix} \begin{pmatrix} c_{13} & 0 & s_{13}e^{-i\delta} \\ 0 & 1 & 0 \\ -s_{13}e^{i\delta} & 0 & c_{13} \end{pmatrix} \begin{pmatrix} c_{12} & s_{12} & 0 \\ -s_{12} & c_{12} & 0 \\ 0 & 0 & 1 \end{pmatrix} \begin{pmatrix} 1 & 0 & 0 \\ 0 & e^{i\alpha} & 0 \\ 0 & 0 & e^{i\beta} \end{pmatrix}. \tag{2.10}$$

In the form as shown in equation 2.10, the mixing matrix is composed of three angles and three phases, and is decomposed into terms that can be associated with different regimes. The sector (23) is identified with atmospheric Δm^2, (12) is associated with solar Δm^2, and (13) is associated with ν_e flavour transitions on short baselines. The Dirac phase, δ, allows for the possibility of CP violation in the appearance modes, where appearance experiments look for neutrinos that were not in the initial beam.

It is expected that all three neutrino species will mix together, but it is useful to consider the simplified case where there are two weak neutrino flavours, ν_α and ν_β, and two mass eigenstates ν_1 and ν_2, with masses m_1 and m_2. The weak eigenstates are then related to the mass eigenstates by:

$$\begin{pmatrix} \nu_\alpha \\ \nu_\beta \end{pmatrix} = \begin{pmatrix} \cos\theta & \sin\theta \\ -\sin\theta & \cos\theta \end{pmatrix} \begin{pmatrix} \nu_1 \\ \nu_2 \end{pmatrix}, \tag{2.11}$$

where θ is the mixing angle between the mass and the flavour eigenstates. Consider a beam of a certain initial flavour, ν_β, with an energy E, and at a distance L from the observer. At the source:

$$|\nu_{(x=0)} \ = |\nu_\beta \ = -\sin\theta|\nu_1 \ + \cos\theta|\nu_2 \ . \tag{2.12}$$

Then at the observer:

$$|\nu_{(x=L)} \ = -\sin\theta e^{iE_1 t}|\nu_1 \ + \cos\theta e^{iE_2 t}|\nu_2 \ , \tag{2.13}$$

where e^{iEt} is time evolution factor from the time dependent Schrödinger equation. This gives a probability that at the detector the ν_β will have evolved into a ν_α of:

$$P_{\nu_\beta \to \nu_\alpha} = |\ \nu_\alpha|\nu_\beta\ |^2 \tag{2.14}$$

$$= |-\sin\theta\cos\theta e^{iE_1 t} + \cos\theta\sin\theta e^{iE_2 t}|^2 \tag{2.15}$$

$$= 2\sin^2\theta\cos^2\theta(1-\cos(E_1 - E_2)t). \tag{2.16}$$

Now $E_i^2 = p^2 + m_i^2$, and in the limit $m_i \quad p$:

$$E_i = \quad \overline{p^2 + m_i^2} \tag{2.17}$$

$$p + \frac{m_i^2}{2p}, \tag{2.18}$$

and:

$$E_1 - E_2 = \frac{m_i^2 - m_2^2}{2p} \tag{2.19}$$

$$= \frac{\Delta m_{12}^2}{2p}. \tag{2.20}$$

The neutrino is highly relativistic, so $t \sim L$, where L is the distance travelled. Assuming $p \sim E$:

$$P_{\nu_\beta \to \nu_\alpha} = \sin^2 2\theta \sin^2 \frac{\Delta m_{21}^2 L}{4E}, \tag{2.21}$$

in natural units. With energy in GeV, length in km, and mass in eV:

$$P_{\nu_\beta \to \nu_\alpha} = \sin^2 2\theta \sin^2 \frac{1.27 \Delta m_{21}^2 L}{4E}. \tag{2.22}$$

This can then be extended to three flavour mixing.

Equation 2.22 shows that if the neutrino has mass, neutrino flavour oscillations are theoretically possible. Davis also gave motivation in the Homestake Mine experiment for neutrino flavour oscillations [12]. The first experiment to observe neutrino oscillations was Super-Kamiokande in 1998 [20], observing atmospheric neutrino oscillations. This gave rise to the design of experiments that would tackle this problem directly. The main two experiments that set out to achieve this were SNO and KAMLAND. KAMLAND first published its results in 2002 [21], shortly followed by SNO [22]. Both experiments giving strong support to solar neutrino oscillations. K2K [23] and MINOS [24], both long-baseline experiments, have independently confirmed the existence of neutrino oscillations.

Also in 2002 the set of 'standard' neutrinos was complete when DONUT published results on the first detection of the tau neutrino, twenty four years after the tau lepton was first observed [25].

Mass Hierarchy

The mass hierarchy of the three generations of neutrinos is still unknown. Two possible hierarchies are shown in figure 2.2. The left plot shows the normal mass hierarchy, with

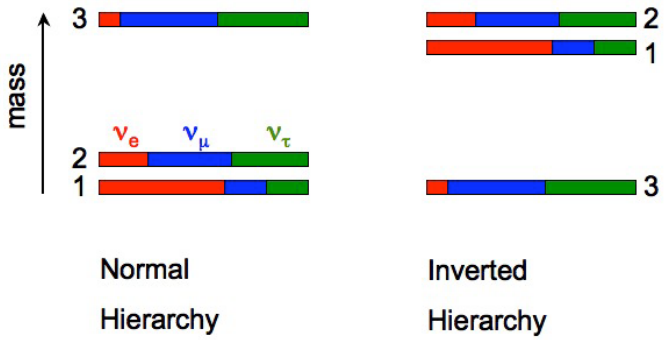

Figure 2.2: *The left plot shows the normal mass hierarchy, where the mass ordering is shown on the vertical axis, and the possible flavour compositions of the mass states indicated by the coloured horizontal bars. The right hand plot shows the inverted mass hierarchy.*

the mass values shown on the vertical axis, and the possible flavour compositions of the mass states indicated by the coloured horizontal bars. The right hand plot shows the inverted mass hierarchy.

Constraints have been made on the mass differences by various experiments. Solar neutrino experiments [26] have constrained $\delta m^2_{21} = 8.0 \pm 0.4 \times 10^{-5}$ eV^2, and long base line experiments [24] have constrained $\delta m_{23} = 2.7 \pm 0.4 \times 10^{-3}$ eV^2 .

Absolute Mass

Solar neutrino experiments and long-base line experiments have made constraints on the differences squared between the masses of the neutrino, but do not describe the absolute mass scale. Table 2.1 shows the current best upper limits of the mass for each neutrino generation (values are taken from [5]).

Future experiments aim to lower these upper limits (or measure the neutrino mass), including particle physics detectors using beta decay/neutrinoless beta decay [9, 27], and cosmology experiments (which are only sensitive to $\Sigma_{i=1,3} m_i$) using CMB gravitational lensing [28].

2.4 UHE Neutrino Astronomy

Despite a lot of successful work on the neutrino, many questions still remain, and much work still has to be done. One field that will play a major role in the understanding of

the neutrino is neutrino astronomy.

The neutrino is the second most abundant particle in the universe, with a number density of 3×10^6 m^{-3} (the photon has a number density of 1×10^7 m^{-3}, and the proton 0.5 m^{-3}). However, the neutrino density is completely dominated by relic neutrinos from the big bang. These relic neutrinos have very low energy and are not directly observable with current techniques. The remaining higher energy neutrinos span a very wide energy range, and it is only the neutrinos at the highest energies that will be considered in this thesis. At ultra-high energies the neutrino flux is small requiring very large detectors to get an analysable detection rate. This forces the use of large natural target materials (water, salt, ice).

The energy that can be detected varies with the technique used. Energies up to 10^{17} eV are the realm of the optical detectors, but at energies $> 10^{17}$ eV, optical detectors become insufficient (see section 3.2). They are optimised for detection of Cerenkov radiation, which has an attenuation length of 50 - 100 m, depending on the material. At energies above 10^{20} eV the predicted number of neutrino per km^3 per year is $\sim$1, so optical arrays are too small to be efficient detectors of UHE neutrinos. In order to detect neutrinos at high energies, many km^3 detectors are required and being designed [29, 30].

2.4.1 The Aims of Neutrino Astronomy

Particle Physics Questions

Particle physics knowledge will be much advanced when the Large Hadron Collider (LHC) [31] starts taking data (hopefully early 2009!), and will collide particles at a centre of mass energy of 14 TeV. The main searches will include searches for the Higgs particle, super-symmetry, and extra dimensions searches [5]. If the LHC finds new physics, and UHE neutrino astronomy finds new physics, will the physics be the same, and directly comparable? New physics would be needed if neutrino astronomy observes an unexplainable excess in neutrinos or if new sources are found. UHE neutrino astronomy will also be able to look at the nucleon neutrino cross section at energies $> E_{\mathrm{LHC}}$.

High-energy astronomy has been much advanced with the invention of the gamma ray telescope [32], but the range of modern high-energy gamma ray telescopes is limited. This is because of the attenuation of gamma rays from distant sources. At 10^{14} eV neutrinos interact with the cosmic background radiation and do not survive the journey from the centre of our galaxy. The neutrinos annihilate into an electron -positron pair:

$$\gamma + \gamma_{BK} \rightarrow e^+ + e^-. \tag{2.23}$$

Neutrino astronomy aims to look back over cosmological interesting distances, as neutrinos suffer no such interactions. UHE neutrino astronomy would also be able to offer insight into the details of the ultimate energy release during the collapse of matter, the origin of cosmic rays, and could even give crucial insights into the nature of dark matter [16].

2.4.2 The Cosmic Ray Spectrum

Figure 2.3 shows the cosmic ray spectrum above 1 GeV. Below this, the spectrum is dominated by coronal ejections.

The spectrum can be well described by a broken power law of the form $\phi \sim E^{-\gamma}$, where $\gamma = 2.7$. There are two features in this diagram that must be described further, the sections labelled the 'knee' and the 'ankle'. Both of these are deviations are caused by a change in the spectral index, γ.

The 'knee', at around 10^{15} eV, remains an unsolved problem. The most popular theory is of a change in the composition of cosmic rays from protons to heavier nuclei [34]. This will be discussed in more detail in section 2.5.1. Other theories include interactions with the galactic dark matter halo, and different acceleration methods to produce the UHE cosmic rays [35].

The second feature is the 'ankle' at 10^{19} eV. This region is considered to be due to the transition from galactic to extragalactic cosmic rays, and is less controversial. Further detail may yet be resolved in the spectrum as more precise data are collected.

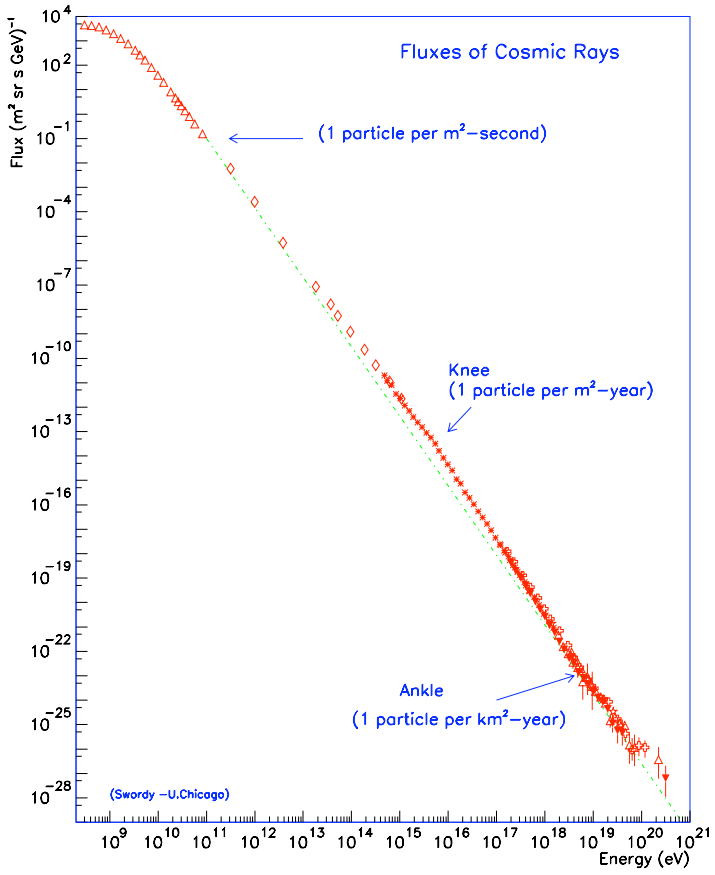

Figure 2.3: *The cosmic ray spectrum, taken from [33]. The figure shows only the high energy cosmic ray spectrum. The distinctive 'knee' and 'ankle' deviations from the power law spectrum can be seen at $\sim 10^{15}$ eV and $\sim 10^{19}$ eV.*

2.4.3 Potential Sources of UHE Neutrinos

The origin and mechanism for accelerating UHE cosmic rays remains one of the major unknown phenomena in astro-particle physics. Many theories have been proposed as to how cosmic rays are accelerated to UHE energies [36], and can be split into two categories - 'bottom-up' and 'top-down' models.

Bottom-up models describe a mechanism where high energy cosmic rays are produced by protons accelerated to high energies. UHE neutrinos are created by proton-proton or proton-photon interactions via pion production and decay. This can happen in the ambient gas and radiation surrounding the accelerating environment or with the CMB. Such accelerators might be active galactic nuclei, AGN, powered by super massive black holes, gamma ray bursts, or shock fronts of supernovae remnants [36].

The second category, top-down, are models in which a UHE neutrino is produced from a high energy relic particles, often through exotic models. Examples of this are the annihilation of super heavy dark matter candidates, the decay of GUT scale particles, and topological defects [37].

Shock Front Acceleration

This method of acceleration is thought to be the primary mechanism for accelerating cosmic rays. As the shock front expands into a medium of decreasing density, it accelerates. The energy of the wavefront can be transferred to the particles in the medium surrounding the shock, and through collisions create high energy particles [38].

High energy cosmic rays can also be created by collision-less acceleration [39]. This mechanism involves the particles being scattered back and fourth across the shock discontinuity. At each cross the particle gains energy. This is because the flow of the shock is converging (the fluid on each side of the discontinuity sees the other as it approaches). This keeps happening until the particle escapes the shock front. An analogy to this is a table tennis ball being scattered back and fourth between two approaching trains.

The upper limit for particles accelerated using this method is a still a debated topic due to the lack of knowledge about regions where this may happen in the universe. Energy limits range up to 10^{20} eV [40]. The predicted energy spectra for particles accelerated this way is $\sim E^{-2}$.

Active Galactic Nuclei

Active Galactic Nuclei (AGN) is a term for a collection of objects in the distant universe which are observed to have enormous energy outputs ($>10^{37}$W). The latest models predict that this energy output is driven by a super massive black-hole (10^7 - 10^9 solar masses) at the centre of the AGN. Tidal disruptions by passing stars form an accretion disk around the black-hole composed of stellar material which, as it spirals into the black-hole, emits radiation. Outflows of ionised gas may be generated perpendicular to the spin axis of the disk. It is in these jets that particles can be accelerated to ultra-high energies.

AGNs can be characterised by i) high luminosities, ii) appearance of jet-like structures iii) a high contrast in brightness between the nucleus and large scale structures. Objects that are classified as AGN are Seyfert galaxies, radio galaxies, BL Lacerate, and Quasars.

Gamma Ray Bursts

Gamma ray bursts were discovered in the late 1960s by the US Vela nuclear test detection satellites [41]. The Vela satellites were designed to detect gamma-radiation emitted by nuclear weapon tests on or under the surface of the Earth. But these satellites also picked up the occasional burst of gamma rays from an unknown source. In 1973, researchers at the US Los Alamos National Laboratory determined that these bursts came from deep space.

Gamma Ray Bursts are short (seconds to hours) very intense flashes of gamma-rays. They occur isotropically in the sky at a rate of about one a day [42]. The isotropy of these events suggests that they are of non-galactic origin, but theories exist where they are produced locally (within the galaxy), and it has yet to be proven either way. The mechanism of the bursts is thought to be the fireball shock model [43].

It is thought that only a small fraction of stars (10^{-6}) undergo this catastrophic energy release towards the end of their evolution. One model suggests that it is the core collapse of massive stars, and another model suggests it originates from the merging of neutron star or black-hole/neutron star binaries. Both these models end with a few solar mass black hole with a torus of debris surrounding them. The sudden release of the gravitational energy in this accretion ring powers the burst. The enormous

compressional heating escapes along the axis of rotation of the accretion ring. This resulting relativistic jet undergoes internal shocks, in which particles can be accelerated. Correlation between UHE particles and Gamma Ray Bursts has yet to be detected [44, 45].

The following mechanisms are examples of a top down models. A result of this is that they do not require any acceleration method.

Z-Burst Neutrinos

Similarly to the CMB, the universe is filled with a homogeneous background of relic neutrinos, which decoupled when the universe cooled down to a temperature of $\mathcal{O}(1\text{ MeV})$ at about 1 second after the big bang. It is predicted that the number density of these neutrinos is 54 cm^{-3} for both neutrinos and anti neutrinos, with a blackbody temperature of 1.95 K [46].

The mean free path for a cosmic ray neutrino to annihilate at the Z resonance on a relic background neutrino is $\mathcal{O}(\text{Hubble Distance})$. This means that for a UHE neutrino, the probability of annihilation is significant. This provides a mechanism for generating a significant flux of nucleons above the GZK cutoff. Each annihilation produces a Z-boson, which then immediately decays (with a lifetime of 3×10^{-25} s), producing nucleons with lower energy, but with a high multiplicity. It is the hadronic channel (70% of the time) which is referred to as the Z burst. Therefore it is predicted that there should be an abundance of necleons around the Z resonance.

Topological Defects

After the big bang, as the universe expanded and cooled, the fundamental forces began developing their own identities. During these symmetry breaking periods (also known as phase transitions) linear topological defects [47, 48] (strings) are produced.

When these topological defects annihilate, or collapse, the energy on the order of the GUT scale is released in the form of super-heavy Higgs or gauge bosons, often referred to as X particles. These X particles can then decay hadronically to give ultra-high energy neutrinos.

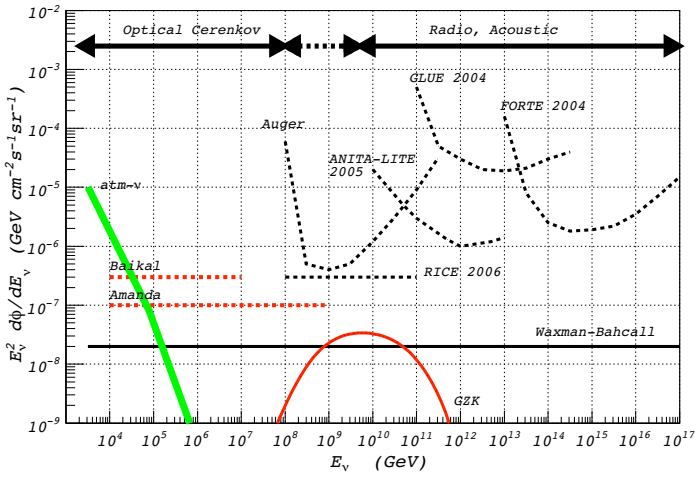

Figure 2.4: *The predicted flux of neutrinos from the GZK mechanism, Waxman-Bachall limit, and the atmospheric neutrino flux. The figure also shows the upper limits of various neutrino experiments. The dates refer to the dates of the published limits, taken from [51].*

2.5 Predictions of the Expected UHE Neutrino Flux

Various predictions have been made for the expected flux of UHE neutrinos based on the standard model of particle physics. The two most common predictions are the Waxman-Bachall [49] upper limit and the cosmogenic flux of neutrinos from the GZK mechanism [50], these are both shown in plot 2.4.

Waxman-Bachall Limit

Waxman and Bachall (WB) [49] calculated that an upper bound can be placed on the flux of cosmic neutrinos arriving on Earth - assuming that they are generated in cosmologically distributed, optically-thin proton accelerators. The value of this flux is 2×10^{-8} E^2 (GeV cm^2 sec sr)$^{-1}$.

If the observed flux of ultra-high energy cosmic rays is the result of cosmologically distributed sources, then the energy injection rate in the 10^{19} - 10^{21} eV energy range is:

$$E_{\rm CR}^2 \frac{d\dot{N}_{\rm CR}}{dE_{\rm CR}}\Big|_{E_0} = \frac{\dot{m}_{\rm CR}^{[10^{19},10^{21}]}}{\ln(10^{21}/10^{19})} \approx 10^{44}\,{\rm erg\,Mpc^{-3}yr^{-1}}\ , \qquad (2.24)$$

where an energy spectrum $\propto E^{-2}$ has been assumed and $E_0 = 10^{19}$ eV. $E_{\rm CR}$ is the energy of the cosmic ray, $\dot{N}_{\rm CR}$ is the injection rate of cosmic rays, and $\dot{n}_{\rm CR}$ is the energy production rate of protons. The energy density of neutrinos produced through photo-pion interactions of these protons is directly related to the injection rate of cosmic rays:

$$E_\nu^2 \frac{dN_\nu}{dE_\nu} \approx \frac{3}{8} f_\pi \, t_{\rm H} \, E_{\rm CR}^2 \frac{d\dot{N}_{\rm CR}}{dE_{\rm CR}}, \tag{2.25}$$

where $t_{\rm H}$ is the Hubble time. f_π is the fraction of the energy which is injected in protons lost to photo-pion interactions. The factor of 3/8 arises since half of the pions are neutral, and thus do not generate neutrinos, and one quarter of the energy of charged pion decays, $\pi^+ \to \mu^+ \nu_\mu \to e^+ \nu_e \nu_\mu \bar{\nu}_\mu$, goes to electrons rather than neutrinos. Thus the expected neutrino flux is:

$$[E_\nu^2 \Phi_\nu]_{\rm WB} \approx (3/8)\, \xi_Z \, f_\pi \, t_{\rm H} \, \frac{c}{4\pi} \, E_{\rm CR}^2 \frac{d\dot{N}_{\rm CR}}{dE_{\rm CR}} \tag{2.26}$$

$$\approx 2.3 \times 10^{-8} \, f_\pi \, \xi_Z \, {\rm GeV \, cm^{-2} \, s^{-1} \, sr^{-1}}, \tag{2.27}$$

where the parameter ξ_Z accounts for the effects of source evolution with redshift, and is expected to be of order unity. $\Phi_\nu = \frac{dN_\nu}{dE_\nu}$ and, E_{CR} and N_{CR} are the energy of the cosmic rays respectively, and number of cosmic rays. The Waxman-Bachall bound is defined by the condition $f_\pi = 1$.

Although figure 2.4 shows an upper limit for the WB flux extending to 1×10^{26} eV, this is only generated on general arguments about Fermi acceleration in astrophysical objects.

GZK Neutrinos

Due to the finite inelastic collision length of protons in the cosmic background radiation (50 Mpc at GZK energies), there is maximum energy of protons of cosmological origin. This is known as the GZK cut-off. The GZK flux is based on the observed flux of ultra-high energy proton cosmic rays, and has uncertainties of an order of magnitude.

The highest energy cosmic rays are energetic enough ($> \sim 10^{19}$ eV) to have photo-production reactions with the cosmic background radiation. The secondary mesons produced in the photo-production, decay into gamma rays and neutrinos, giving a flux

of high-energy neutrinos:

$$p + \gamma_{cmb} \rightarrow \pi^+ + n \tag{2.28a}$$

$$\pi^+ \rightarrow \mu^+ + \nu_\mu \tag{2.28b}$$

$$\mu^+ \rightarrow e^+ + \bar{\nu_\mu} + \nu_e \tag{2.28c}$$

$$n \rightarrow p + e^- + \bar{\nu}_e \tag{2.28d}$$

Using a model of neutrino production due to proton interactions on CMB photons:

$$\frac{dN}{dE} \propto E^{-\alpha} exp(-E/E_c), \tag{2.29}$$

over the full lifetime of the universe, calculations of the flux of GZK neutrinos can be made [52]. This is shown in figure 2.5.1. GZK neutrinos are of significant interest for the early studies of UHE neutrinos, as it is assumed that these will provide a guaranteed flux of UHE neutrinos which can be directly compared with theory. For energies above the GZK cut-off point, comparing the measured flux with theory becomes more difficult, due to lack of theory. To date 49 events of energy above 10^{20} eV have been detected by the Flys Eye [53], AGASA [54], and the Pierre-Auger [55] experiments.

2.5.1 A Possible Problem for UHE Neutrino Astronomy

So far it has been assumed that the GZK neutrino flux will come from high energy protons undergoing photo-meson interactions with the cosmic microwave background. If, however, a substantial fraction of the cosmic ray primaries are heavy nuclei rather than protons, they would preferentially lose energy through photo-disintegration when the UHE heavy nuclei interacts with the cosmic infra-red background and splits into lighter nuclei, so the corresponding neutrino flux may be substantially depleted - in the worst case scenario by a factor of 15 [34].

Heavy nuclei, with their higher electric charge, would be more strongly deflected by magnetic fields and thus would be more likely to appear as an isotropic distribution of events. Additionally, heavy nuclei propagate over cosmological distances differently than protons, raising the possibility that they could originate from more distant sources.

Heavy nuclei could result from the field around the cosmic accelerator not being

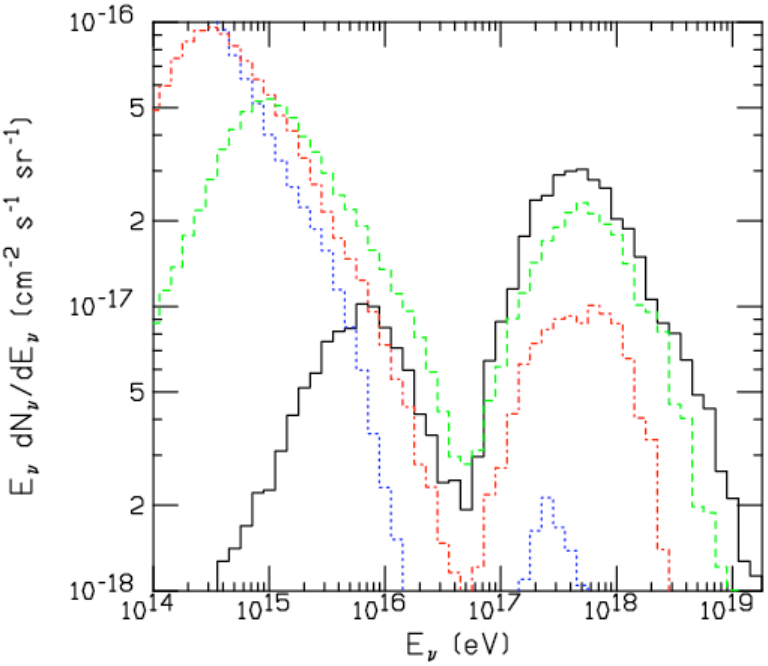

Figure 2.5: *The neutrino spectrum produced in the propagation of the UHE heavy nuclei - ^{4}HE (green, dashed), ^{16}O (red,dot-dashed), and ^{56}Fe (blue, dots) - compared to the result for protons (black, solid line). Taken from [34].*

dense enough to photo-disintegrate the heavy nuclei before it escapes the influence of the accelerator. It is however expected that for the higher energies of interest in this study E $> 10^{19}$ eV, most large nuclei will photo-disintegrate at the source and hence a flux of UHE neutrinos is still expected at Earth. The notable exception that is stated in [34] is for starburst galaxies, where most large nuclei are expected to escape intact. Figure 2.5.1 shows neutrino spectrum for heavy nuclei and protons.

2.6 Interactions of UHE Neutrinos

For UHE neutrinos the cross section is sufficiently high that the Earth becomes opaque to the neutrinos. This means that only the detection of downward going neutrinos is possible at UHE, opposed to upward going neutrinos that are searched for by the lower energy neutrino telescopes. But the lower energy telescopes suffer from a background of neutrinos from the interaction of high energy cosmic rays with the atmosphere, which will not affect UHE neutrino telescopes.

The cross section, σ, for an ultra-high energy neutrino interaction with a nucleon

via a single boson exchange has not been experimentally measured above 4.7×10^{13} eV, but has been calculated by a number of groups, for example [56]. The differential cross section for charged current interactions can be expressed in terms of the measured structure functions of the target nuclei - F_2 and xF_3 [57]:

$$\frac{d^2\sigma}{dQ^2dy} = \frac{G_F^2}{2\pi y} \left(\frac{M_W^2}{Q^2 + M_W^2} \right)^2 (F_2(x,Q^2)(1-y+y^2/2) \pm y(1-y/2)xF_3(x,Q^2)), \quad (2.30)$$

where G_F is the Fermi weak coupling, M_W is the mass of the W boson, Q^2 is the square of the four momentum transferred to the target nucleon, $y = \nu/E$ where ν is the energy transferred to the nucleon ($\nu = E - E'$ with E and E' the energies of the incident and scattered leptons), and $x = Q^2/2M\nu$ is the fraction of the momentum of the target nucleon carried by the struck quark. The $\pm$ refers to neutrino/anti-neutrino interactions. y is in effect the fraction of the neutrinos energy that is converted into the energy in the hadron shower. The structure functions F_2 and xF_3 are the sum of the quark distribution functions which have been parameterised by fitting data. The parton distribution functions are then extrapolated to the required energy. A similar expression can be written for neutral current interactions. A parameterised cross section is defined in [58], and will be used in this analysis:

$$\sigma = 2.501 \times 10^{-39} \times E^{0.3079}, \quad (2.31)$$

where the energy, E, is in GeV, and the cross section, σ, is in m^2. An example of predicted cross sections is shown in figure 2.6. The numbers in equation 2.31 are based on a ratio of charged to neutral current interactions.

2.7 Summary

Despite a lot of successful work on the neutrino, many questions still remain, and much work still has to be done. One field that will play a major role in the understanding of the neutrino is UHE neutrino astronomy. UHE neutrino astronomy will also be able to study physics on the GUT scale, measure the nucleon neutrino cross section at energies unachievable on the Earth, and look at regions in the universe hidden to conventional EM astronomy. It is expected that there will be a 'guaranteed' flux of neutrinos at GZK

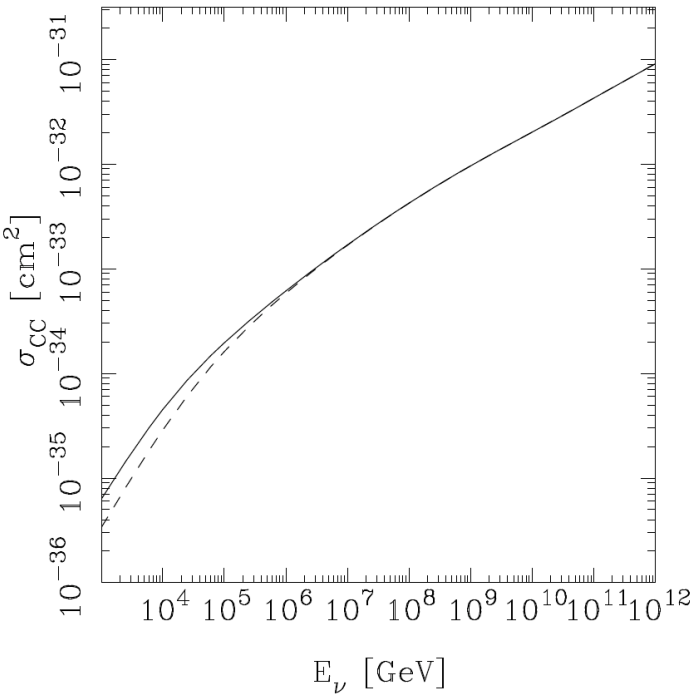

Figure 2.6: *The cross section of UHE neutrinos. The solid line shows the neutrino cross section and the dashed shows the anti neutrino cross section.Taken from [58].*

energies.

Chapter 3

Current Optical, Air Shower, Radio, and Acoustic Experiments

3.1 Introduction

The last chapter described the motivation for UHE neutrino telescopes. This chapter will describe the leading experiments in the search for UHE neutrinos. Each method will be discussed separately, each illustrated by a selection of experiments.

3.2 Optical Cerenkov Detector Experiments

Cerenkov radiation is emitted when a charged particle travels faster than the speed of light through a dielectric medium. As the charged particle travels through a dielectric medium, electrons in the atoms of the medium become excited and polarised by the magnetic field of the traversing particle. Photons are emitted as the electrons return to equilibrium [59]. If the particle is travelling slower than the photons, then the photons will interfere destructively, but when the particle is travelling faster than the speed of light in the medium, the photons constructively interfere and a Cerenkov light cone is seen. A schematic diagram of this can be seen in figure 3.1.

Up-going neutrinos interact below the Earth's surface or with the surrounding medium of the detector via a charged current reaction to produce a high energy muon $\nu_\mu(\overline{\nu}_\mu) + N \rightarrow \mu^-(\mu^+) + X$. The energy of this muon is between half and three-quarters

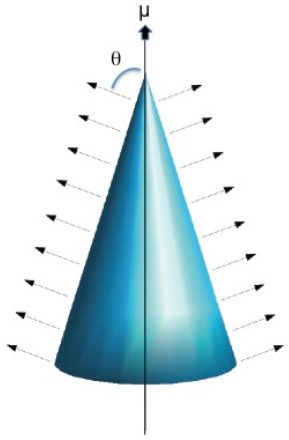

Figure 3.1: *A schematic of the Cerenkov light cone radiating from a muon travelling through a dielectric medium. θ is the opening angle of the Cerenkov cone.*

of the neutrino energy, with the remainder of the energy going into the hadronic cascade, X. This muon travels through the medium, effectively collinear to the incident neutrino direction, creating a Cerenkov light cone.

The number of Cerenkov photons produced, N, within a wavelength interval $d\lambda$, per distance dx is given by:

$$\frac{d^2N}{dxd\lambda} = \frac{2\pi\alpha}{\lambda^2} \times \quad 1 - \frac{1}{\beta^2 n^2} \quad , \tag{3.1}$$

where $\beta = v/c$ and v is the speed of the muon, α is the fine structure constant (1/137), and n is the refractive index. The opening angle of the Cerenkov cone is given by:

$$\cos\theta = \frac{1}{\beta n}. \tag{3.2}$$

Using photo-multiplier tubes, optical Cerenkov detectors search for this light cone. By reconstructing the cone, the muon path, and hence the neutrino direction, can be calculated. The total amount of light generated from secondary charged particle emission along the muon path gives an approximate measurement of the muon energy.

Muons resulting from low energy atmospheric cosmic rays will be shielded by the

Earth. Therefore by looking for upward going muons, only the showers originating from inside the Earth (from the interaction of a high energy neutrino) will be considered. This means that a Southern hemisphere telescope will look at the Northern hemisphere sky, and a Northern hemisphere telescope will look at the Southern hemisphere sky. These experiments are limited in the effective volume that they can operate over by the attenuation of light in the medium. For the South Pole ice the absorption length has a mean value of 100 m and a scattering length of 25 m [60]. For water the absorption length is $\mathcal{O}(200)$ m.

AMANDA/ICECUBE

AMANDA (Antarctic Muon And Neutrino Detector Array) [61] , is a detector of 667 downward pointing PMTs situated 1.5 km under the south pole ice. The detector covers the area of a cylinder with a height of 500 m and a diameter of 200 m. To drill the holes for the strings a hot water drill is used. The holes are drilled at 1 cm s^{-1}, and take 3 - 4 days to drill a 50 cm diameter hole to 2 km. After the holes are drilled, the strings are lowered in and the water freezes around the strings. It takes 35 hours for the water to freeze completely.

For data taken between 2000 - 2004 (1001 days of live time), the AMANDA collaboration has published many important results for neutrino astronomy [62]. A select few of these will be described with no order of importance. The first is the search for neutrino point sources. This search was performed by looking for an excess of events from the direction of 32 pre-selected objects using a sample of 4282 up going muon tracks. For this search no excess was found. A search was also carried out looking for an excess anywhere in the Northern hemisphere sky. Again no significant excess was found.

The next search was for the diffuse flux (see section2.5). This search found 6 events on an average predicted atmospheric neutrino background of 6.1. Therefore no excess of signal was found, and an upper limit of $E^2\phi < 8.8 \times 10^{-8}$ GeV cm^{-2} s^{-1} sr^{-1} was determined at 90% confidence level. This can be seen on figure 2.4.

As a natural extension to AMANDA, the ICECUBE detector is currently being constructed [63]. A schematic of the detector can be seen in figure 3.2. The detector is due for completion in 2011, and will consist of 80 strings, each containing 60 optical

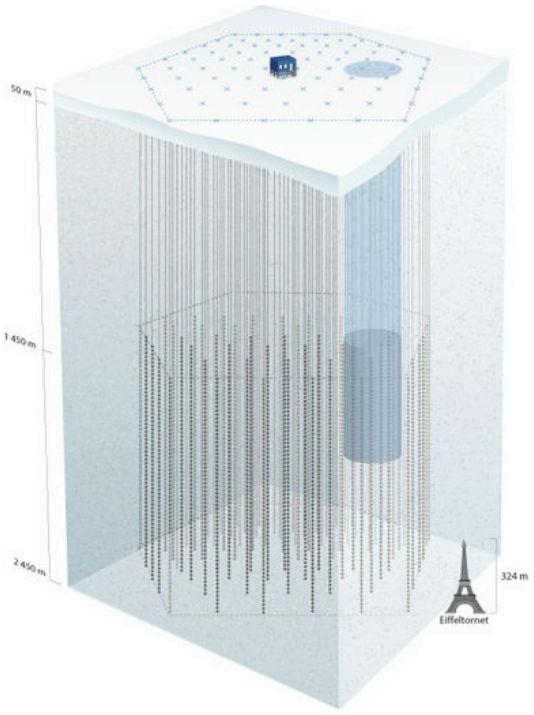

Figure 3.2: *A schematic of the ICECUBE array, taken from [64]. The embedded AMANDA detector can be seen as the blue cylinder.*

modules. The completed detector will cover an area of 1 km^3. At the time of writing, 40 strings had been fully deployed, and the detector was on target to be completed by 2011.

ANTARES

ANTARES (Astronomy with a Neutrino Telescope and Abyssal environmental RESearch) [65] is situated at a depth of 2500 m in the Mediterranean Sea, just off the coast of France. The detector consists of an array of 900 photomultiplier tubes (PMTs) on 12 vertical strings, spread over an area of about 0.1 km^2 and with an active height of about 350 m. ANTARES is also now considering the possibility of acoustic detection of neutrinos [66]. The optical detector was completed on May 30^{th} 2008.

NEMO

The NEMO array (NEutrino Mediterranean Observatory) [67] is situated 50 km off Capo Passero, Sicily. The optical array will consist of 4096 PMTs. The site is at an

average depth 3500 m and will consist of 54 500 m high strings spaced at 200 m. The NEMO collaboration claim better sensitivity than ICECUBE to point sources. NEMO is also considering the deployment of acoustic modules on its array. At the time of writing, the NEMO collaboration had successfully completed phase 1, involving the deployment and successful readout of 1 string of optical detectors.

Lake Baikal

The Lake Baikal experiment [68] is situated 1 km under the water of Lake Baikal in Siberia. It has 192 optical modules on 8 strings. It is the oldest experiment in this field, and began in the late 1970's. Its current configuration has been running since 1998, and is currently upgrading to incorporate new strings to increase its sensitivity.

3.3 Air Shower Detector Experiments

Air shower detectors measure high energy cosmic rays incident on the atmosphere using two different methods. The first method is to detect the Cerenkov radiation of the muons from extended air showers as they pass through detectors situated on the Earth's surface. The second method is to detect the fluorescence light from nitrogen molecules excited by the high energy cosmic ray air shower itself.

PIERRE-AUGER Observatory - Cosmic Rays

The AUGER [55] experiment is designed to measure the higher end of the cosmic ray spectrum, $E > 10^{18}$ eV. The observatory covers an area of 3000 km^2 and contains 1600 Cerenkov detectors and 24 fluorescence detectors. AUGER started taking data in 2001, and has been taking data continuously since then. The experiment uses two types of detectors, ground based Cerenkov detectors and air fluorescence light detectors.

Auger has detected 27 UHE cosmic ray events with an energy $\geq 6 \times 10^{19}$ eV in seven years worth of data, and has linked these to nearby AGN [69]. These events can be seen in figure 3.3, which shows the high energy cosmic ray events superimposed on a map of the known AGN.

The AUGER experiment has also been able to confirm the GZK suppression of UHE cosmic rays [50], as shown in figure 3.4. The figure shows the fractional differences

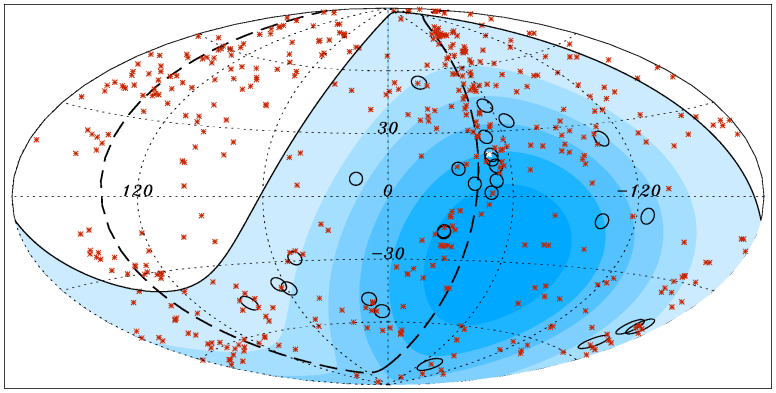

Figure 3.3: *The high energy cosmic ray events (black circles) superimposed on a map of the known AGN (red crosses). The solid black line represents the field of view of the observatory, with the coloured bands showing the relative exposure times. Taken from [69]*

between the Auger data compared to a spectrum with an index of 2.69 (the shape of the spectrum is discussed in section 2.5). It can be seen that at $1 \times 10^{19.4}$ eV there begins a suppression of the high energy cosmic ray flux. This is consistent with the GZK calculation for the suppression of UHE cosmic rays (section 2.5).

PIERRE-AUGER Observatory - Neutrinos

The PIERRE-AUGER observatory is also able to distinguish showers originating from high energy neutrinos. This enables the collaboration to place a limit on the flux of these neutrinos. This limit is competitive with optical, radio, and acoustic techniques, and is shown in figure 2.4.

Neutrino showers can be distinguished in two ways. The first method is to look for late showers - showers originating close to the ground detectors. This is achieved by looking at the EM component of the shower at the ground. Cosmic ray showers happen high in the atmosphere, whereas neutrinos are able to penetrate the atmosphere and interact near the detectors. Because cosmic ray showers happen high in the atmosphere, the EM component of the shower is highly suppressed at ground level due to the attenuation in the atmosphere.

The second method is to look for Earth skimming τ neutrinos. These neutrinos can interact in the nearby mountains producing a τ lepton which in turn decays via a charged current interaction from which the shower can be detected. This shower has

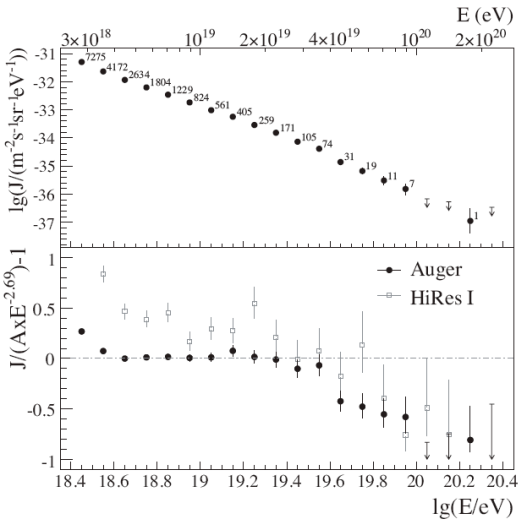

Figure 3.4: *The suppression of UHE cosmic rays, consistent with the GZK mechanism. The upper panel shows the differential flux J as a function of energy, and the lower panel shows the fractional differences between AUGER and HiRes I data compared with a spectrum with an index of 2.69. Taken from [50].*

unique characteristics and can easily be distinguished from other showers. This is the method used to produce the limit shown in figure 2.4.

3.4 Radio Cerenkov Detector Experiments

When a neutrino interacts with matter, an electromagnetic or hadronic shower results. As the shower develops there becomes an excess negative charge. This is predominantly due to Compton scattering and annihilation [70]. This negative charge excess is $\mathcal{O}(20\%)$, and is travelling very close to the speed of light in a vacuum, and in the medium it creates a Cerenkov signal. At wavelengths much longer than the shower size, this radiation is coherent leading to highly polarised Cerenkov radiation being emitted. This was first described by Askaryan in 1962 [71].

The advantage of looking for radio Cerenkov over optical Cerenkov is the attenuation length. In ice this is many km, and in salt it is expected to be $\mathcal{O}$(100 m - 1000 m), although water is opaque to radio waves. This means that the effective volume becomes much greater per detector, and a less dense array of detectors is needed. As for acoustic emission, the radiation is coherent meaning the energy of the Cerenkov pulse increases as the square of the shower energy.

RICE

RICE (Radio Ice Cerenkov Experiment) [72] used the AMANDA strings to attach radio dipole antennas. It consists of an 18 channel array of radio receivers distributed about a cube of length 200 m, at a depth between 100 - 300 m.

RICE was operational for 5 years and collected 1.5 years of useful data. The final set of data includes 1×10^6 events, from which 43 remain after analysis cuts. These 43 were examined by hand, and were all discarded due to defects. Using these data RICE have placed a rather stringent upper limit on the UHE neutrino flux. This is shown in figure 2.4.

ANITA

ANITA (the Antarctic Impulsive Transient Antenna) [73] searches for radio emissions from the Antarctic ice using a balloon circumnavigating the ice-sheet at an altitude of 40 km. The first flight with the ANITA prototype, ANITA-lite took place in 2004, achieving an 18.4 day flight [74].

The first flight of the full experiment took place in December 2006, with a flight time of 35 days. The next flight will be in late 2008. The effective area of the telescope is 10^6 km^2. With the data from the ANITA-lite experiment and the 2006 flight, the ANITA collaboration have found no neutrino like signals. For all 3 flights, the ANITA Monte Carlo predicts 0.1 - 1.0 events. Using these data ANITA have managed to place an upper limit on the UHE neutrino flux. This is shown in figure 2.4.

GLUE

GLUE (the Goldstone Lunar Ultra-high energy Experiment) [37] searches for 10 ns microwave pulses appearing from subsurface electromagnetic cascades from the lunar regolith, appearing in coincidence at two large radio telescopes separated by 20 km. The radio antennas are situated at the Goldstone Tracking Facility near Barstow, California. By using the moon to a depth of about 10 m as the target, the effective volume of the detector is 100,000 km^3. The experiment ran for 120 hours, but no neutrino candidate events were found. Using this data GLUE have managed to place an upper limit on the UHE neutrino flux. This is shown in figure 2.4.

F E

F r e (a t O orb t Rec r g f nsi t Ev nts) [5 a a te i t ing i a circu ar o bit an alt ud of 00 k Laun d i 97 it r cor d dio e ssions r g n a the s sur e at e Gre nland c -s et. g e - he t o de m t e c i vo me of he e im nt 1.8×10^6 m^3.

The exp r me t w or gin lly d sig stu he oss ity of us ng ra n ls o e e t u lear e a on . It w a er reali th t t i data oul also be use sear h o UHE n n ev nt D ring the li e i o E 99 9, 4 m l on e nt we e de e w o p i g l of t ut . sing t s ta O av na ed t l ce an u p r li t on he U e tr no flu . Thi is show n re 2 4

3.5 A s i De ect Experi nt

Th h dr ni r e ec r magn c c s ad s n dep s t t a n y, oni t i s me i m (e u e 1 . heat dissipat s sl wly, so he ul e is n e n on of t e e w re the nerg wa p d. This in r d a i-po ar ousti lse it le din o p ss hi i sed n e l in e tio 1 .

UN

T SAUN St d of co ultr -hi e ergy u ete t n) [76] xpe i nt i ial y sev n hydrophone u e r m a 56 avy hydrop o e rray e array is ar an ed n hexag n l n u at epth e we 570 and 160 m th hy o ne sp ced 1.5 m pa t. The pe i nt s sed n the n u f e O ea , a d ep s n s ated ar the s.

A ed ovel e iq e i l bra n the ra ig ed ight ul s e dr p f om sta ar boa an t e n l eas d as th b l mplode unde res r . SA ND w fi st gr p t publ s a i o t e t o flux a us ic e hniq 77] T ir ec n phas of o ation i cu r n y d way, a ng full u o the 5 y op e rr

17 17 17

± 0

> 18

τ

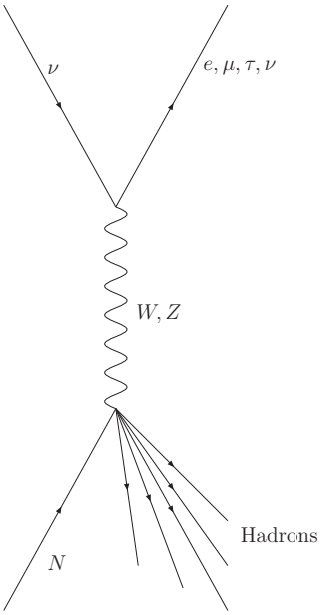

$\times$ 19

θ

$$\frac{d^2E}{drdz} = L(z, E_L) \times R(r, z, E_L)$$

$L(z, E_L)$

$R(r, z, E_L)$ E_L $_{10}(E)$ E

$L(z, E_L)$

$$L(z, E_l) = P_{1L} \quad \frac{z - P_{2L}}{P_{3L} - P_{2L}} \quad \frac{P_{3L} \,!\, P_{2L}}{P_{4L} + P_{5L}\, z + P_{6L}\, z^2} \; exp \quad \frac{P_{3L} - z}{P_{4L} + P_{5L}z + P_{6L}z^2}$$

$$\frac{P_{1L}}{E} = 2.760 \times 10^{-3} - 1.974 \times 10^{-4} E_L + 7.450 \times 10^{-6} E_L^2,$$

$$P_{2L} = -210.9 - 6.968 \times 10^{-3} E_L + 0.11551 E_L^2,$$

$$P_{3L} = -41.50 + 113.9 E_L - 4.103 E_L^2,$$

$$P_{4L} = 8.012 + 11.44 E_L - 0.5434 E_L^2,$$

$$P_{5L} = 0.7999 \times 10^{-5} - 0.004843E_L - 0.0002552E_L^2$$

$$P_{5L} = 4.563 \times 10^{-5} - 3.504 \times 10^{-6}E_L + 1.315 \times 10^{-7}E_L^2.$$

P_{1L} P_{3L} z

P_{2L} P_{4L} P_{5L} P_{6L}

z

$$R(r, z, E_l) = \frac{1}{I} \left(\frac{r}{P_{1R}}\right)^{(P_{2R}-1)} \left(1 + \frac{r}{P_{1R}}\right)^{(P_{2R}-4.5)}$$

$$I = \int_0^\infty \left(\frac{r}{P_{1R}}\right)^{(P_{2R}-1)} \left(1 + \frac{r}{P_{1R}}\right)^{(P_{2R}-4.5)} dr = P_{1R}\frac{\Gamma(4.5 - 2P_{2R})\Gamma(P_{2R})}{\Gamma(4.5 - P_{2R})}$$

Γ P_{nR} n

$$P_{nR} = A + Bz + Cz^2.$$

P_{1R}

$$A = 0.01287E_L^2 - 0.2573E_L + 0.9636,$$

$$B = -0.4697 \times 10^{-4}E_L^2 - 0.0008072E_L + 0.0005404$$

$$C = 0.7344 \times 10^{-7}E_L^2 - 1.375 \times 10^{-6}E_L + 4.488 \times 10^{-6}.$$

P_{2R}

$$A = -0.8905 \times 10^{-3}E_L^2 - 0.007727E_L + 1.969,$$

$$B = 0.1173 \times 10^{-4}E_L^2 - 0.0001782E_L - 5.093 \times 10^{-6}$$

$$C = -0.1058 \times 10^{-7} E_L^2 + 0.1524 \times 10^{-6} E_L - 0.1069 \times 10^{-8}.$$

$$q(\rho, z, t) = \frac{1}{2\pi} f_z(z) g_z(\rho, z) H \quad t - \frac{z}{c_0} \quad ,$$

z ρ z

t f_z g

H

$$f_z(z) = \frac{E}{X_0} b \frac{(bu)^{a-1} exp(-bu)}{\Gamma(a)},\ u = z/X_0,$$

X_0 a b

E

a b

g_z

ρ

$$\frac{g_z(\rho, z)}{g_0} = \begin{cases} x^{n_1} & : \qquad \geq 1 \\ x^{n_2} & : \end{cases}$$

$$g_i = \frac{1}{\rho_i^2} \frac{(2 - n_1)(n_2 - 1)}{n_2 - n_1}$$

$x = \rho_i/\rho$ i z n_1 n_2

$$\begin{aligned} n_1 &= 1.66 \pm 0.02 - (0.29 \pm 0.02)(z/z_{max}) \\ n_2 &= 4.35 \pm 0.05 - (1.10 \pm 0.04)(z/z_{max}) \end{aligned} .$$

z r

E

$$\frac{d^2E}{drdz} = Ek \left(\frac{z}{z_{max}}\right)^t \exp(t - z/\lambda) 2\pi r \Gamma(r),$$

$z_{max} = 0.9X_0 \ln(E/E_c)$ $X_0 = 36.1$ $^{-2}$

E_c z_{max}/λ λ

$\log_{10}(E/10^4$ $)$ $^{-2}$ $^{t-1}$ $\exp(t)\lambda\Gamma(t)$

$$\rho(r) = \frac{1}{r_M^2} a^{s-2} (1+a)^{s-4.5} \frac{\Gamma(4.5-s)}{2\pi\Gamma(s)\Gamma(4.5-2s)},$$

$a = r/r_M$ $r_M = 9.04$ $^{-2}$ s

$$P(t) = \frac{E_0 \beta \varepsilon}{4\pi C_p r} \frac{d}{dt}(\delta(r/c - t))dV,$$

$P(t)$ β $\times$ $^{-4}$ $^{-1}$

C_p $^{-1}$ $^{-1}$

E_0 ε

c $^{-1}$

t r

-2

$$\frac{\beta c^2}{C_p}.$$

β Cp

$\tilde{a}(i\omega)$

$$\tilde{a}(i\omega) = \frac{\omega^2}{\omega_0 c_s} + \left(\frac{1}{r_1}\right)\frac{i\omega}{\omega_1 + i\omega} + \left(\frac{1}{r_2}\right)\frac{i\omega}{\omega_2 + i\omega},$$

$$\omega = 2\pi f \qquad \omega_0 = 0.79 \times 10^{12} \qquad c_s = 1500 \quad ^{-1}$$

$$f_1 = 91.2 \qquad f_2 = 1.31 \qquad r_1 = 157.8 \qquad r_2 = 45.6$$

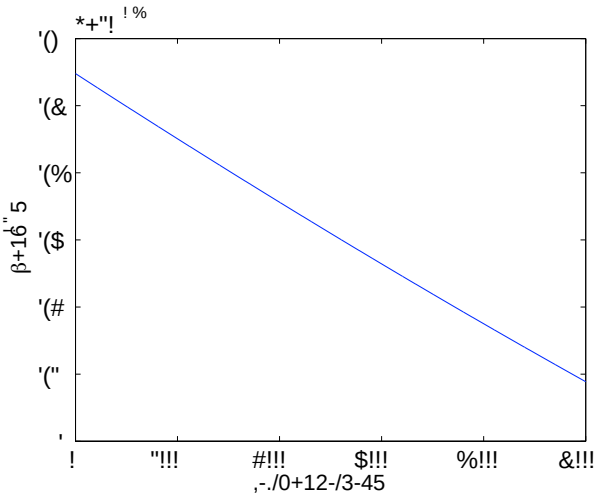

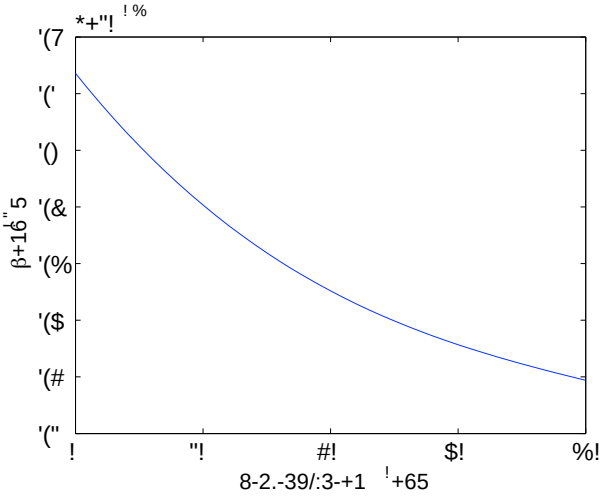

C

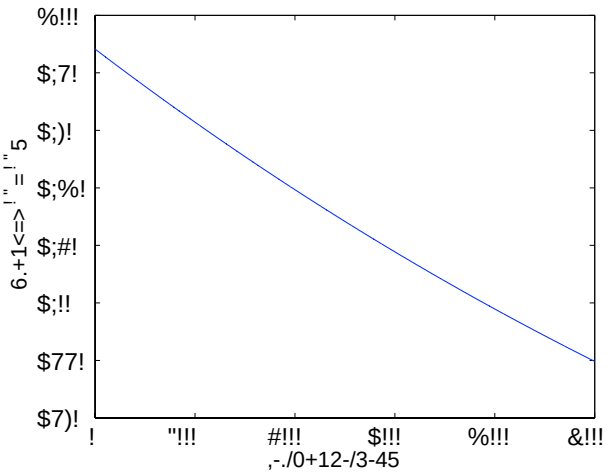

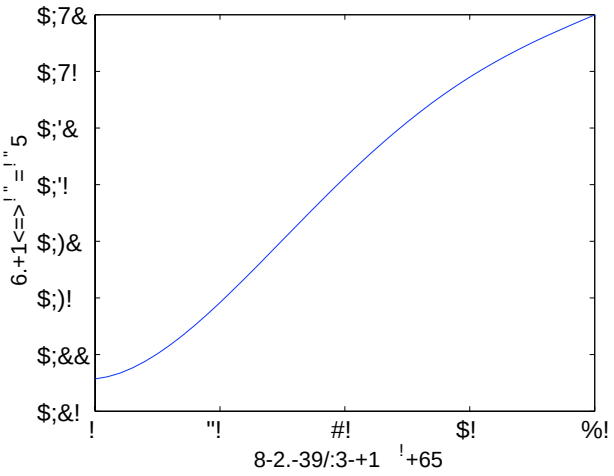

C

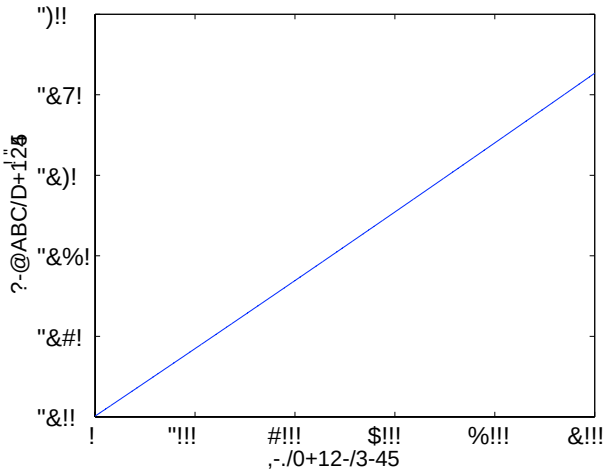

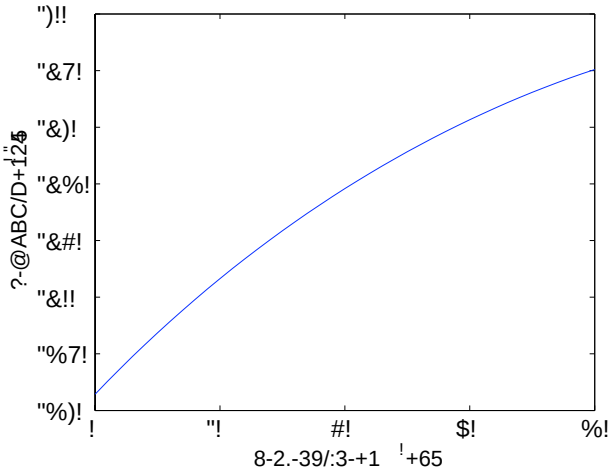

C

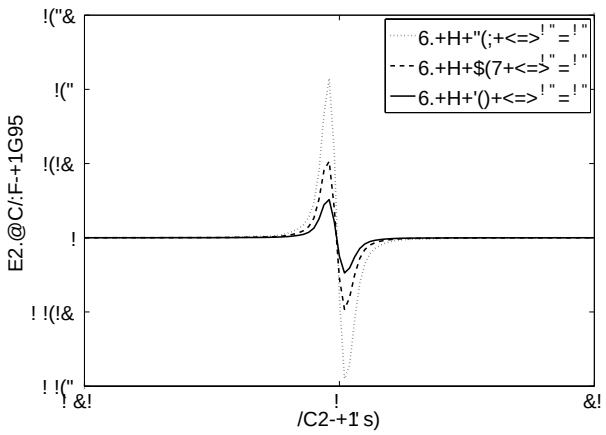

β Cp

β Cp

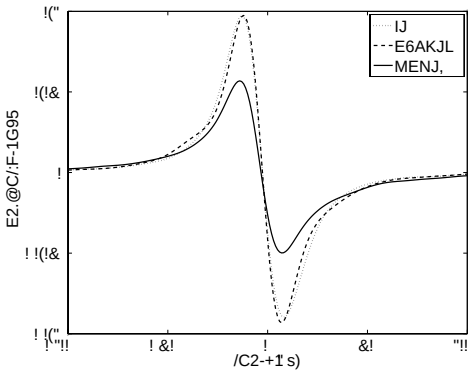

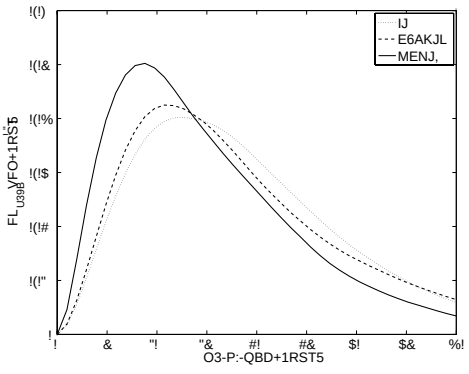

$$10^{20}$$

$$E_{frac}$$

$$= \frac{|P_{max}| - |P_{min}|}{|P_{max}| + |P_{min}|}.$$

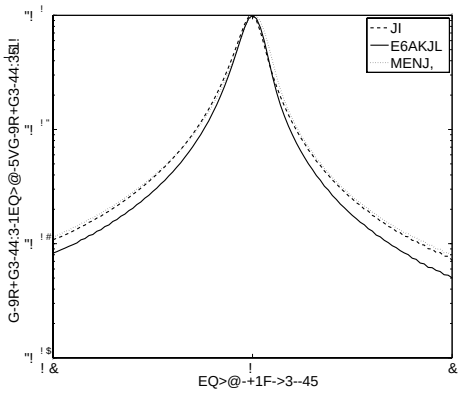
JI
E6AKJL
MENJ,
EQ>@-+1F->3--45

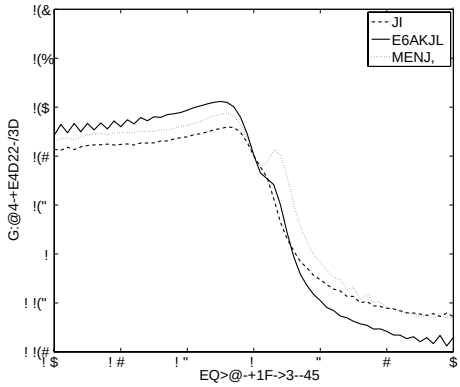
JI
E6AKJL
MENJ,
G:@4-+E4D22-/3D
EQ>@-+1F->3--45

10^{20}

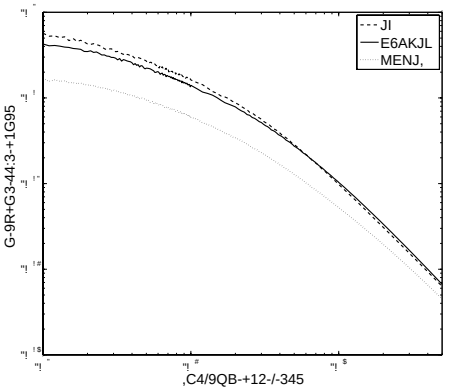
JI
E6AKJL
MENJ,
G-9R+G3-44:3-+1G95
,C4/9QB-+12-/-345

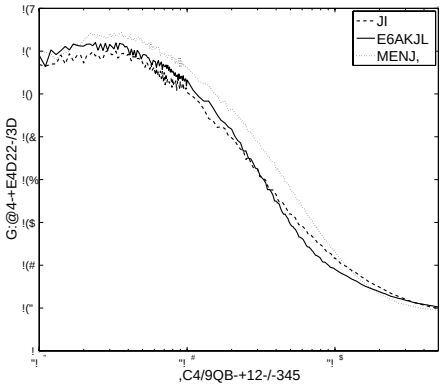
JI
E6AKJL
MENJ,
G:@4-+E4D22-/3D
,C4/9QB-+12-/-345

10^{20}

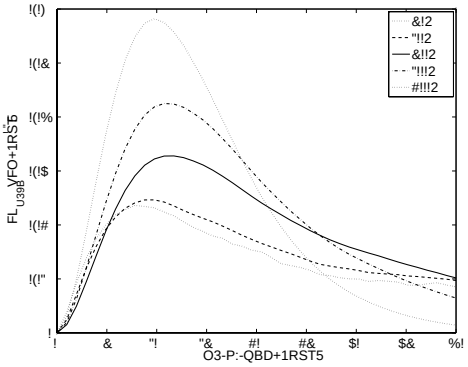
!(!)
!(!&
!(!%
!(!$
!(!#
!(!"
!
&!2
"!!2
&!!2
"!!!2
#!!!2
!
&
"!
"&
#!
#&
$!
$&
%!
O3-P:-QBD+1RST5

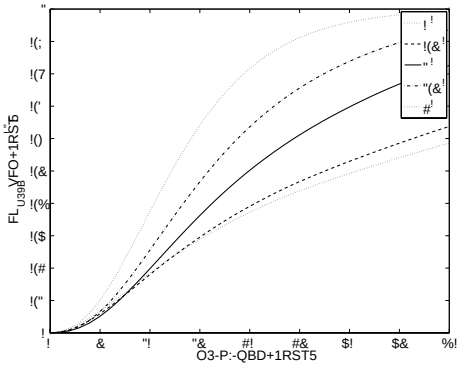
!(;
!(7
!(
!0
!(&
!(%
!($
!(#
!("
!
!
&
"!
"&
#!
#&
$!
$&
%!
O3-P:-QBD+1RST5

10^{20}

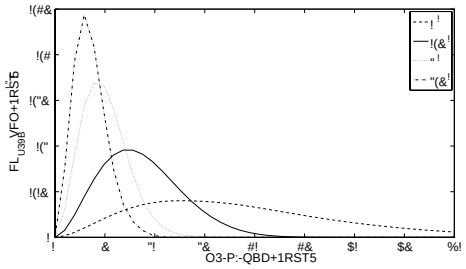
!(#&
!(#
!("&
!("
!(!&
!
!
&
"!
"&
#!
#&
$!
$&
%!
O3-P:-QBD+1RST5

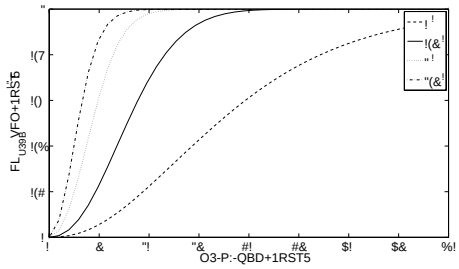
"
!(7
!0
!(%
!(#
!
!
&
"!
"&
#!
#&
$!
$&
%!
O3-P:-QBD+1RST5

10^{20}

- 10^{19} 10^{21}

  μ

- 10^{15}

  μ

- 10^{19}

  μ

  μ

  10^{19}

$$P_{max} = \frac{\beta}{4\pi C_p} \frac{E}{R},$$

β $_p$ E

R

$\pm$

θ

x, y

z

	x	y	z			

(x, y, z) z

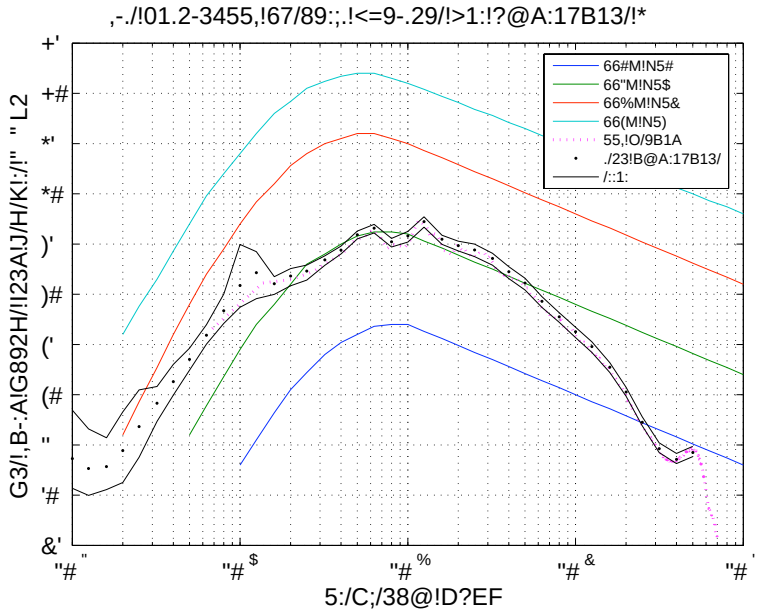
,-./!01.2-3455,!67/89:;.!<=9-.29/!>1:!?@A:17B13/!*
66#M!N5#
66"M!N5$
66%M!N5&
66(M!N5)
55,!O/9B1A
./23!B@A:17B13/
/::1:
G3/!,B-:AIG892H/!I23AIJ/H/KI:/!" " L2
5:/C;/38@!D?EF

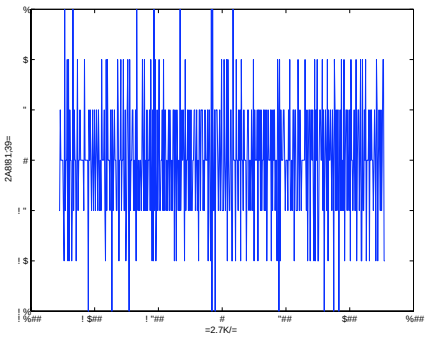
2A881;39=
=2.7K/=

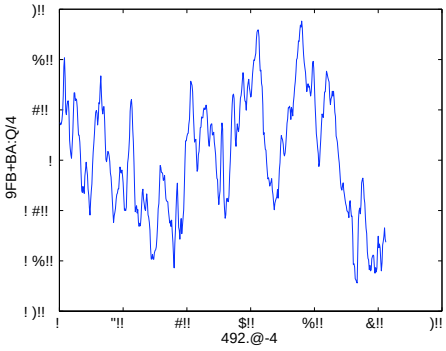
9FB+BA:Q/4
492.@-4

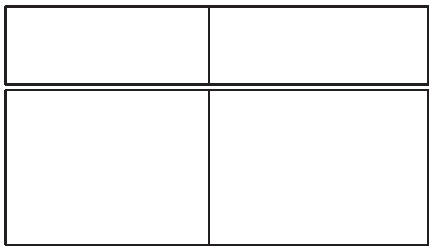

- $\times$ 6

  rd

-

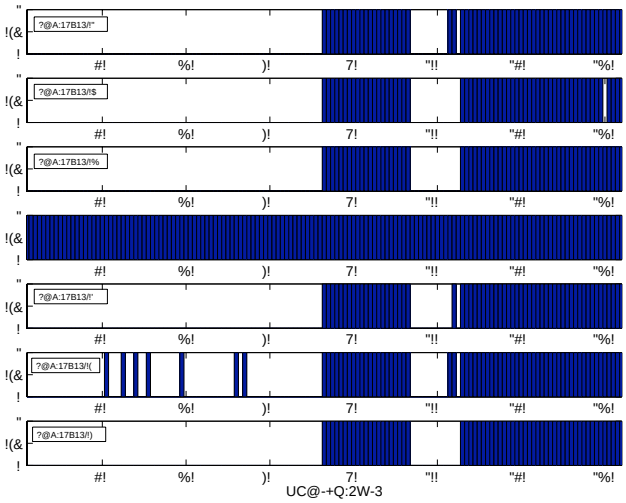

$\times$ 6

$\times$ 6

-

-

- $\sim \quad f$
-
-
-
-
-
- st

$x(t) \qquad y(t)$

$$C_{xy}(\tau) = \int_{-\infty}^{\infty} x(t)\, y(t-\tau)\, dt,$$

τ

1×10^{11}

rd

—

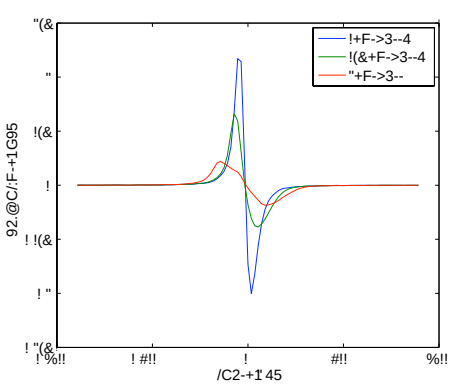
!+F->3--4
!(&+F->3--4
"+F->3--
"(&
"
!(&
!
! !(&
! "
! "(&
! %!!
! #!!
!
#!!
%!!
92.@C/.F-+1G95
/C2-+1'45

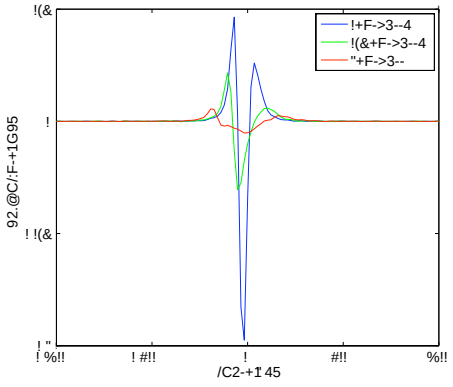
!+F->3--4
!(&+F->3--4
"+F->3--
!(&
!
! !(&
! "
! %!!
! #!!
!
#!!
%!!
92.@C/.F-+1G95
/C2-+1'45

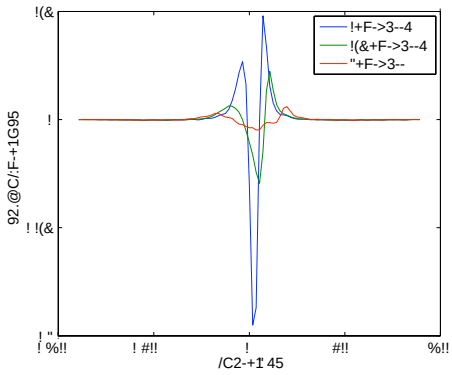
!+F->3--4
!(&+F->3--4
"+F->3--
!(&
!
! !(&
! "
! %!!
! #!!
!
#!!
%!!
92.@C/.F-+1G95
/C2-+1'45

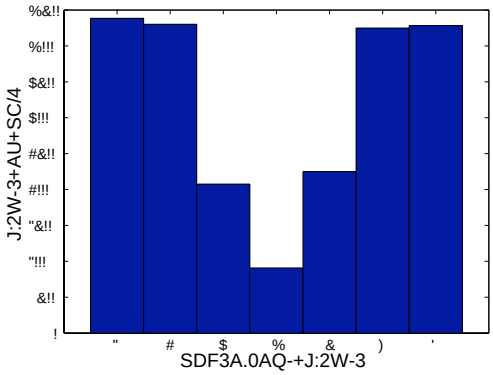
%&!!
%!!!
$&!!
$!!!
#&!!
#!!!
"&!!
"!!!
&!!
!
J:2W-3+AU+SC/4
"
#
$
%
&
)
'
SDF3A.0AQ-+J:2W-3

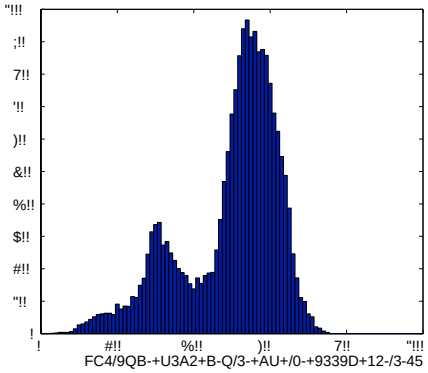
"!!!
:!!
7!!
'!!
)!!
&!!
%!!
$!!
#!!
"!!
!
!
#!!
%!!
)!!
7!!
"!!!
FC4/9QB-+U3A2+B-Q/3-+AU+/0-+9339D+12-/3-45

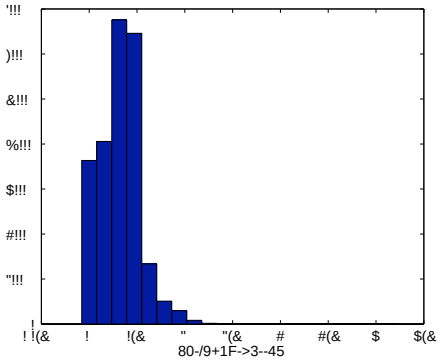
'!!!
)!!!
&!!!
%!!!
$!!!
#!!!
"!!!
!
! !(&
!
!(&
"
"(&
#
#(&
$
$(&
80-/9+1F->3--45

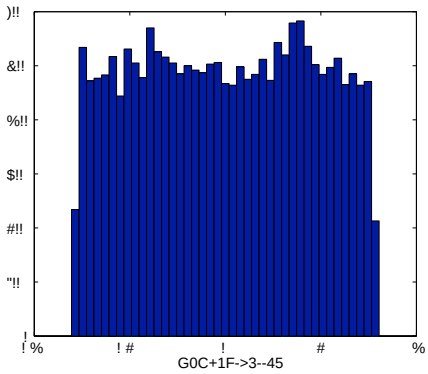
)!!
&!!
%!!
$!!
#!!
"!!
!
! %
! #
!
#
%
G0C+1F->3--45

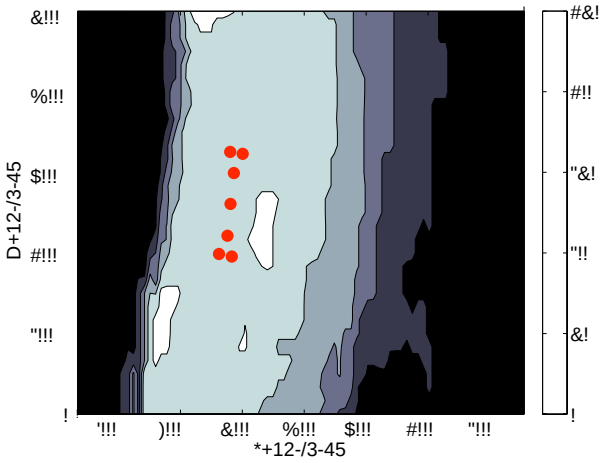

± 1

$\pm$

-
-
-
-
-
-
-
-

•

× 21

21

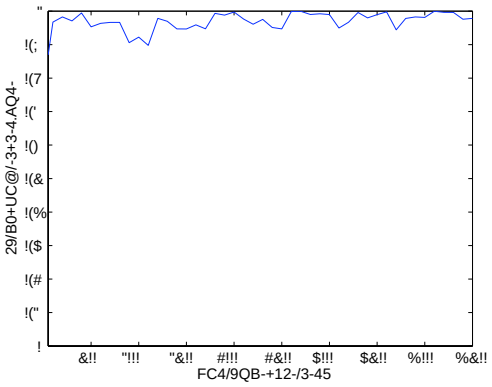
"
!(;
!(7
!('
!()
!(&
!(%
!($
!(#
!("
!
29/B0+UC@/-3+3-4.AQ4-
&!!
"!!!
"&!!
#!!!
#&!!
$!!!
$&!!
%!!!
%&!!
FC4/9QB-+12-/3-45

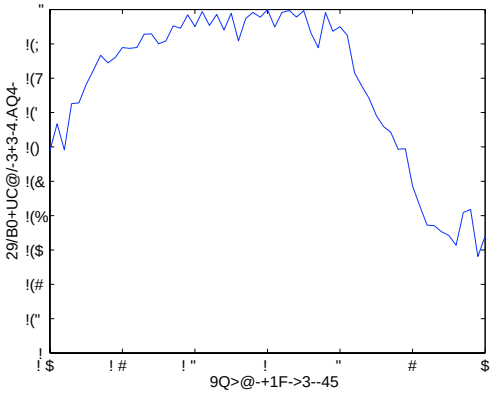
"
!(;
!(7
!('
!()
!(&
!(%
!($
!(#
!("
!
29/B0+UC@/-3+3-4.AQ4-
! $
! #
! "
!
"
#
$
9Q>@-+1F->3--45

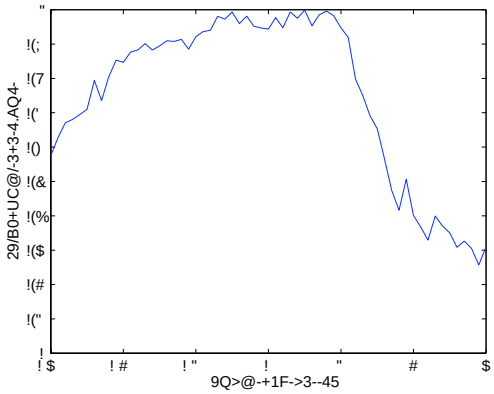
"
!(;
!(7
!('
!()
!(&
!(%
!($
!(#
!("
!
29/B0+UC@/-3+3-4.AQ4-
! $
! #
! "
!
"
#
$
9Q>@-+1F->3--45

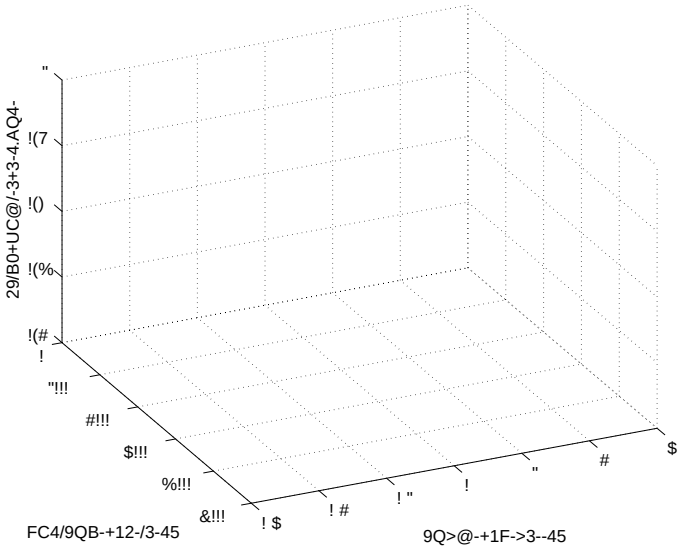
29/B0+UC@/-3+3-4.AQ4-
"
!(7
!()
!(%
!(#
!
"!!!
#!!!
$!!!
%!!!
&!!!
! $
! #
! "
!
"
#
$
FC4/9QB-+12-/3-45
9Q>@-+1F->3--45

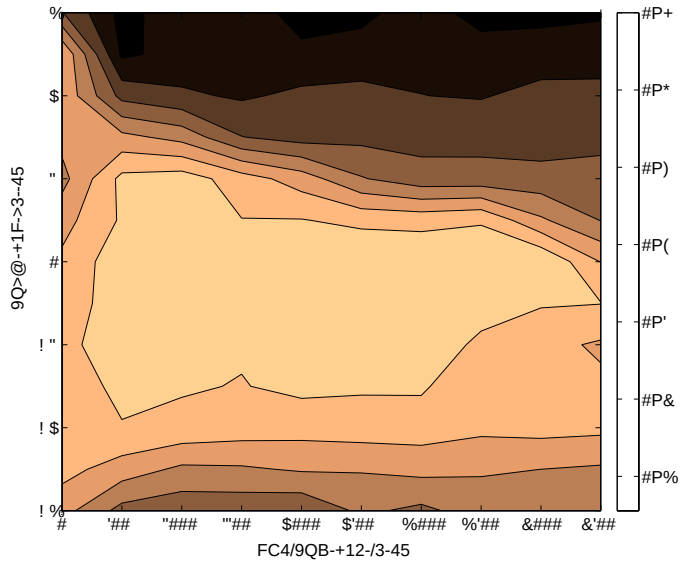
9Q>@-+1F->3--45
%
$
"
#
! "
! $
! %
#P+
#P*
#P)
#P(
#P'
#P&
#P%
#
'##
"###
'"##
$###
$'##
%###
%'##
&###
&'##
FC4/9QB-+12-/3-45

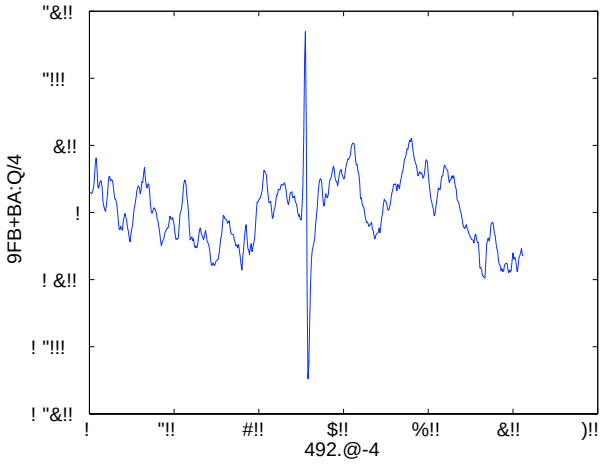
"&!!
"!!!
&!!
!
! &!!
! "!!!
! "&!!
9FB+BA:Q/4
!
"!!
#!!
$!!
%!!
&!!
)!!
492.@-4

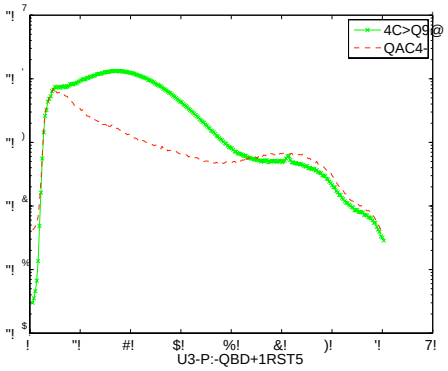

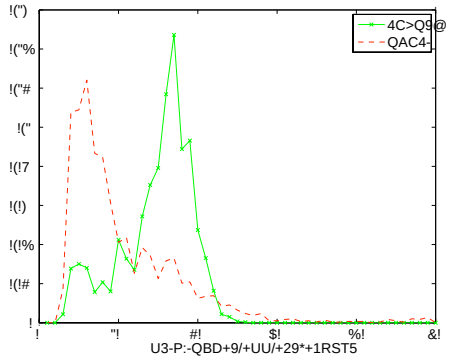

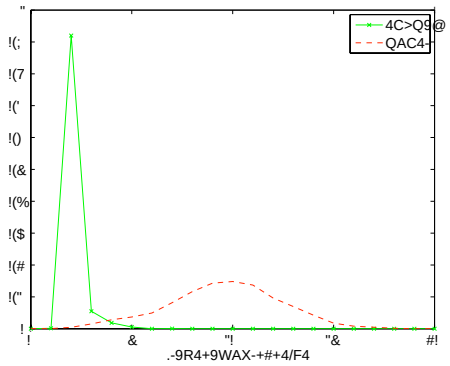

$\times$ 21

rd

$$= \frac{E \ (x-\mu)^3}{\sigma^3}$$

μ x σ x $E(t)$

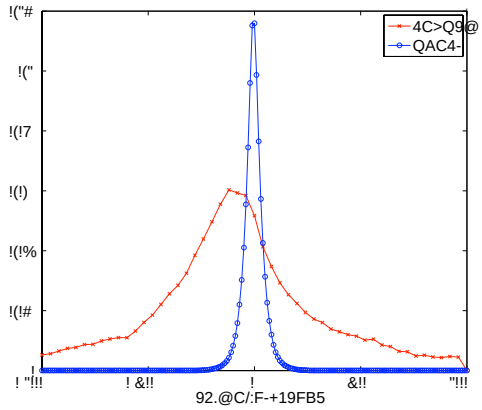

$\times$ 21

t

th

$$= \frac{E\ (x-\mu)^4}{\sigma^4}$$

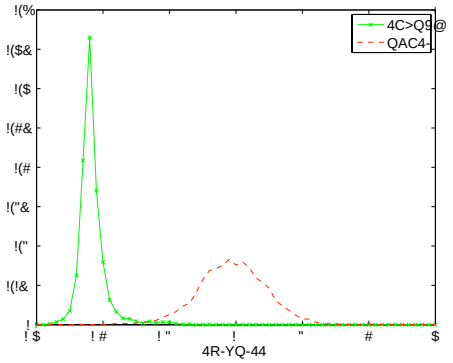

$\times$ 21

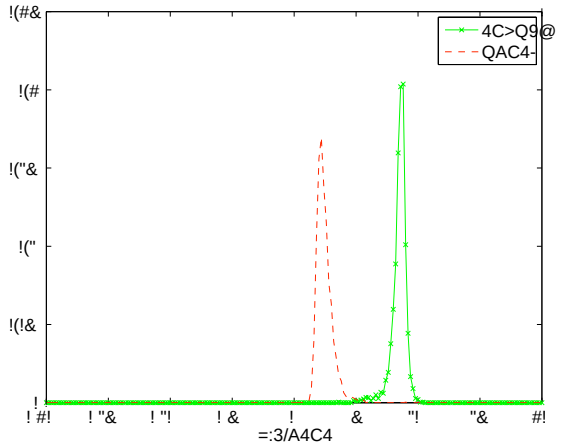

$\times$ 21

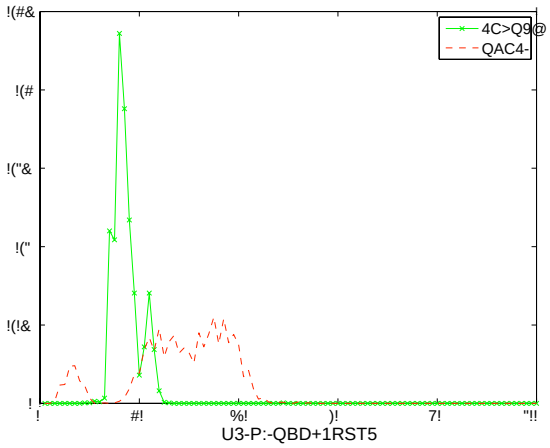

× 21

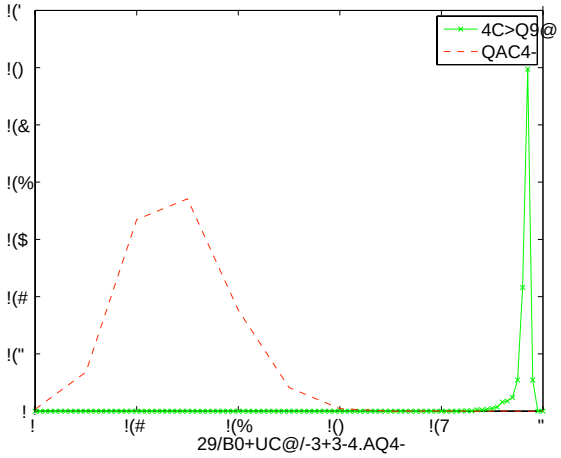

× 21

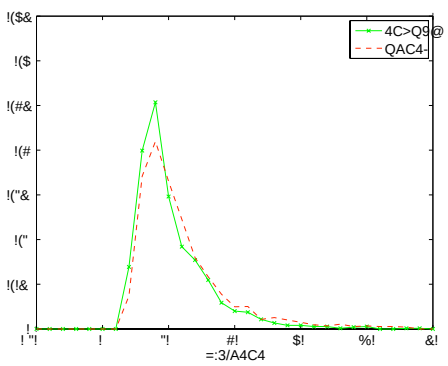

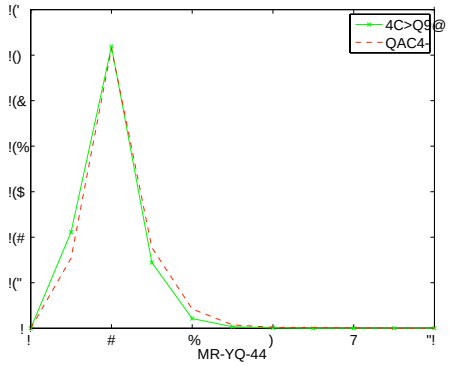

× 21

21

20

× 21

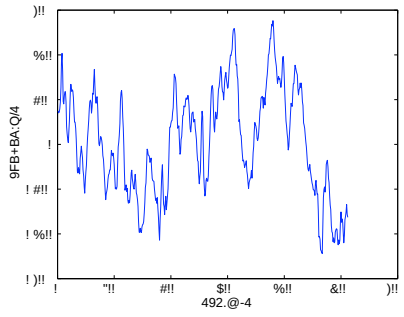

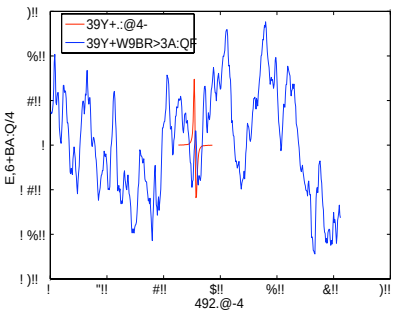

20

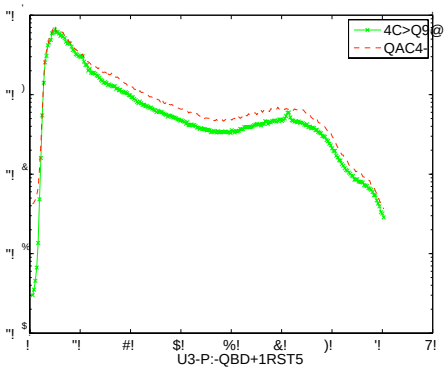

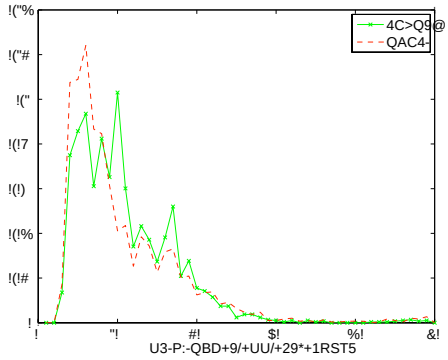

$\times$ 20

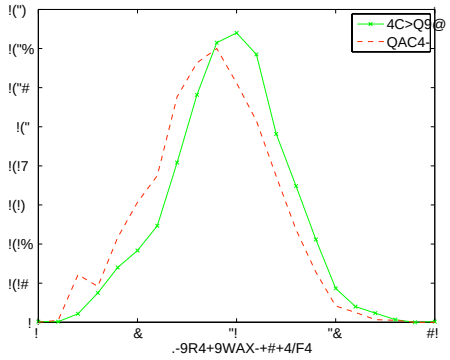

$\times$ 20

20

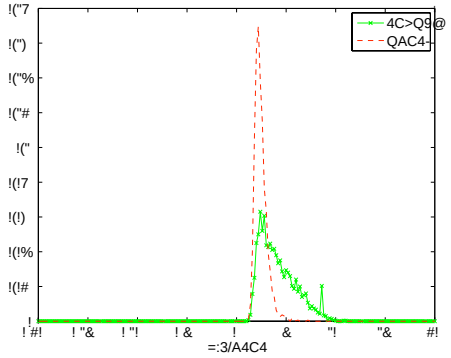

$\times$ 20

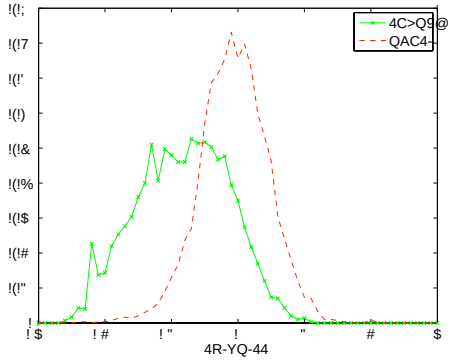

$\times$ 20

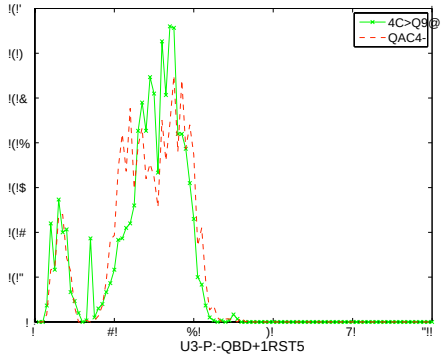

$\times$ 20

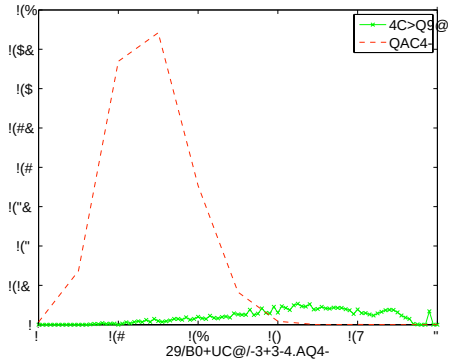

$\times$ 20

$$= \frac{\qquad\qquad}{+}$$

$$= \frac{\qquad\qquad}{\qquad\qquad}.$$

20 21

20

20 21 21

21

20

20 21 20

$\times$ 20

$\pm$

$\pm$

$-$ $-$

20

21

21

20

20

21

20

20

21

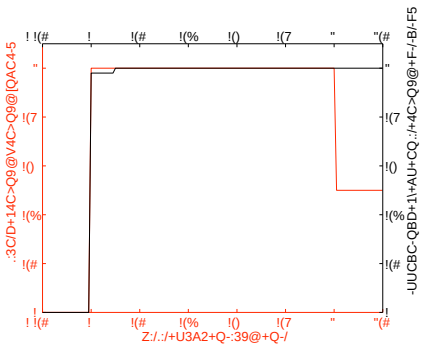

21

21

20

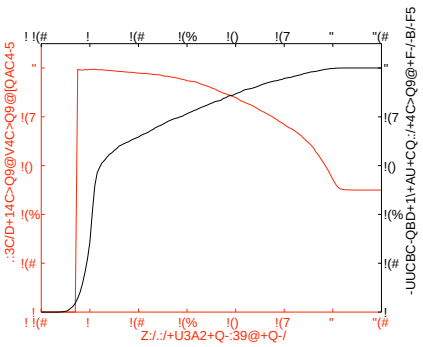

21

20

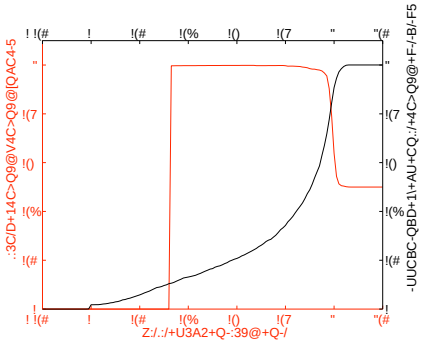

21

21

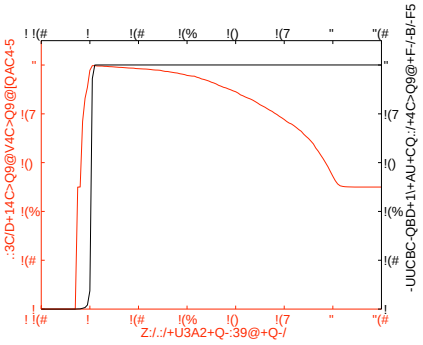

20

20

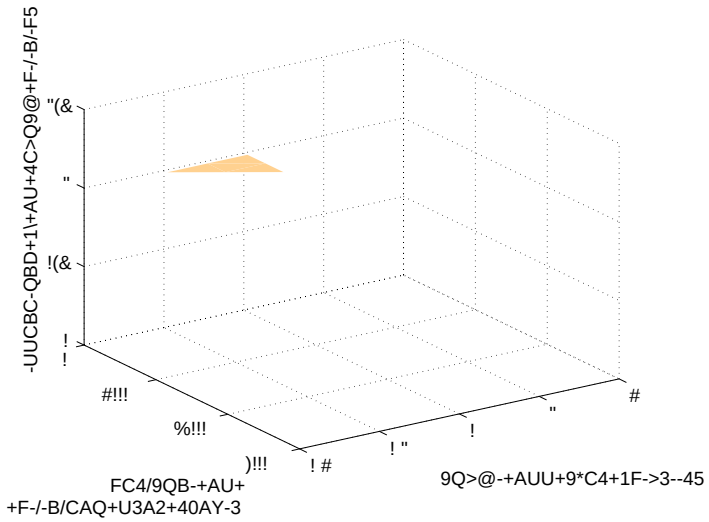
-UUCBC-QBD+1\+AU+4C>Q9@+F-/-B/-F5
"(&
"
!(&
!
!
#!!!
%!!!
)!!!
! #
! "
!
"
#
FC4/9QB-+AU+
+F-/-B/CAQ+U3A2+40AY-3
9Q>@-+AUU+9*C4+1F->3--45

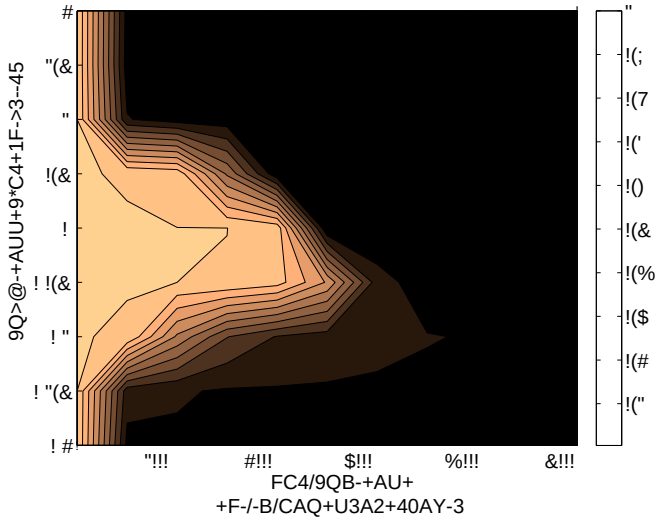
9Q>@-+AUU+9*C4+1F->3--45
#
"(&
"
!(&
!
! !(&
! "
! "(&
! #
"!!!
#!!!
$!!!
%!!!
&!!!
FC4/9QB-+AU+
+F-/-B/CAQ+U3A2+40AY-3
"
!(;
!(7
!('
!()
!(&
!(%
!($
!(#
!("

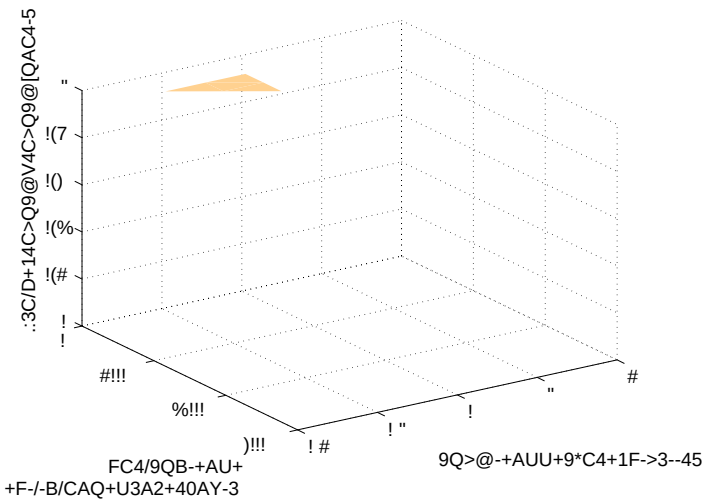
.:3C/D+14C>Q9@V4C>Q9@[QAC4-5
"
!(7
!()
!(%
!(#
!
!
#!!!
%!!!
)!!!
! #
! "
!
"
#
FC4/9QB-+AU+
+F-/-B/CAQ+U3A2+40AY-3
9Q>@-+AUU+9*C4+1F->3--45

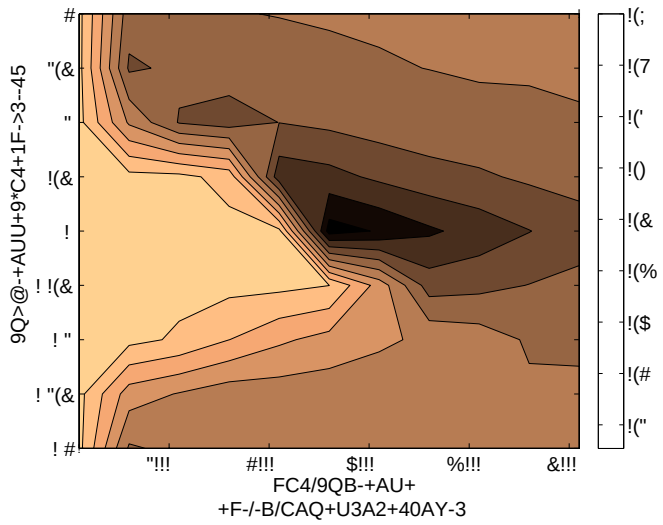
9Q>@-+AUU+9*C4+1F->3--45
#
"(&
"
!(&
!
! !(&
! "
! "(&
! #
"!!!
#!!!
$!!!
%!!!
&!!!
FC4/9QB-+AU+
+F-/-B/CAQ+U3A2+40AY-3
!(;
!(7
!('
!()
!(&
!(%
!($
!(#
!("

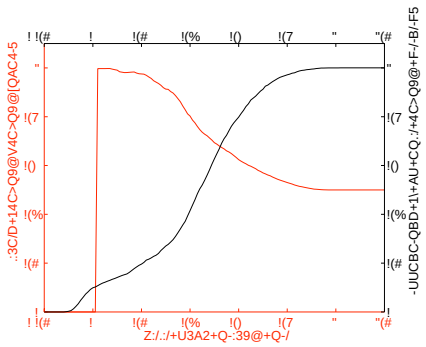

20

—

—

20

—

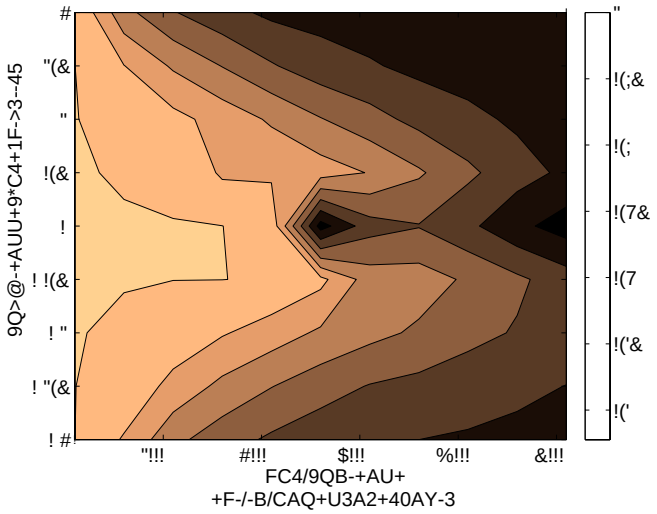
#
"(&
"
!(&
!
! !(&
! "
! "(&
! #
9Q>@-+AUU+9*C4+1F->3--45
"!!!
#!!!
$!!!
%!!!
&!!!
FC4/9QB-+AU+
+F-/-B/CAQ+U3A2+40AY-3
"
!(;&
!(;
!(7&
!(7
!('&
!('

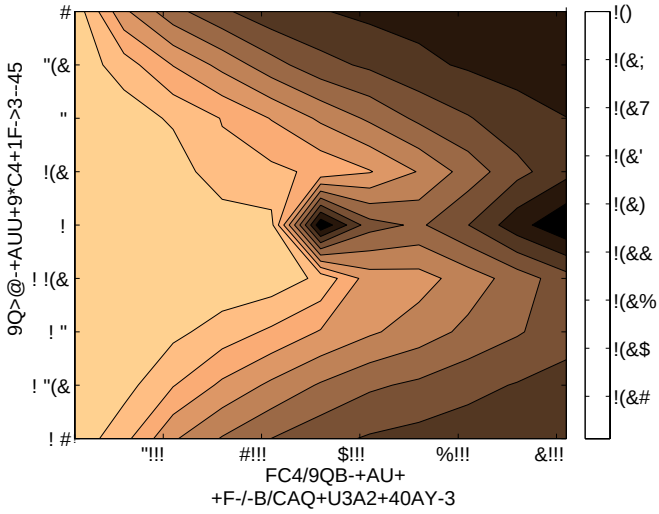
#
"(&
"
!(&
!
! !(&
! "
! "(&
! #
9Q>@-+AUU+9*C4+1F->3--45
"!!!
#!!!
$!!!
%!!!
&!!!
FC4/9QB-+AU+
+F-/-B/CAQ+U3A2+40AY-3
!()
!(&;
!(&7
!(&'
!(&)
!(&&
!(&%
!(&$
!(&#

-
-
-
-
-

χ^2

-

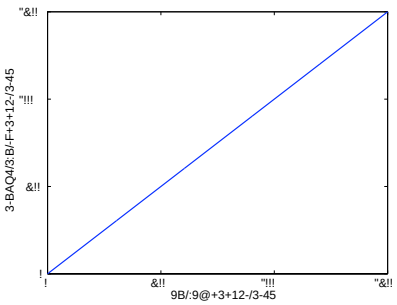

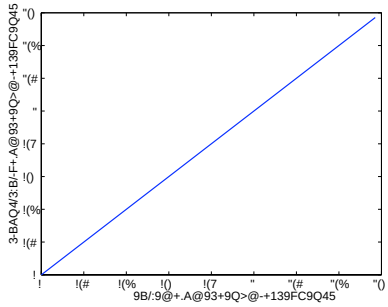

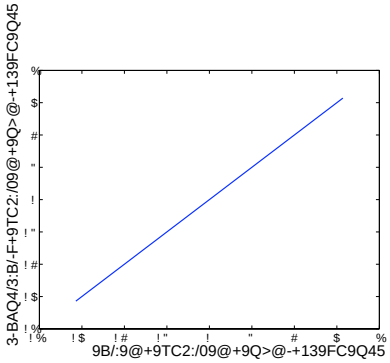

r

r

θ

ϕ

x, y z

χ^2

x, y, z

χ^2

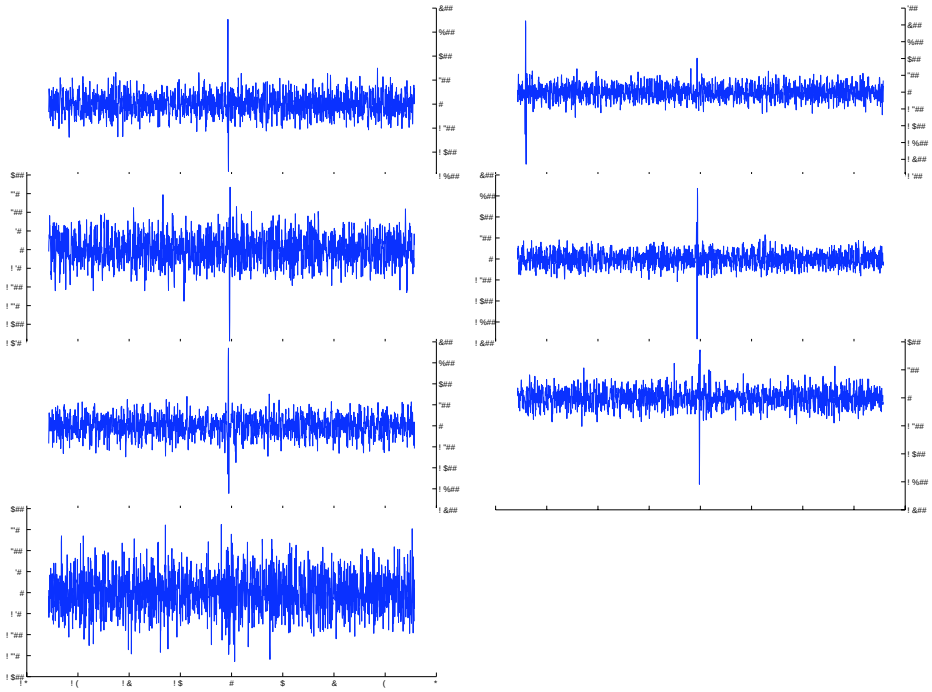

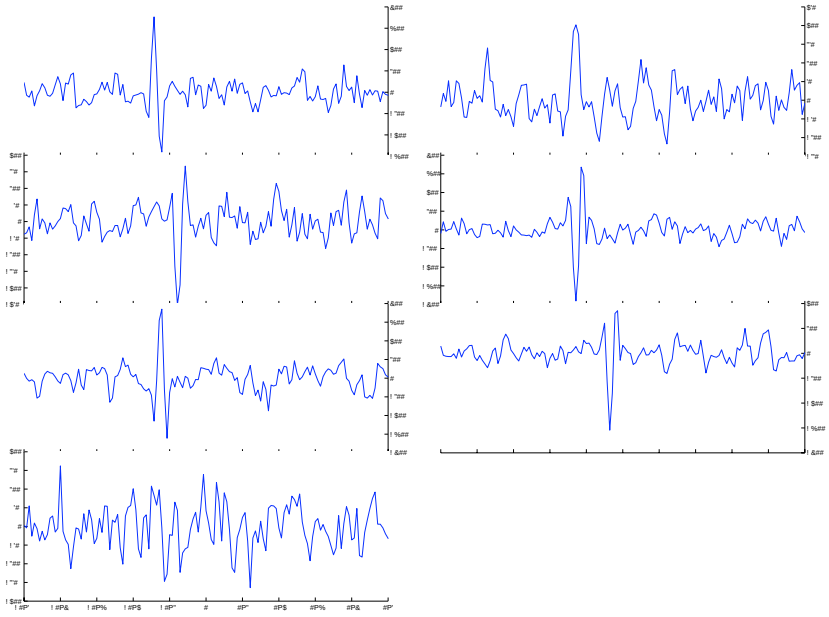

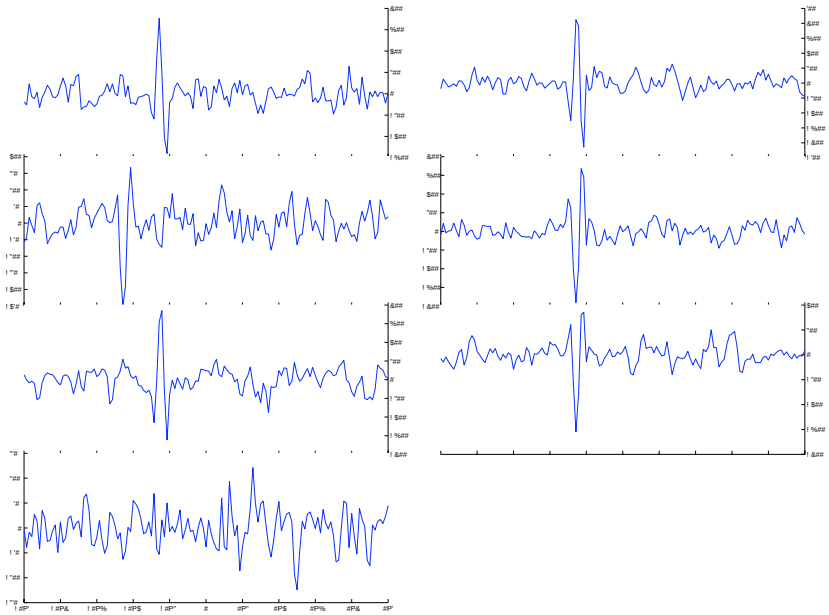

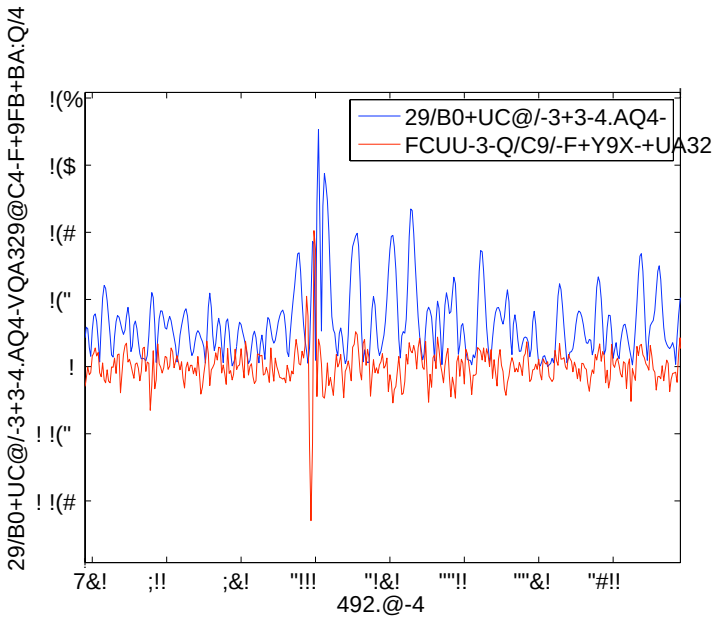
29/B0+UC@/-3+3-4.AQ4-VQA329@C4-F+9FB+BA:Q/4
!(%
!($
!(#
!("
!
! !("
! !(#
29/B0+UC@/-3+3-4.AQ4-
FCUU-3-Q/C9/-F+Y9X-+UA32
7&!
;!!
;&!
"!!!
"!&!
""!!
""&!
"#!!
492.@-4

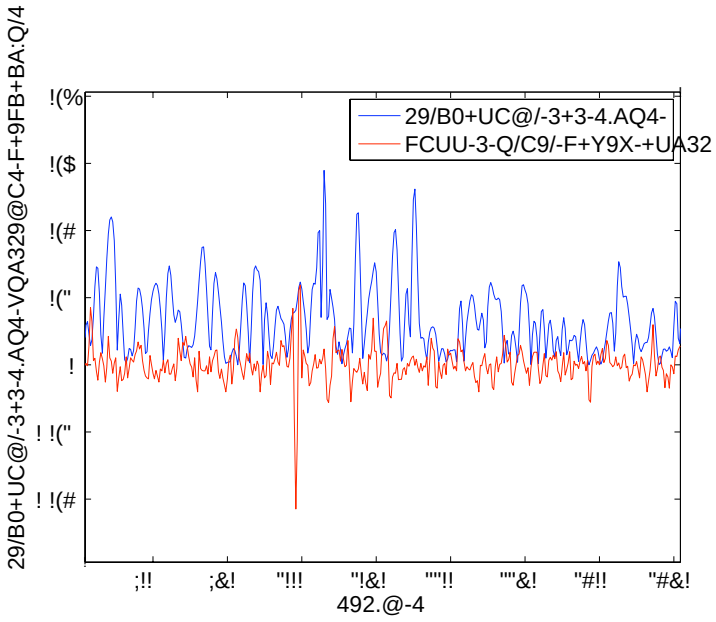
29/B0+UC@/-3+3-4.AQ4-VQA329@C4-F+9FB+BA:Q/4
!(%
!($
!(#
!("
!
! !("
! !(#
29/B0+UC@/-3+3-4.AQ4-
FCUU-3-Q/C9/-F+Y9X-+UA32
;!!
;&!
"!!!
"!&!
""!!
""&!
"#!!
"#&!
492.@-4

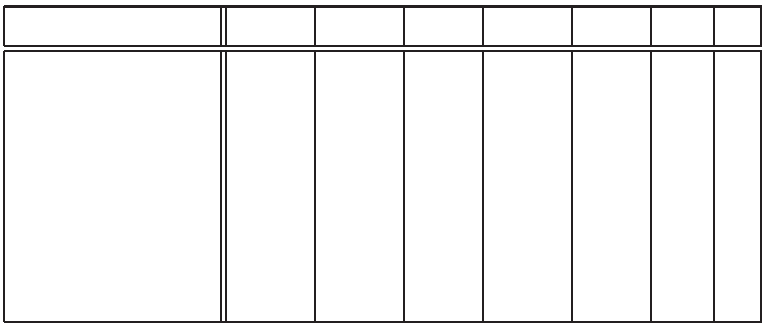

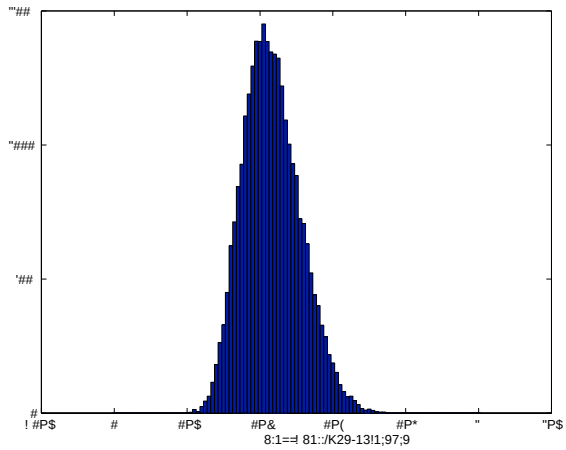
'"##
'"###
'##
#
! #P$
#
#P$
#P&
#P(
#P*
"
"P$
8:1=ꟾ 81::/K29-13!1;97;9

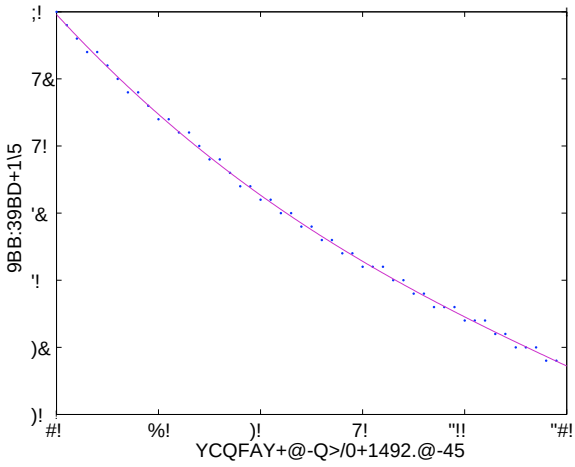
;!
7&
7!
'&
'!
)&
)!
9BB:39BD+1\5
#!
%!
)!
7!
"!!
"#!
YCQFAY+@-Q>/0+1492.@-45

$$= \quad -0.0036 \times \qquad ^2 - 0.62 \times \qquad + 96 \quad .$$

-
-
-
-

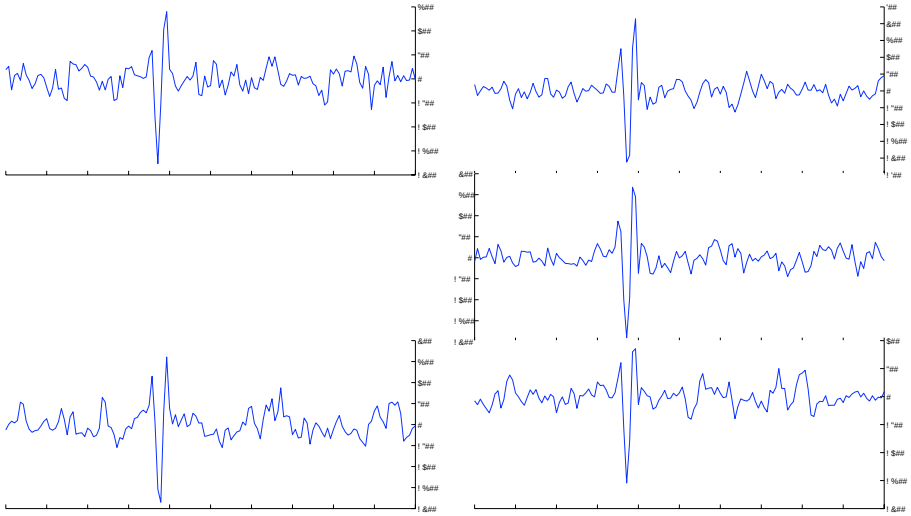

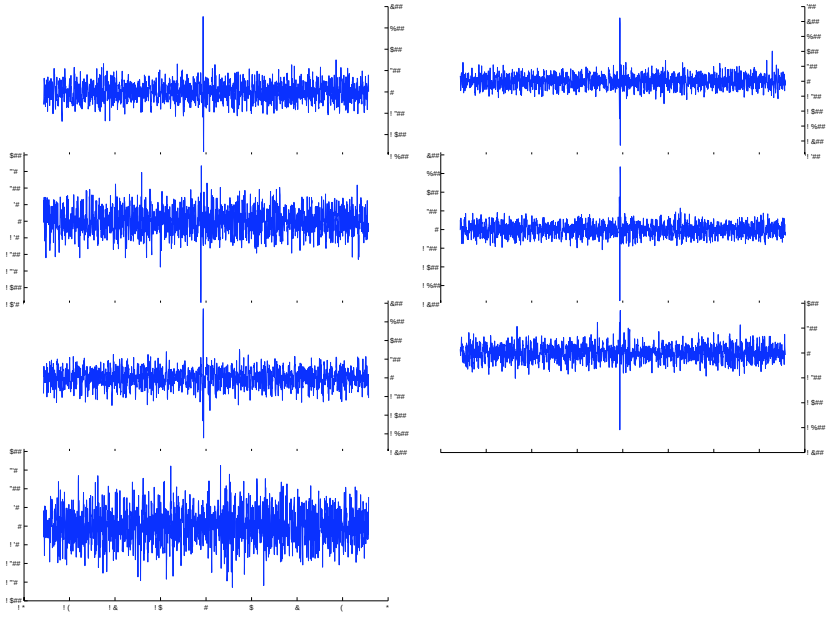

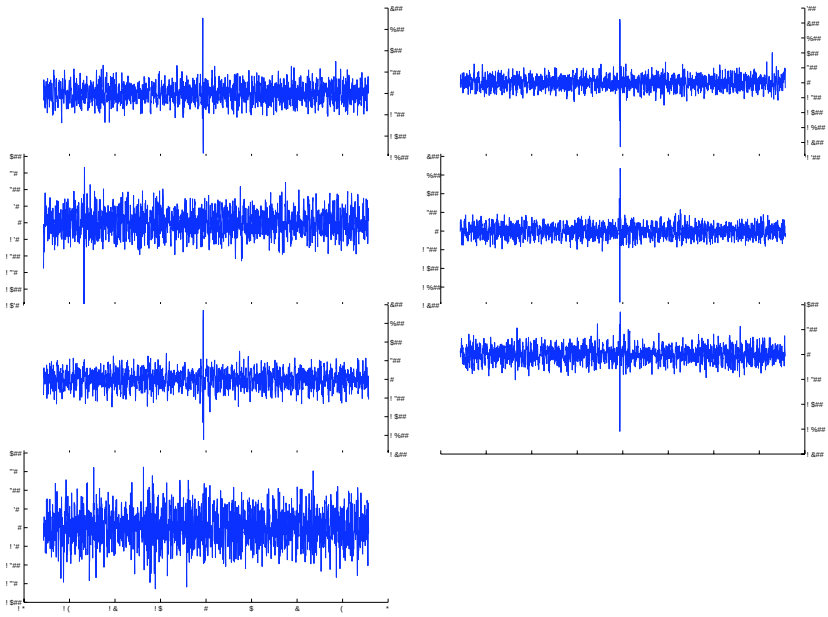

20	
20.5	
21	
21.5	
22	
22.5	
23	

—

—

21.5 21 20

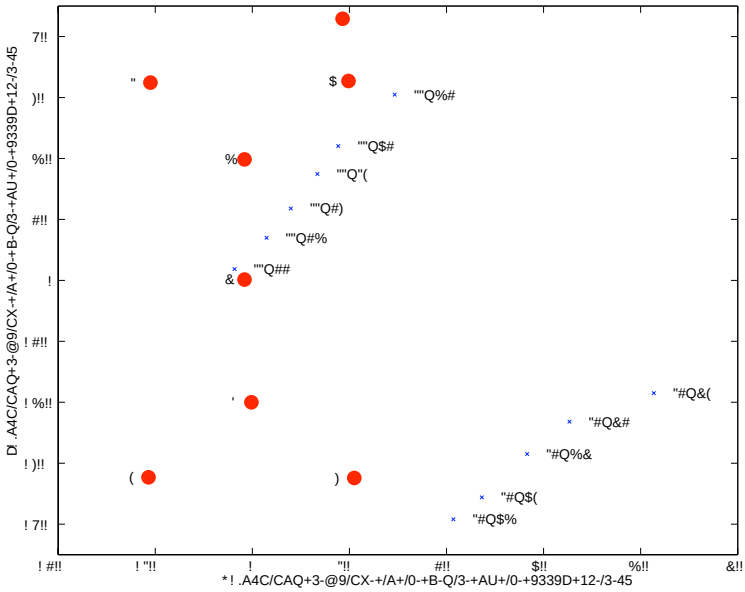
7!!
)!!
%!!
#!!
!
! #!!
! %!!
!)!!
! 7!!
D! .A4C/CAQ+3-@9/CX-+/A+/0-+B-Q/3-+AU+/0-+9339D+12-/3-45
! #!!
! "!!
!
"!!
#!!
$!!
%!!
&!!
*! .A4C/CAQ+3-@9/CX-+/A+/0-+B-Q/3-+AU+/0-+9339D+12-/3-45
"
$
%
&
'
(
)
""Q%#
""Q$#
""Q"(
""Q#)
""Q#%
""Q##
"#Q&(
"#Q&#
"#Q%&
"#Q$(
"#Q$%

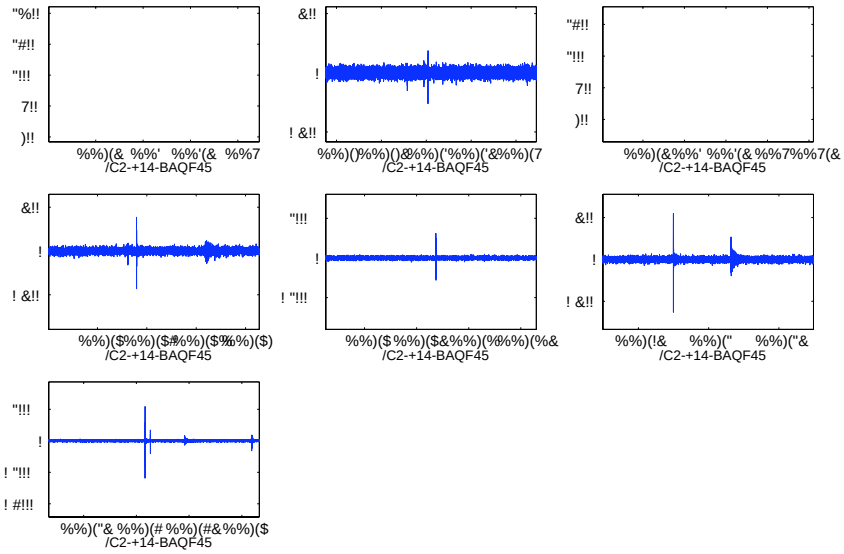
"%!!
"#!!
"!!!
7!!
)!!
%%)(& %%' %%'(& %%7
/C2-+14-BAQF45
&!!
!
! &!!
%%)()%%)(),&%%)('%%)('&%%)(7
/C2-+14-BAQF45
"#!!
"!!!
7!!
)!!
%%)(&%%' %%'(&%%7%%7(&
/C2-+14-BAQF45
&!!
!
! &!!
%%)($%%)($#%%)($%%)($)
/C2-+14-BAQF45
"!!!
!
! "!!!
%%)($%%)($&%%)(%%%)(%&
/C2-+14-BAQF45
&!!
!
! &!!
%%)(!& %%)(" %%)("&
/C2-+14-BAQF45
"!!!
!
! "!!!
! #!!!
%%)("& %%)(# %%)(#&%%)($
/C2-+14-BAQF45

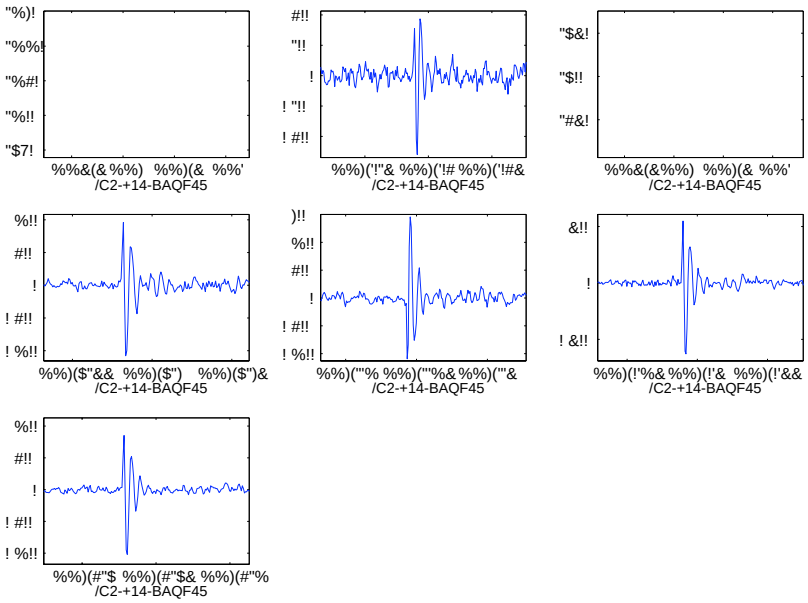
"%)!
"%%!
"%#!
"%!!
"$7!
%%&(&%%) %%)(& %%'
/C2-+14-BAQF45
#!!
"!!
!
! "!!
! #!!
%%)('!"& %%)('!# %%)('!#&
/C2-+14-BAQF45
"$&!
"$!!
"#&!
%%&(&%%) %%)(& %%'
/C2-+14-BAQF45
%!!
#!!
!
! #!!
! %!!
%%)($"&& %%)($") %%)($")&
/C2-+14-BAQF45
)!!
%!!
#!!
!
! #!!
! %!!
%%)('"% %%)('"%& %%)('"&
/C2-+14-BAQF45
&!!
!
! &!!
%%)(!'%& %%)(!'& %%)(!'&&
/C2-+14-BAQF45
%!!
#!!
!
! #!!
! %!!
%%)(#"'$ %%)(#"'$& %%)(#"'%
/C2-+14-BAQF45

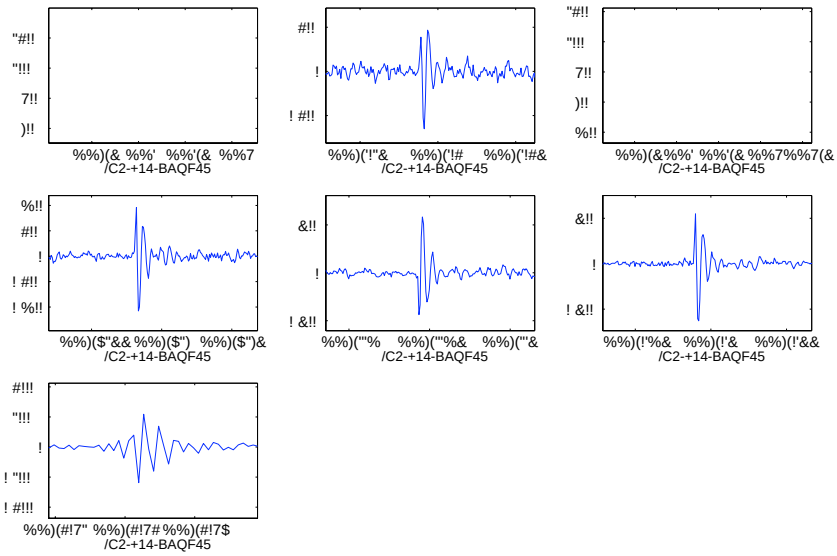
"#!!
"!!!
7!!
)!!
%%)(& %%' %%'(& %%7
/C2-+14-BAQF45
#!!
!
! #!!
%%)('!"& %%)('!# %%)('!#&
/C2-+14-BAQF45
"#!!
"!!!
7!!
)!!
%%)(&%%' %%'(& %%7%%7(&
/C2-+14-BAQF45
%!!
#!!
!
! #!!
! %!!
%%)($"&& %%)($") %%)($")&
/C2-+14-BAQF45
&!!
!
! &!!
%%)('"% %%)('"%& %%)('"&
/C2-+14-BAQF45
&!!
!
! &!!
%%)(!'%& %%)(!'& %%)(!'&&
/C2-+14-BAQF45
#!!!
"!!!
!
! "!!!
! #!!!
%%)(#!7" %%)(#!7# %%)(#!7$
/C2-+14-BAQF45

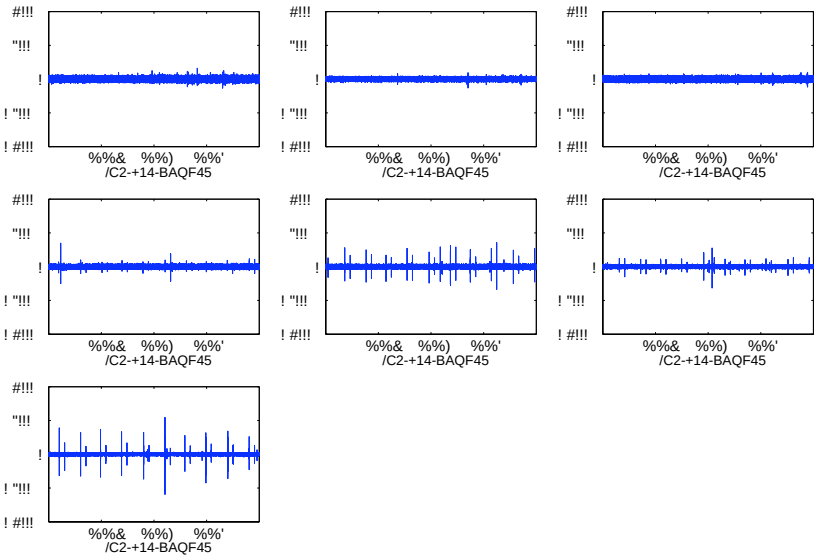
#!!!
"!!!
!
! "!!!
! #!!!
%%& %%) %%'
/C2-+14-BAQF45

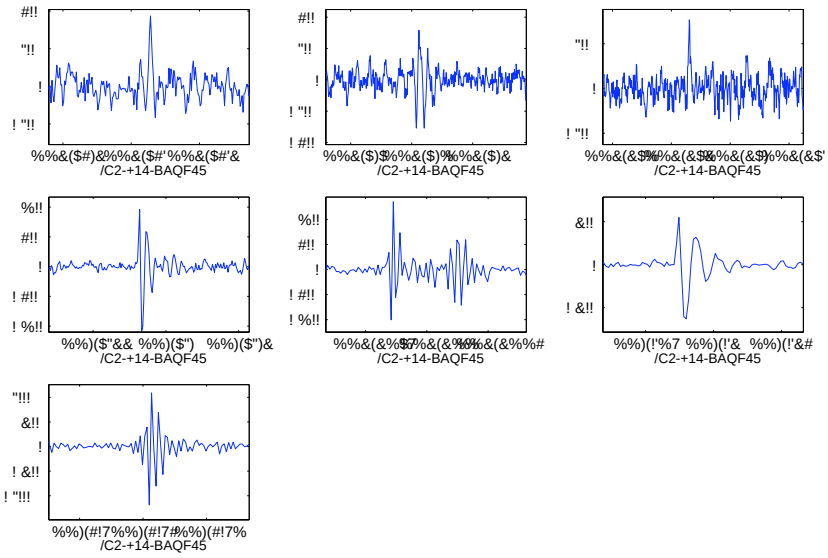
#!!
"!!
!
! "!!
! #!!
%%&($#)&%%&($#'%%&($#'&
/C2-+14-BAQF45

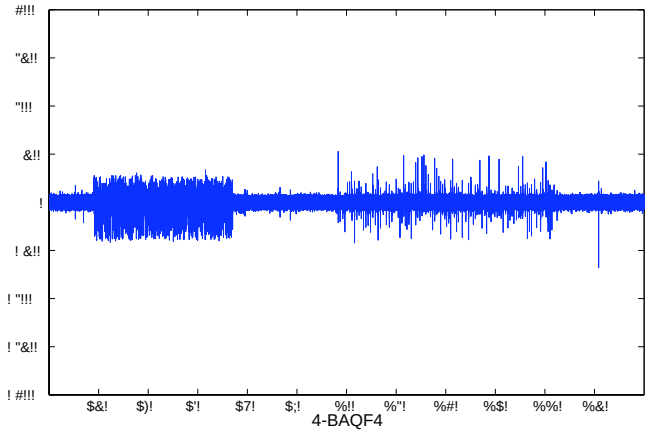
#!!!
"&!!
"!!!
&!!
!
! &!!
! "!!!
! "&!!
! #!!!
$&!
$)!
$'!
$7!
$;!
%!!
%"!
%#!
%$!
%%!
%&!
4-BAQF4

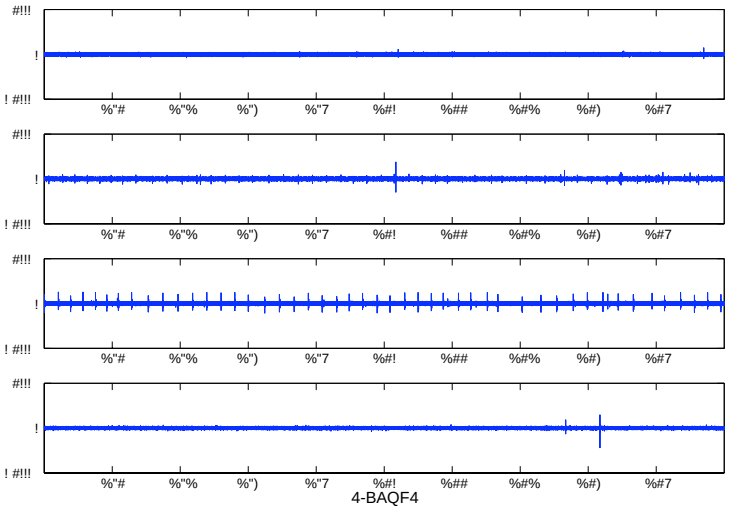
#!!!
!
! #!!!
%"#
%"%
%")
%"7
%#!
%##
%#%
%#)
%#7
4-BAQF4

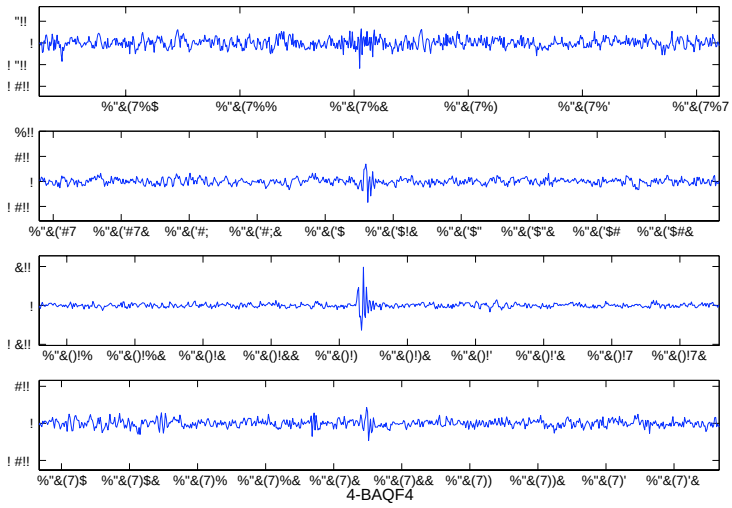

4-BAQF4

~

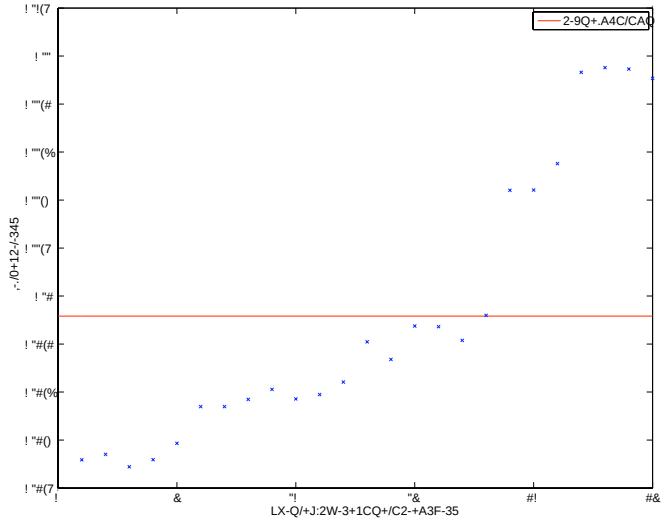

(x, y)

$\sim$

$\frac{1}{r}$ $\frac{1}{r^2}$

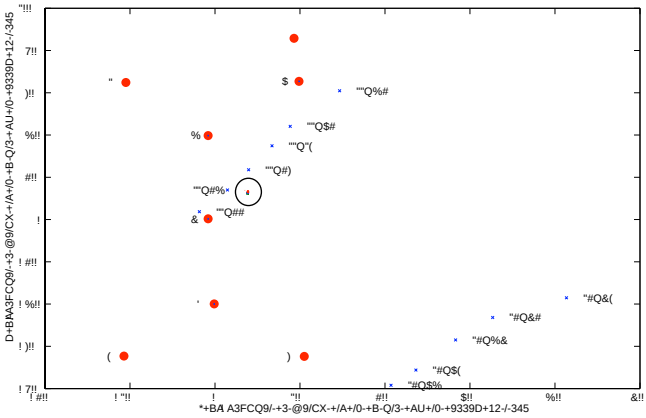
"!!!
7!!
)!!
%!!
#!!
!
! #!!
! %!!
!)!!
! 7!!
D+BA43FCQ9/-+3-@9/CX-+/A+/0-+B-Q/3-+AU+/0-+9339D+12-/-345
! #!!
! "!!
!
"!!
#!!
$!!
%!!
&!!
*+BA A3FCQ9/-+3-@9/CX-+/A+/0-+B-Q/3-+AU+/0-+9339D+12-/-345
$
"
%
&
(
)
'
""Q%#
""Q$#
""Q'(
""Q#)
""Q#%
""Q##
"#Q&(
"#Q&#
"#Q%&
"#Q$(
"#Q$%

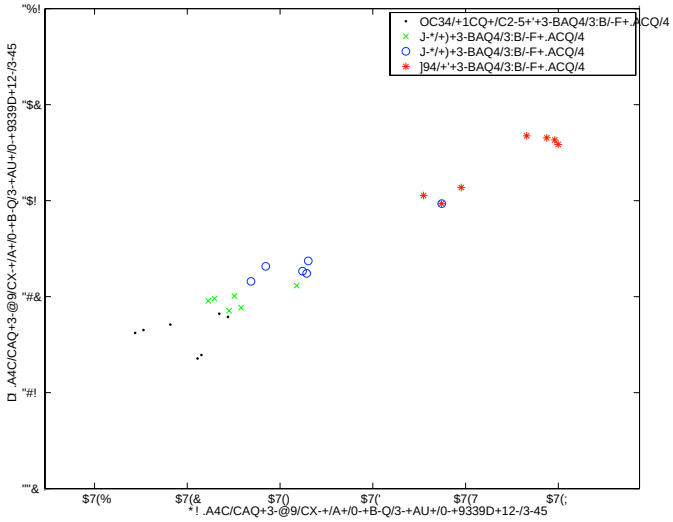
"%!
"$&
"$!
"#&
"#!
""&
D .A4C/CAQ+3-@9/CX-+/A+/0-+B-Q/3-+AU+/0-+9339D+12-/3-45
$7(%
$7(&
$7()
$7('
$7(7
$7(;
*! .A4C/CAQ+3-@9/CX-+/A+/0-+B-Q/3-+AU+/0-+9339D+12-/3-45
OC34/+1CQ+/C2-5+'+3-BAQ4/3:B/-F+.ACQ/4
J-*/+)+3-BAQ4/3:B/-F+.ACQ/4
J-*/+)+3-BAQ4/3:B/-F+.ACQ/4
]94/+'+3-BAQ4/3:B/-F+.ACQ/4

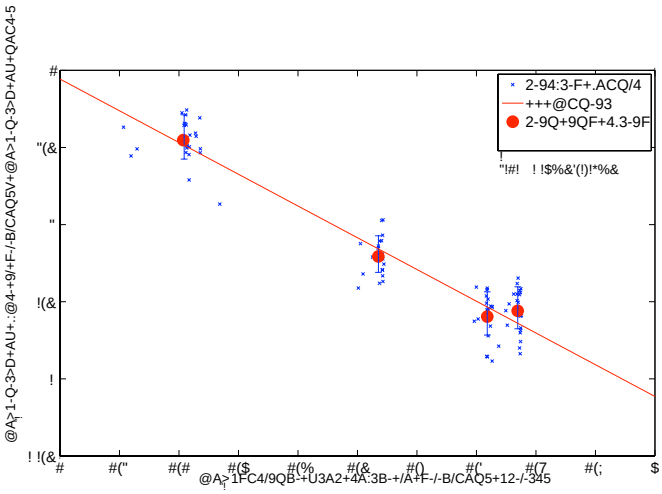
2-94:3-F+.ACQ/4
+++@CQ-93
2-9Q+9QF+4.3-9F
"!#! ! !$%&'(!)!*%&
@A>1-Q-3>D+AU+QAC4+5
@A>1FC4/9QB-+U3A2+4A:3B-+/A+F-/-B/CAQ5+12-/-345

$\pm$ ^{2}

$\alpha(E)$

α

$$\alpha(E) = \frac{\times \qquad \times}{},$$

$$\frac{1}{} = \qquad \times \qquad \times \qquad .$$

$\times 10^{23}$

$$s = \quad \lambda(E)\Phi(E)dE,$$

$\lambda(E)$

E $\Phi(E)$

s

s

$$s \leq s_{up} = -\log \beta,$$

$1-\beta$ β

$$s_{up} = 2.3.$$

$\Phi(E)$

$$\Phi(E) \leq \frac{s_{up}}{E\lambda(E)},$$

$\lambda(E)$

$\log(E^2 \times \Phi(E))$ $\approx E^{-2}$

$\dot{a}$ $\dot{b}$ $\dot{b}$ (x, y)

$\dot{a}$ $\dot{b}$

$\dot{a} \times \dot{b}$

$\dot{a}$ $\dot{b}$

$\dot{a} \times \dot{b}$ $\dot{a}$

$(\dot{a} \times \dot{b}) \times \dot{a},$

(x, y)

θ_0

θ_0 θ_{oa}

$$\tan(\theta_{oa}) = x/$$

$$x \approx \times \cos(90 - \theta_0)$$

$$x \approx \times \sin(\theta_0)$$

$$\theta_{oa} \approx \tan^{-1} \frac{\times \sin(\theta_0)}{} ,$$

θ_0

θ_{oa}

θ_{oa}

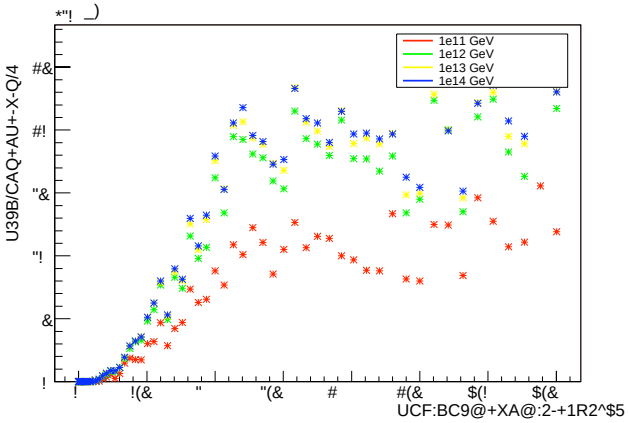

x y

3

$\times$ $\times$

π

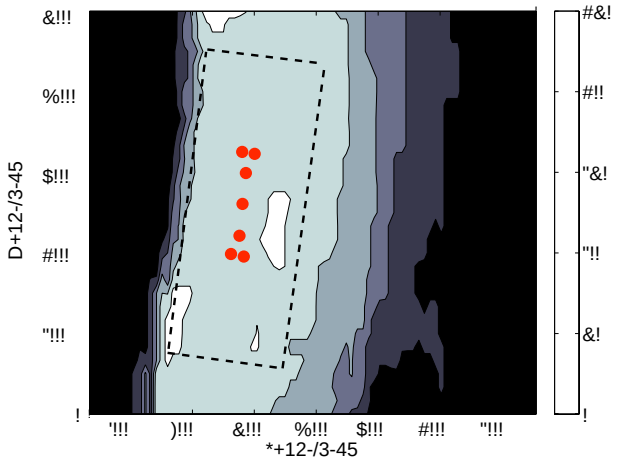

$$P(x) = P_0 e^{-\frac{x}{8500}},$$

x

$$\dot{\boldsymbol{p}} = \dot{\boldsymbol{p}}_0 + c\dot{\boldsymbol{d}},$$

$\dot{\boldsymbol{p}}$ $\dot{\boldsymbol{p}}_0$

$\dot{\boldsymbol{d}}$ (x, y, z)

$\dot{\boldsymbol{p}}$

$$p_x = p_{0x} + cd_x$$

$$p_y = p_{0y} + cd_y$$

$$p_z = p_{0z} + cd_z,$$

$\dot{\boldsymbol{p}}_0$

$$R = |\dot{\boldsymbol{p}}| = \quad \overline{p_x^2 + p_y^2 + p_z^2},$$

$\dot{\boldsymbol{p}}$ $\dot{\boldsymbol{p}}$

c

$$R = |\dot{\boldsymbol{p}}|$$
$$R = \quad \overline{\dot{\boldsymbol{p}} \cdot \dot{\boldsymbol{p}}}$$
$$R = \quad \overline{(\dot{\boldsymbol{p}}_0 + c\dot{\boldsymbol{d}}) \cdot (\dot{\boldsymbol{p}}_0 + c\dot{\boldsymbol{d}})}$$
$$0 = c^2 \quad \dot{\boldsymbol{d}} \cdot \dot{\boldsymbol{d}} \quad + c \quad 2\dot{\boldsymbol{p}}_0 \cdot \dot{\boldsymbol{d}} \quad + \dot{\boldsymbol{p}}_0 \cdot \dot{\boldsymbol{p}}_0 - R^2,$$

c

$c(\quad) \qquad c(\quad)$

$c \quad c(\quad)$

$\dot{\boldsymbol{p}}$

$\dot{\boldsymbol{p}}_0 - \dot{\boldsymbol{p}}(c \quad)$

$$= e^{(-\qquad\qquad)},$$

$$= \qquad\qquad \times \qquad\qquad \times N_{av} \times \qquad\qquad ,$$

N_{av}

$\times$ 21

(x, y)

20	$\times$	-3	$\times$	-3	$\times$	-4	$\times$	-5
20.5	$\times$	-3	$\times$	-3	$\times$	-4	$\times$	-5
21	$\times$	-3	$\times$	-3	$\times$	-4	$\times$	-5
21.5	$\times$	-3	$\times$	-3	$\times$	-4	$\times$	-5
22	$\times$	-3	$\times$	-3	$\times$	-4	$\times$	-5

20	$\times$ -5		
20.5	$\times$ -5		$\times$ -5
21	$\times$ -5		$\times$ -5
21.5	$\times$ -5		$\times$ -5
22	$\times$ -5		$\times$ -5

$\sim$

x, y

z y

x

$\pm$ $-$

z

$\sim$ $-$

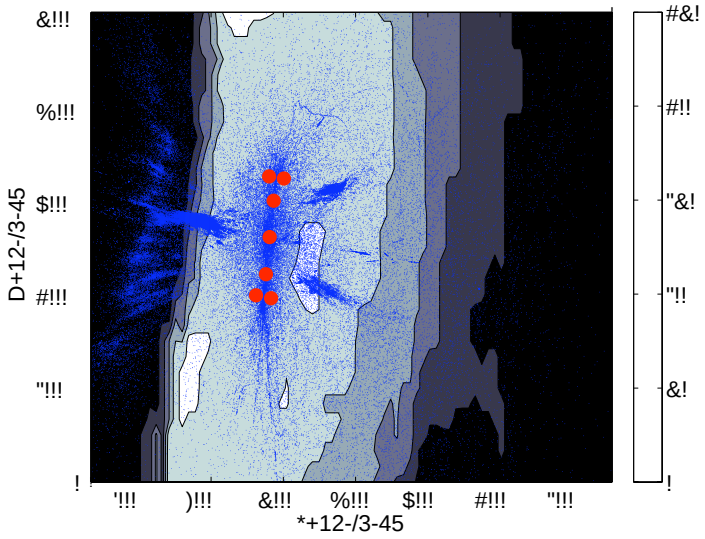
&!!!
%!!!
$!!!
#!!!
"!!!
!
D+12-/3-45
'!!!
)!!!
&!!!
%!!!
$!!!
#!!!
"!!!
*+12-/3-45
#&!
#!!
"&!
"!!
&!
!

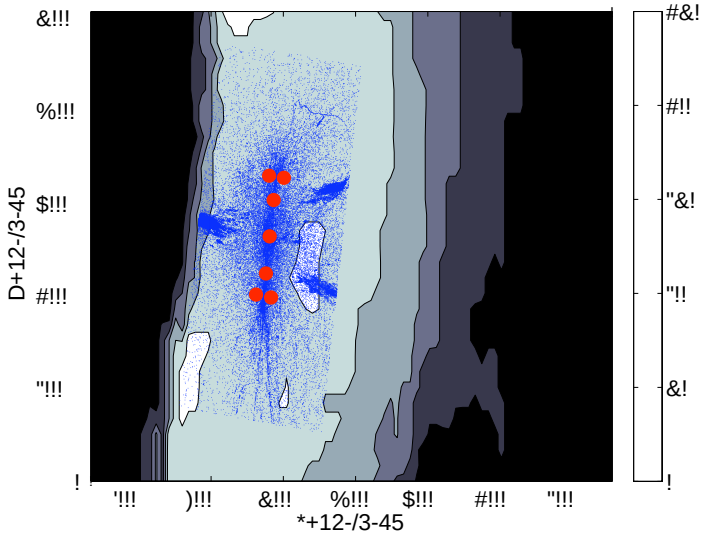
&!!!
%!!!
$!!!
#!!!
"!!!
!
D+12-/3-45
'!!!
)!!!
&!!!
%!!!
$!!!
#!!!
"!!!
*+12-/3-45
#&!
#!!
"&!
"!!
&!
!

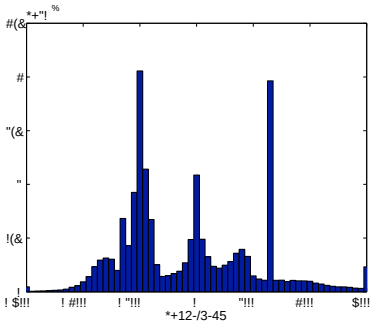

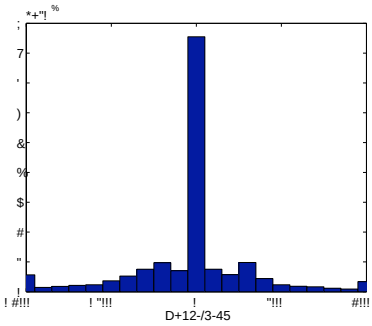

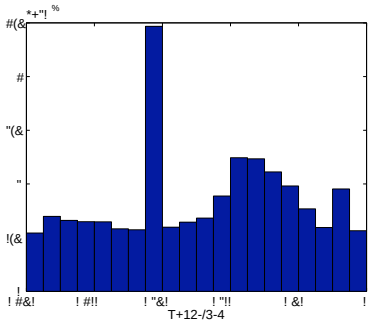

x

y z

—

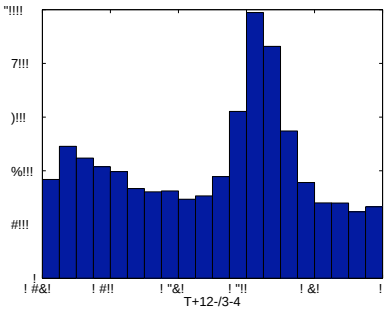

$$z$$

20	
20.25	
20.5	
21	
21.5	
22	
22.5	
23	

$$\sim$$

$$>$$

20.5

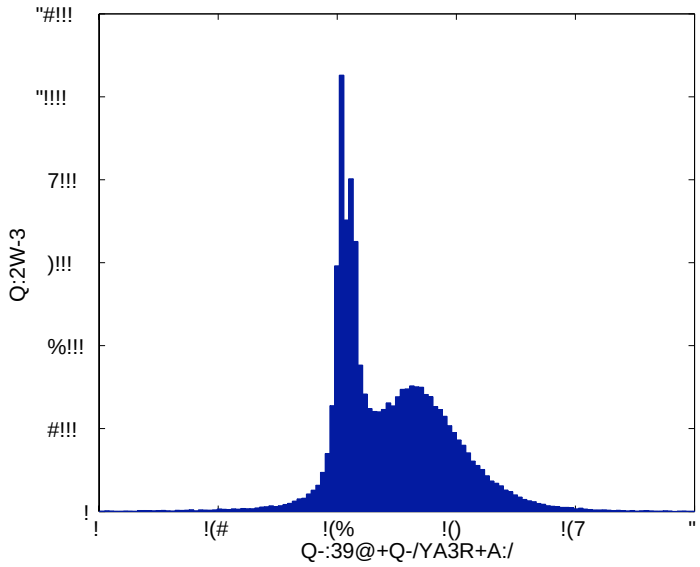
"#!!!
"!!!!
7!!!
)!!!
%!!!
#!!!
!
Q:2W-3
!
!(#
!(%
!()
!(7
"
Q-:39@+Q-/YA3R+A:/

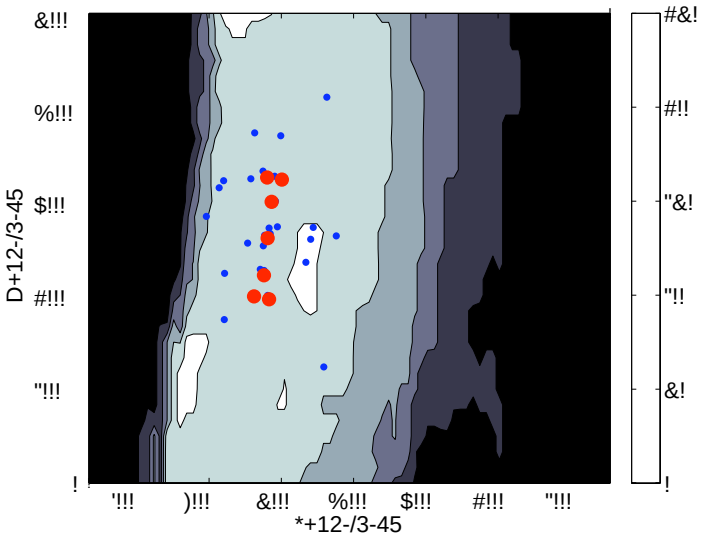
&!!!
%!!!
$!!!
#!!!
"!!!
!
D+12-/3-45
'!!!
)!!!
&!!!
%!!!
$!!!
#!!!
"!!!
*+12-/3-45
#&!
#!!
"&!
"!!
&!
!

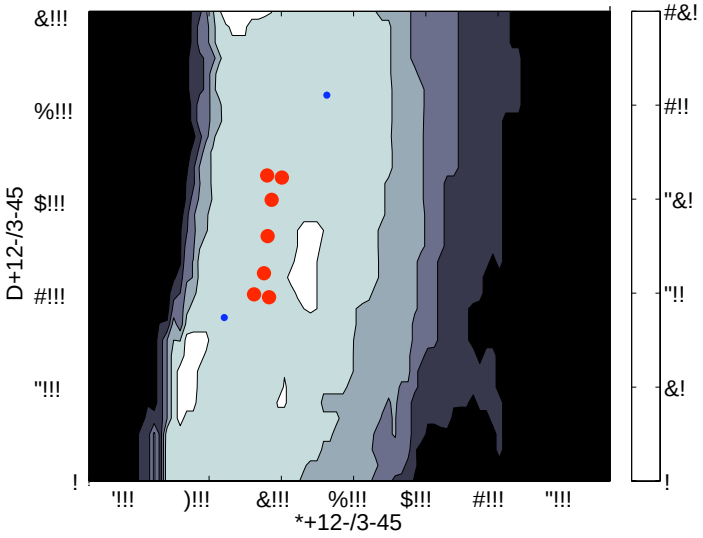
&!!!
%!!!
$!!!
#!!!
"!!!
!
D+12-/3-45
'!!!
)!!!
&!!!
%!!!
$!!!
#!!!
"!!!
*+12-/3-45
#&!
#!!
"&!
"!!
&!
!

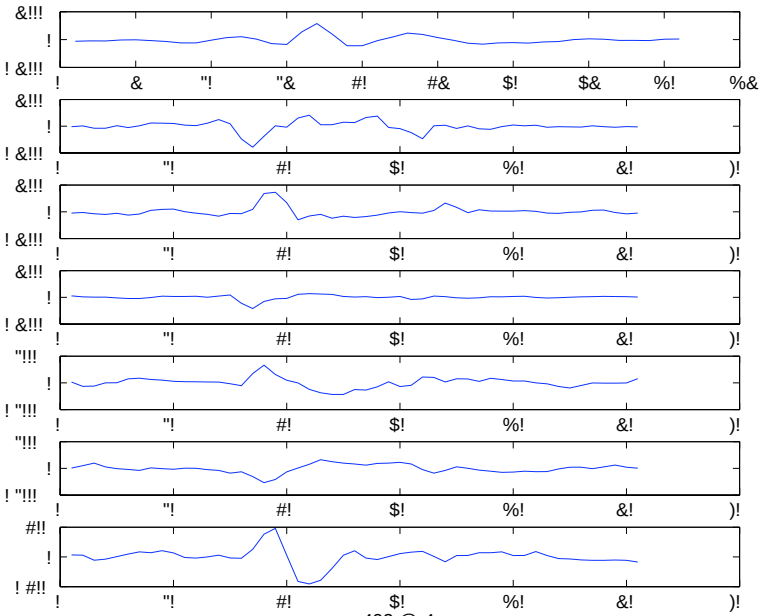

492.@-4

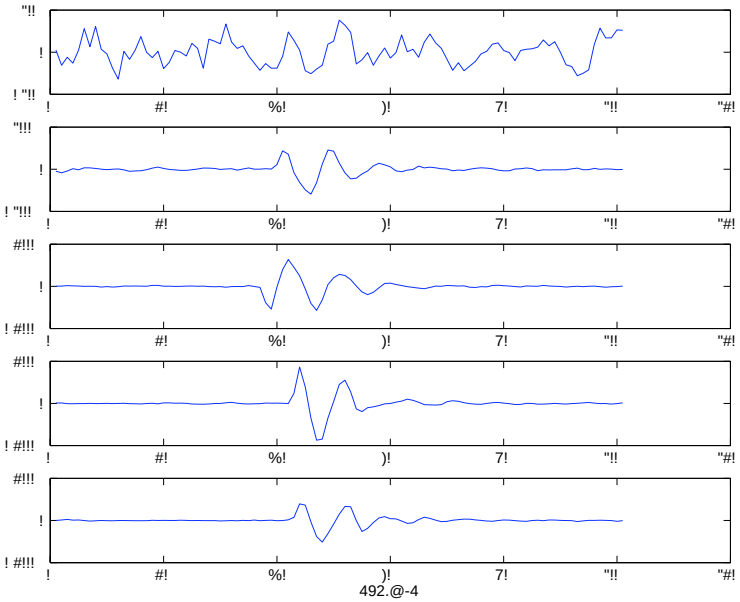

th

th

—

—

—

$\times$ 20.5

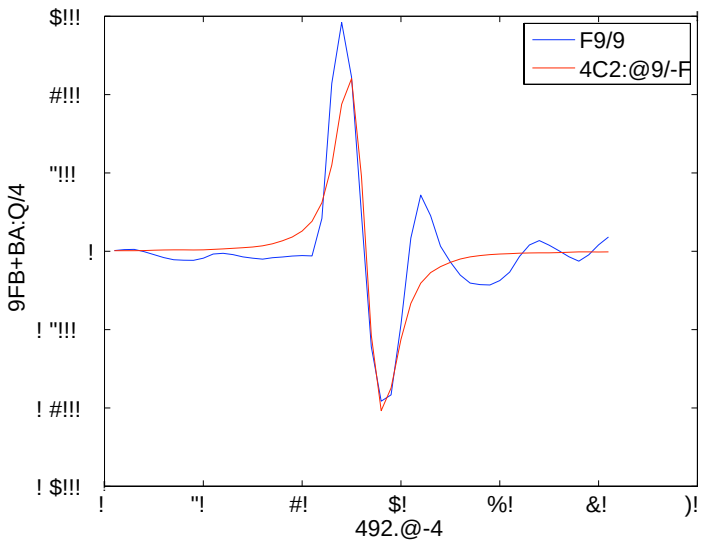
$!!!
#!!!
"!!!
!
! "!!!
! #!!!
! $!!!
9FB+BA:Q/4
F9/9
4C2:@9/-F
!
"!
#!
$!
%!
&!
)!
492.@-4

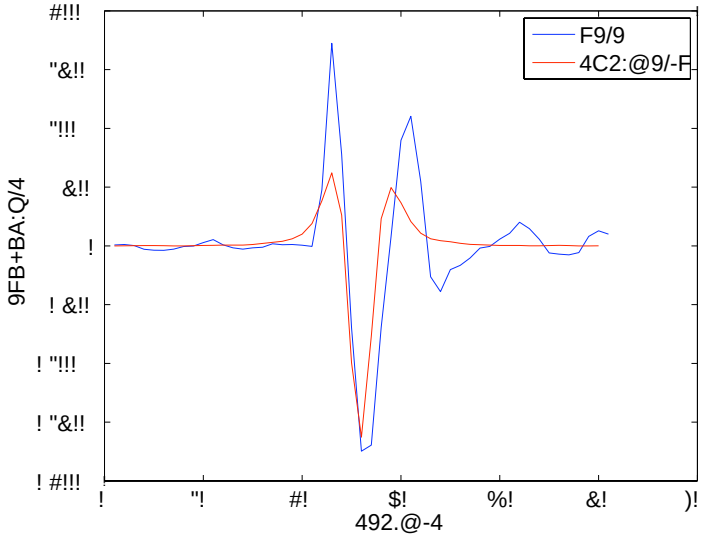
#!!!
"&!!
"!!!
&!!
!
! &!!
! "!!!
! "&!!
! #!!!
9FB+BA:Q/4
F9/9
4C2:@9/-F
!
"!
#!
$!
%!
&!
)!
492.@-4

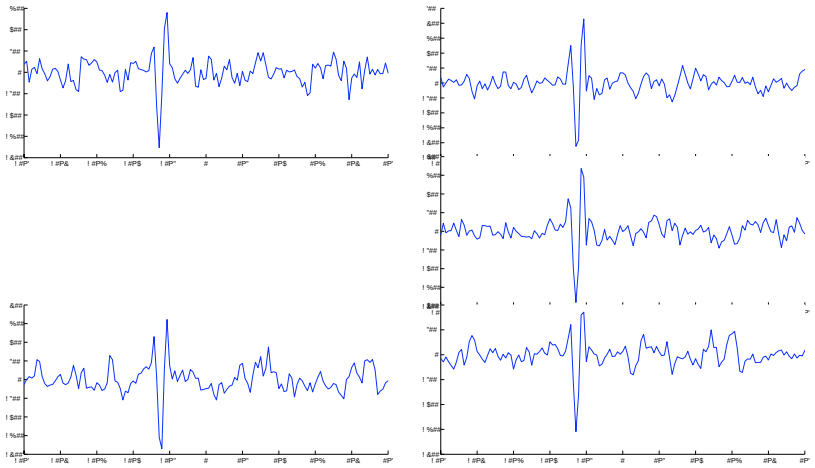

$\phi(E)$

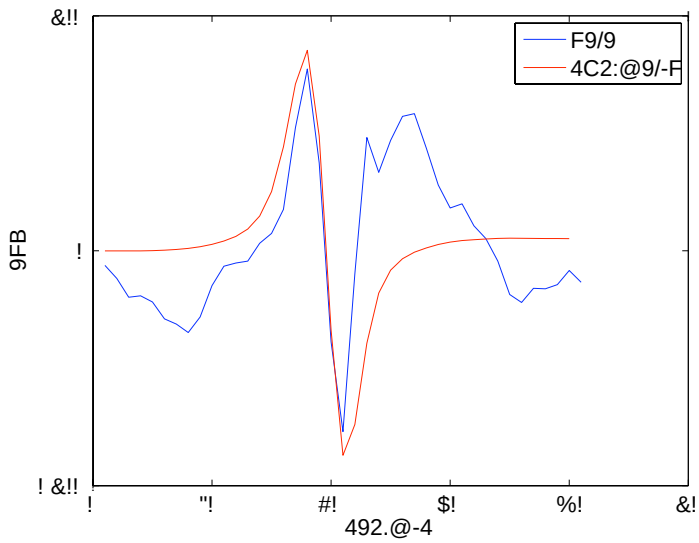

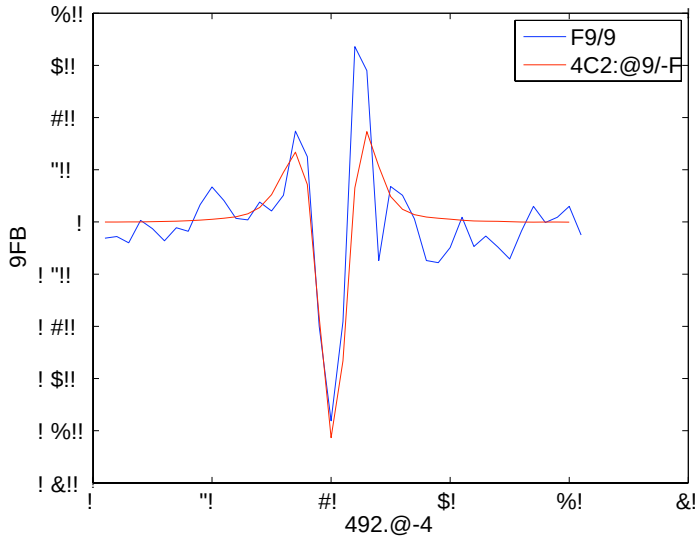

× 20.5

	$\alpha(E)$ $_{2}$	^{2}! $-2\ -1\ \ -1$
20		
20.25		
20.5		
21		
21.5		
22		
22.5		
23		

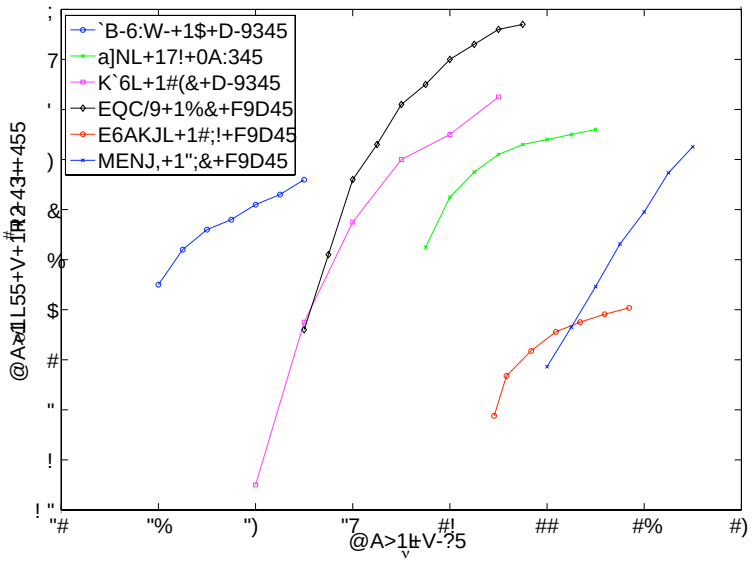

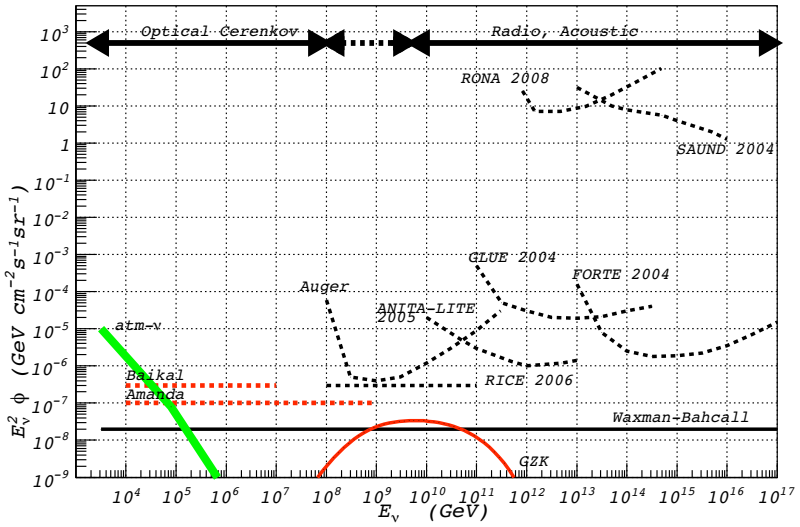
Optical Cerenkov
Radio, Acoustic
RONA 2008
SAUND 2004
GLUE 2004
FORTE 2004
Auger
ANITA-LITE 2005
atm-ν
Baikal
Amanda
RICE 2006
Waxman-Bahcall
GZK
$E_\nu^2\ \phi\ (GeV\ cm^{-2}s^{-1}sr^{-1})$
E_ν (GeV)

20.5									
21									
21.5									
22									
22									
22.5									

20.5 21 21.5 22			

$$= L_7 + L_6 \times E_6/E_7 + L_5 \times E_5/E_7 + L_4 \times E_4/E_7$$

L_x x E_y

y

$x \qquad y$

Δ

$x \qquad y$

$\overline{x^2 + y^2 + z^2}$

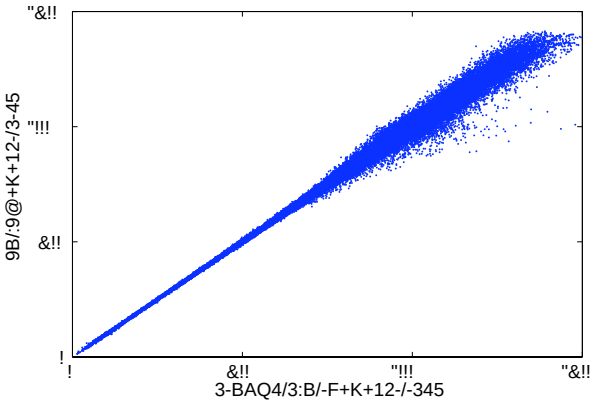
"&!!
"!!!
&!!
!
9B/:9@+K+12-/3-45
!
&!!
"!!!
"&!!
3-BAQ4/3:B/-F+K+12-/-345

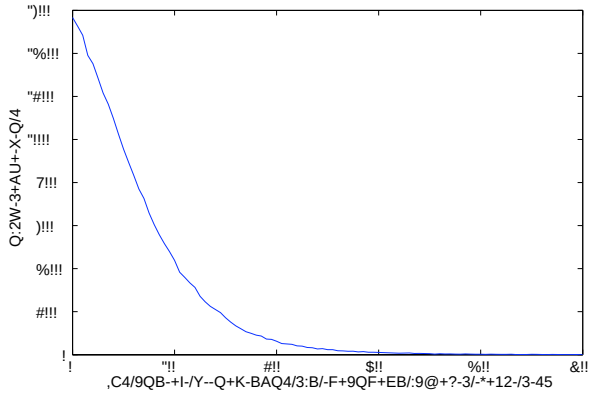
)!!!
"%!!!
"#!!!
"!!!!
7!!!
)!!!
%!!!
#!!!
!
Q:2W-3+AU+-X-Q/4
!
"!!
#!!
$!!
%!!
&!!
,C4/9QB-+I-/Y--Q+K-BAQ4/3:B/-F+9QF+EB/:9@+?-3/-*+12-/3-45

3

$\times$ 20

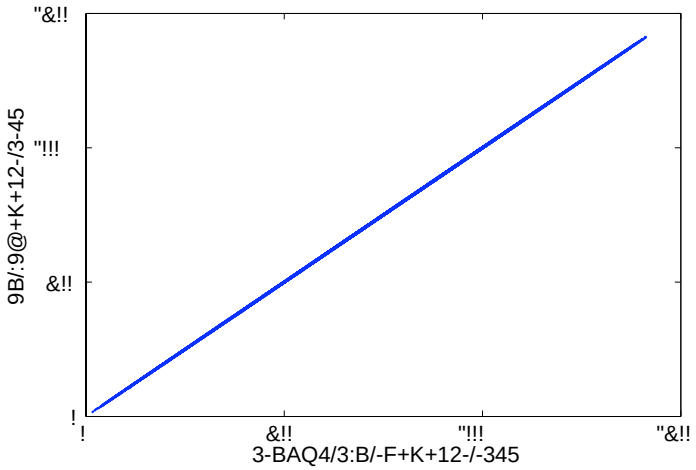
"&!!
"!!!
&!!
!
!
&!!
"!!!
"&!!
9B/:9@+K+12-/3-45
3-BAQ4/3:B/-F+K+12-/-345

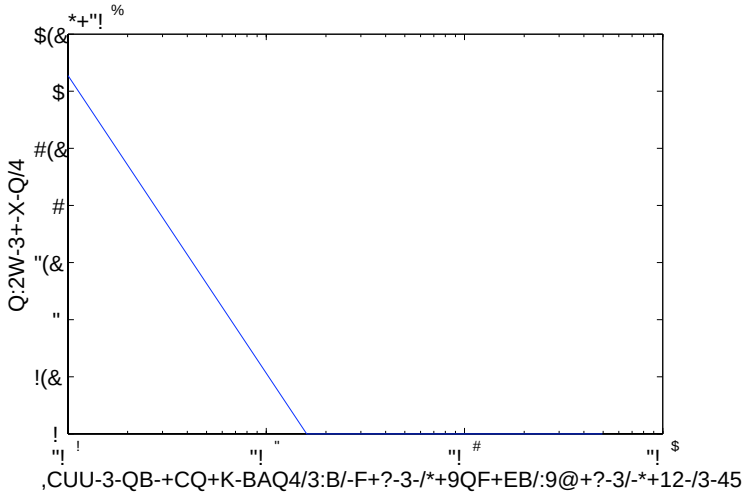
*+"! %
$(&
$
#(&
#
"(&
"
!(&
!
"! !
"! "
"! #
"! $
Q:2W-3+-X-Q/4
,CUU-3-QB-+CQ+K-BAQ4/3:B/-F+?-3-/*+9QF+EB/:9@+?-3/-*+12-/3-45

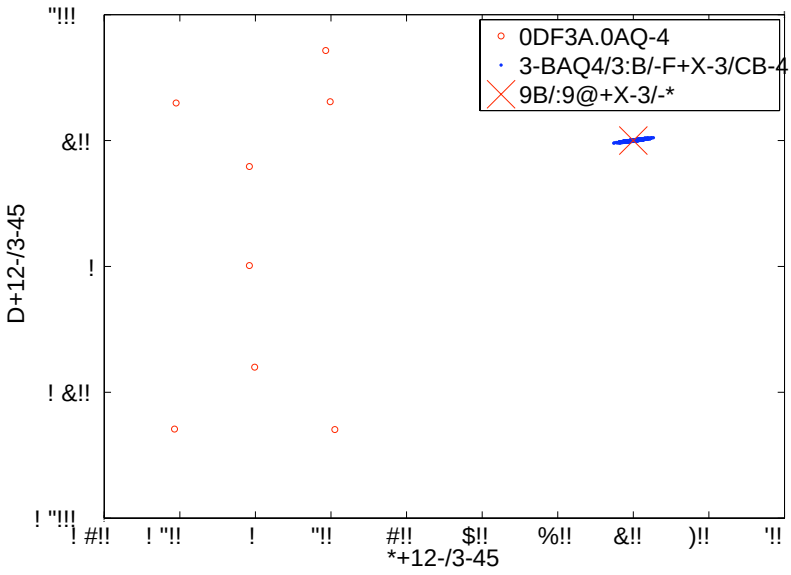
"!!!
&!!
!
! &!!
! "!!!
D+12-/3-45
0DF3A.0AQ-4
3-BAQ4/3:B/-F+X-3/CB-4
9B/:9@+X-3/-*
! #!!
! "!!
!
"!!
#!!
$!!
%!!
&!!
)!!
'!!
*+12-/3-45

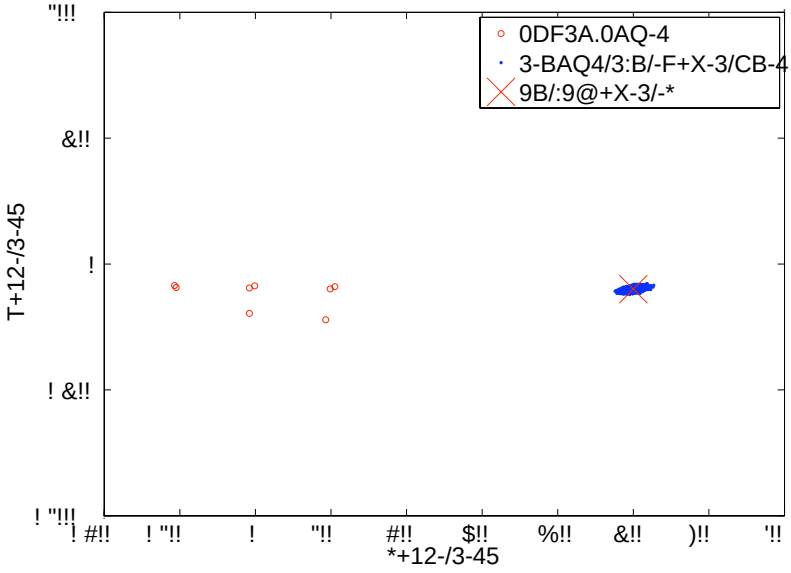
"!!!
&!!
!
! &!!
! "!!!
T+12-/3-45
0DF3A.0AQ-4
3-BAQ4/3:B/-F+X-3/CB-4
9B/:9@+X-3/-*
! #!!
! "!!
!
"!!
#!!
$!!
%!!
&!!
)!!
'!!
*+12-/3-45

(x, y) (x, z)

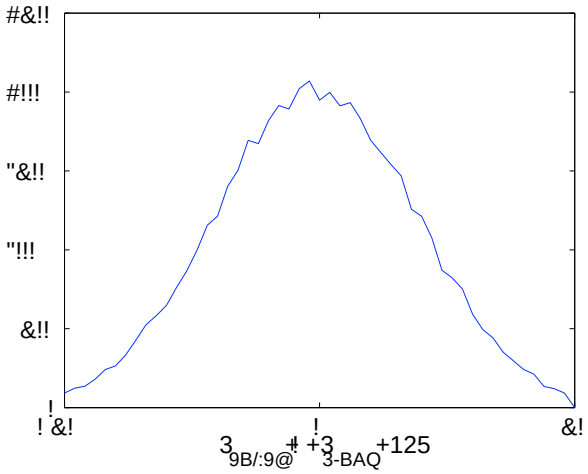

$\alpha \qquad \phi$

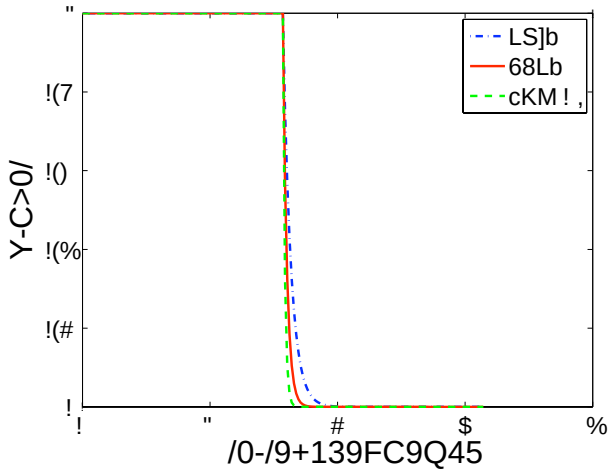

θ

20.5 21 21.5 22 22.5 22	

α ϕ

	$\alpha(E)$ 2	$^2\phi$ -2 -1 -1
20		
20.25		
20.5		
21		
21.5		
22		
22.5		
23		

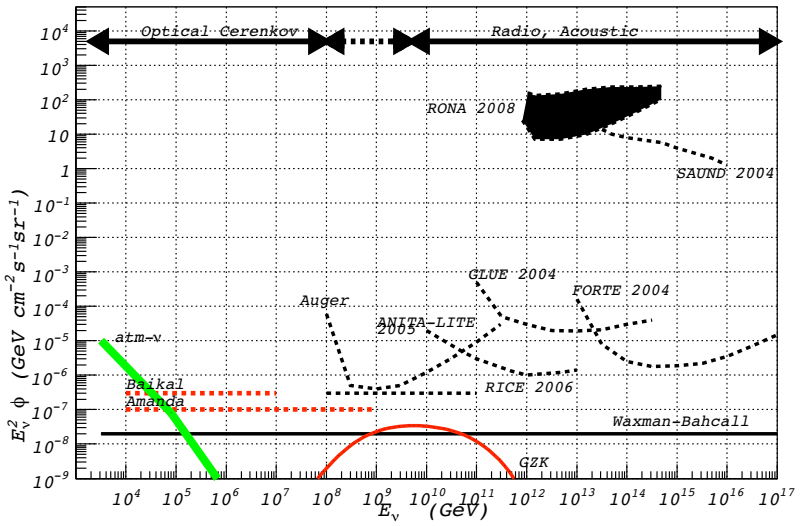

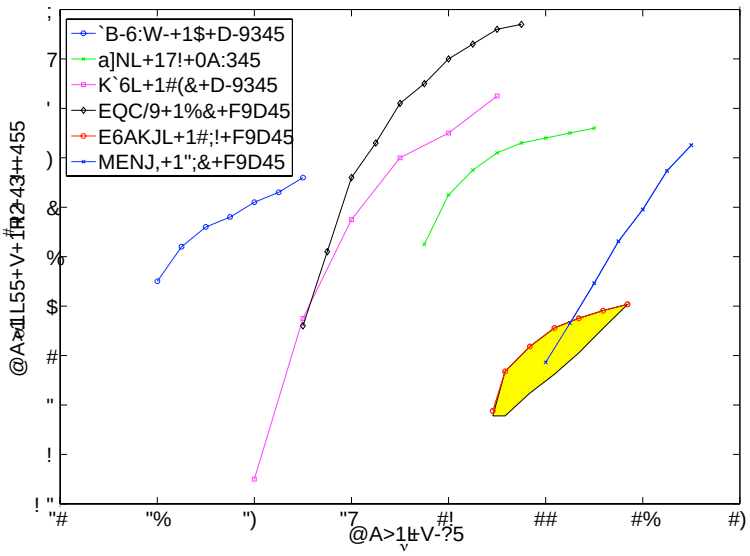
`B-6:W-+1$+D-9345
a]NL+17!+0A:345
K`6L+1#(&+D-9345
EQC/9+1%&+F9D45
E6AKJL+1#;!+F9D45
MENJ,+1";&+F9D45
@A>1L55+V+1R2-43++455
@A>1L+V-?5
"#
"%
")
"7
#!
##
#%
#)
;
7
'
)
&
%
$
#
"
!
! "

E^2 $\approx E^{-2}$

E^2

$\alpha(E) \qquad \lambda(E)$

E $E + dE$

$$dN = \frac{d\phi}{dE}\lambda(E)dE,$$

$d\phi/dE$ $^{-1}$ $^{-2}$ $^{-1}$ $^{-1}$

$$\frac{d\phi}{dE} = AK(E),$$

20	$\times \quad -4$
20.5	$\times \quad -3$
21	$\times \quad -3$
21.5	$\times \quad -3$
22	$\times \quad -3$

$K(E)$

$$N = s_{up} = \int_{E_1}^{E_2} dN = \int_{E_1}^{E_2} \frac{d\phi}{dE}\lambda(E)dE = A \int_{E_1}^{E_2} K(E)\lambda(E)dE.$$

$$A = \frac{s_{up}}{\int_{E_1}^{E_2} K(E)\lambda(E)dE},$$

$$\frac{d\phi}{dE} = AK(E) = \frac{s_{up}K(E)}{\int_{E_1}^{E_2} K(E)\lambda(E)dE}.$$

- $K(E) \propto \quad E^2$
- $K(E) \propto \qquad\qquad\qquad\qquad \log(E)$

	$^2\phi$ -2 -1 -1			
		^{2}		
20.5				
21				
21.5				
22				
22.5				
23				

^{2}

^{2}

^{3}

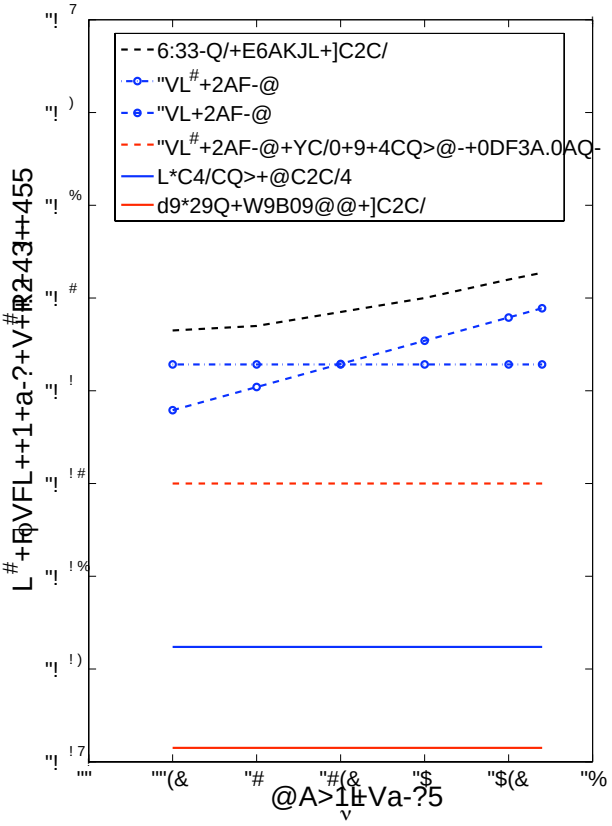
6:33-Q/+E6AKJL+]C2C/
"VL#+2AF-@
"VL+2AF-@
"VL#+2AF-@+YC/0+9+4CQ>@-+0DF3A.0AQ-
L*C4/CQ>+@C2C/4
d9*29Q+W9B09@@+]C2C/
"$(&
"%

$$0 = \frac{1}{2}mv^2 - \frac{GmM}{R},$$

m v M

R G

6.67×10^{-11} ^{3} $^{-1}$ $^{-2}$

$$\begin{aligned}\frac{1}{2}mv^2 &= \frac{GmM}{R} \\ c &= \left(\frac{2GM}{R}\right)^{1/2} \\ R &= 2GM/c^2,\end{aligned}$$

15

−12

4 −3

$$E = 4 \times 10^9 \quad ,$$

−3

$$\frac{dE}{dx} = \frac{4 \times 10^9}{6 \times 10^4 \times 10^5}$$
$$\frac{dE}{dx} = 0.7 \qquad ^{-1}.$$

−1 v c

$^{-1}$

$^{-1}$

$\pm$

$$1 \quad = 36.62\ \mu$$

$$1 \quad = 2731$$

$$1 \quad = 10 \quad .$$

$\sim$ ^{3}

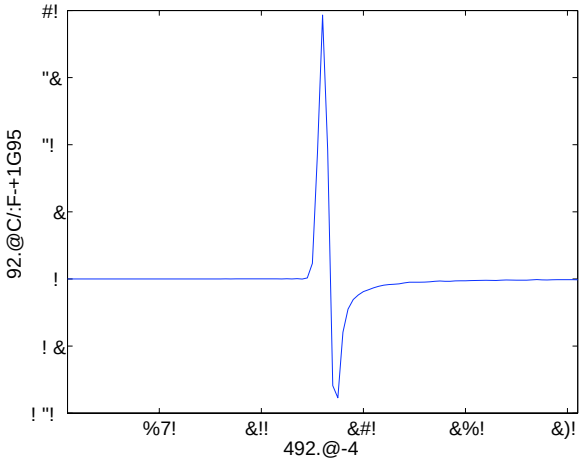
#!
"&
"!
&
!
! &
! "!
92.@C/:F-+1G95
%7!
&!!
&#!
&%!
&)!
492.@-4

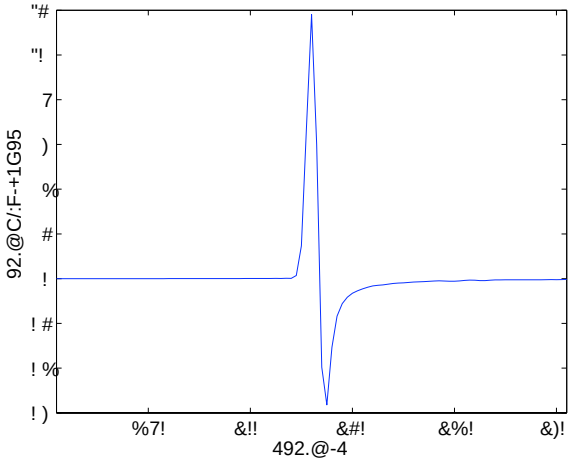
"#
"!
7
)
%
#
!
! #
! %
!)
92.@C/:F-+1G95
%7!
&!!
&#!
&%!
&)!
492.@-4

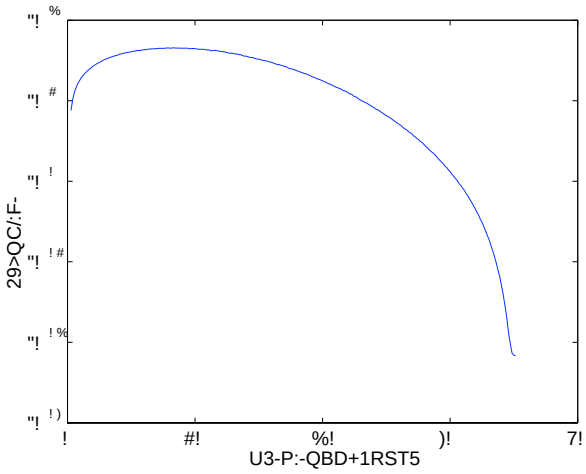
"! %
"! #
"! !
! #
! %
!)
29>QC/:F-
!
#!
%!
)!
7!
U3-P:-QBD+1RST5

$$P(t) = \frac{E_0 \beta \varepsilon}{4\pi C_p r} \frac{d}{dt}(\delta(r/c - t))dV,$$

β

C_p E_0 ε

c t

r

C -1 L β -1 -1 -1 p γ	$\times$ -5	$\times$ -5	$\times$ -5

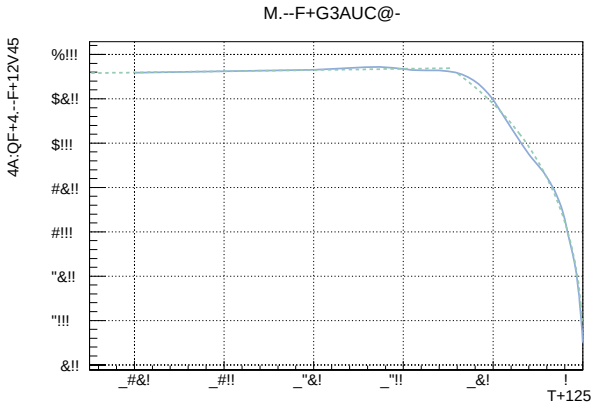

γ $\frac{2}{L} \times \beta$ p

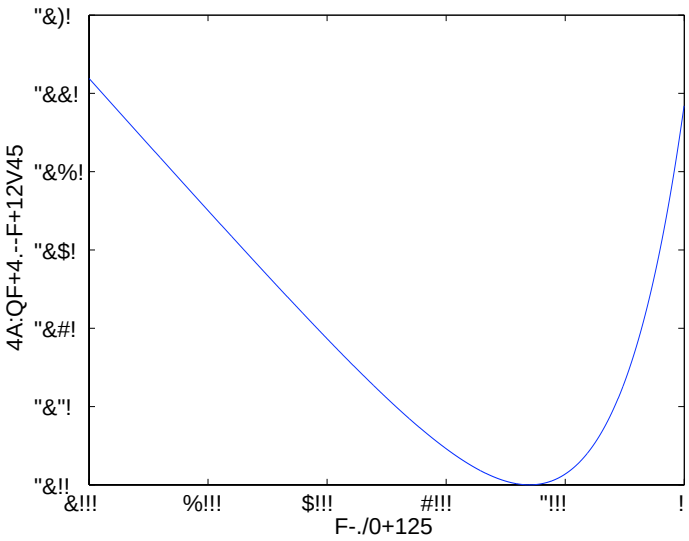
"&)!
"&&!
"&%!
"&$!
"&#!
"&"!
"&!!
4A:QF+4.--F+12V45
&!!!
%!!!
$!!!
#!!!
"!!!
!
F-./0+125

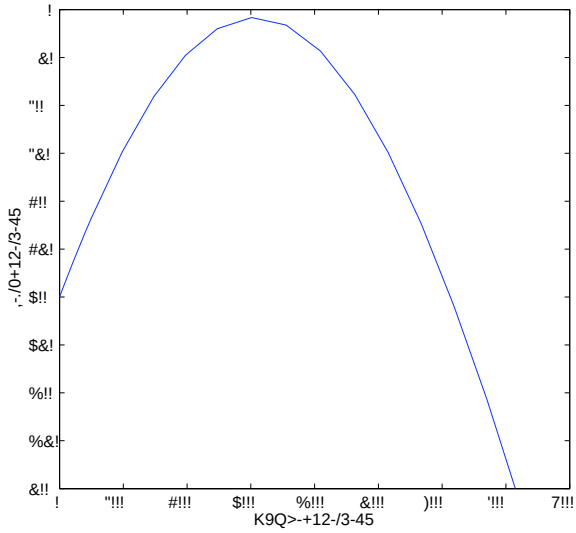
!
&!
"!!
"&!
#!!
#&!
$!!
$&!
%!!
%&!
&!!
,-./0+12-/3-45
!
"!!!
#!!!
$!!!
%!!!
&!!!
)!!!
'!!!
7!!!
K9Q>-+12-/3-45

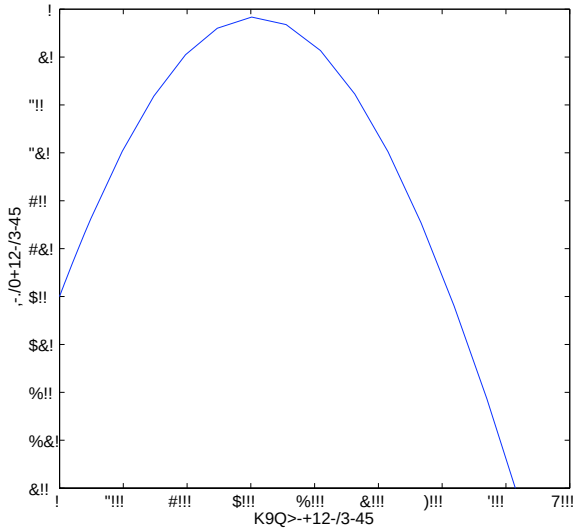
!
&!
"!!
"&!
#!!
#&!
$!!
$&!
%!!
%&!
&!!
,-./0+12-/3-45
!
"!!!
#!!!
$!!!
%!!!
&!!!
)!!!
'!!!
7!!!
K9Q>-+12-/3-45

$\sim$

x z

$-$

x

$-$

$-$

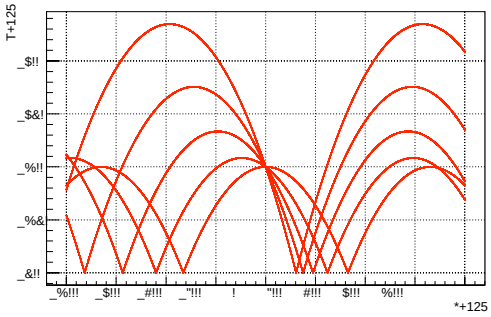
T+125
_$!!
_$&!
_%!!
_%&
_&!!
_%!!!
_$!!!
_#!!!
_"!!!
!
"!!!
#!!!
$!!!
%!!!
*+125

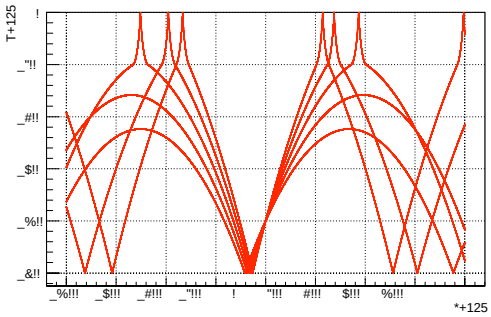
T+125
!
_"!!
_#!!
_$!!
_%!!
_&!!
_%!!!
_$!!!
_#!!!
_"!!!
!
"!!!
#!!!
$!!!
%!!!
*+125

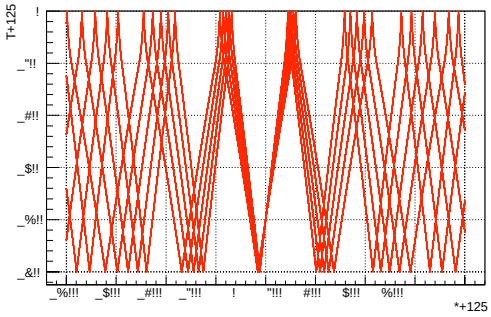
T+125
!
_"!!
_#!!
_$!!
_%!!
_&!!
_%!!!
_$!!!
_#!!!
_"!!!
!
"!!!
#!!!
$!!!
%!!!
*+125

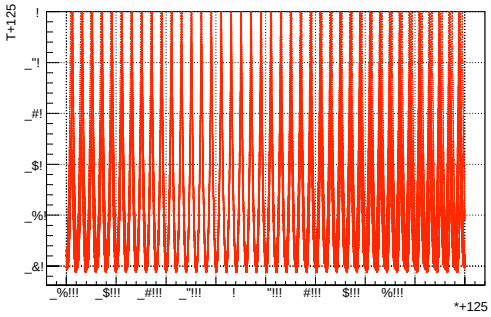
T+125
!
_"!
_#!
_$!
_%!
_&!
_%!!!
_$!!!
_#!!!
_"!!!
!
"!!!
#!!!
$!!!
%!!!
*+125

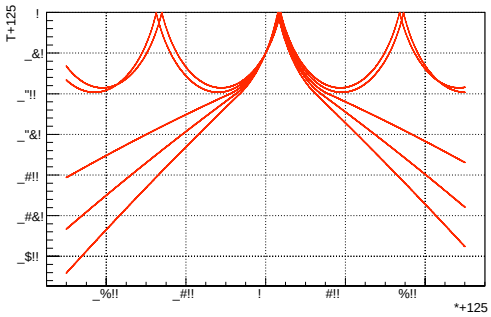
T+125
!
_&!
_"!!
_"&!
_#!!
_#&!
_$!!
_%!!
_#!!
!
#!!
%!!
*+125

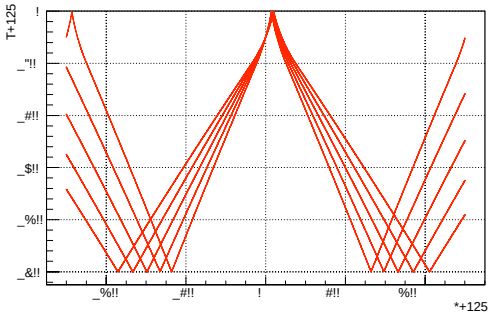
T+125
!
_"!!
_#!!
_$!!
_%!!
_&!!
_%!!
_#!!
!
#!!
%!!
*+125

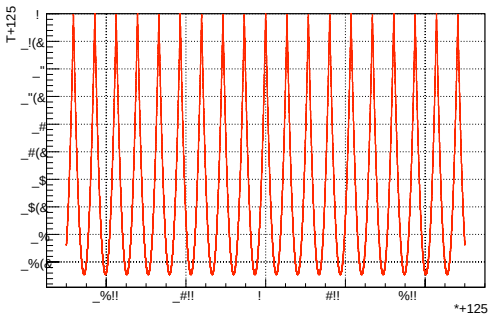
T+125
!
_!(&
_"
_"(&
_#
_#(&
_$
_$(&
_%
_%(&
_%!!
_#!!
!
#!!
%!!
*+125

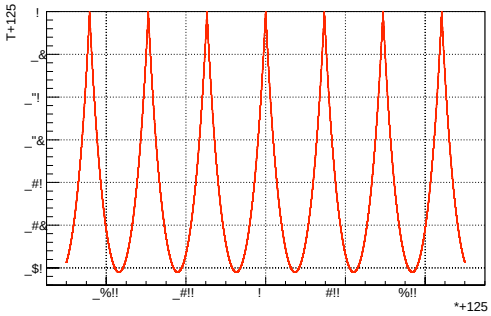
T+125
!
_&
_"!
_"&
_#!
_#&
_$!
_%!!
_#!!
!
#!!
%!!
*+125

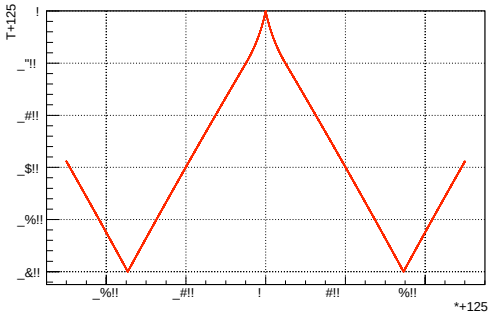
T+125
!
_"!!
_#!!
_$!!
_%!!
_&!!
_%!!
_#!!
!
#!!
%!!
*+125

$$Z_{water} = \rho_{water} \times V_{water}$$

$$Z_{ice} = \rho_{ice} \times V_{ice}$$

$$R_{reflect} = \frac{Z_{ice} - Z_{water}}{Z_{ice} + Z_{water}}$$

$V_{water} = 1440$ $^{-1}$ $V_{ice} = 3990$ $^{-1}$ $\rho_{water} = 1$ $^{-3}$ $\rho_{ice} =$ 0.918 $^{-3}$

18 19 20 21

3

3

3

18

$+ \quad z$

$\times \quad 22$

2

2 $\times \quad -4 \quad 2$

2

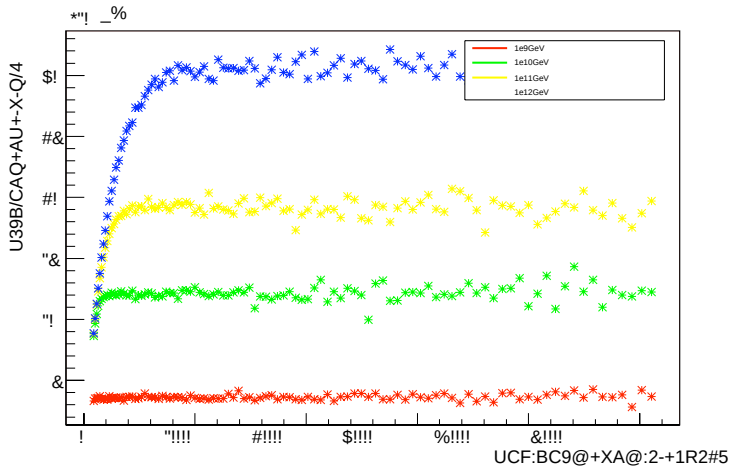
*"! _%
U39B/CAQ+AU+-X-Q/4
$!
#&
#!
"&
"!
&
1e9GeV
1e10GeV
1e11GeV
1e12GeV
!
"!!!!
#!!!!
$!!!!
%!!!!
&!!!!
UCF:BC9@+XA@:2-+1R2#5

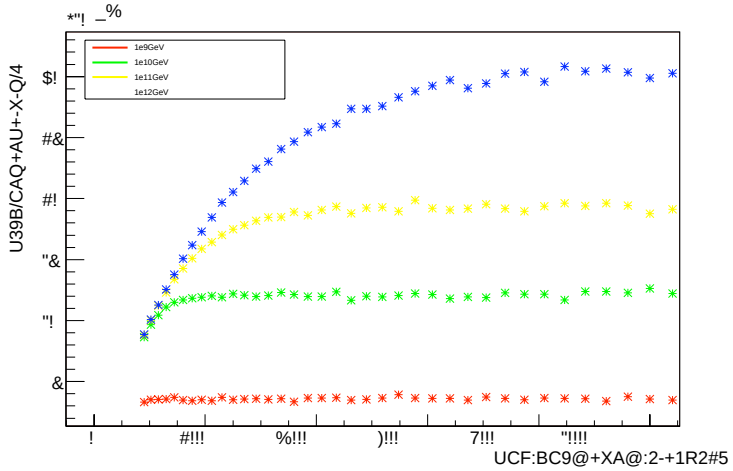
*"! _%
U39B/CAQ+AU+-X-Q/4
$!
#&
#!
"&
"!
&
1e9GeV
1e10GeV
1e11GeV
1e12GeV
!
#!!!
%!!!
)!!!
7!!!
"!!!!
UCF:BC9@+XA@:2-+1R2#5

18 19 20 21

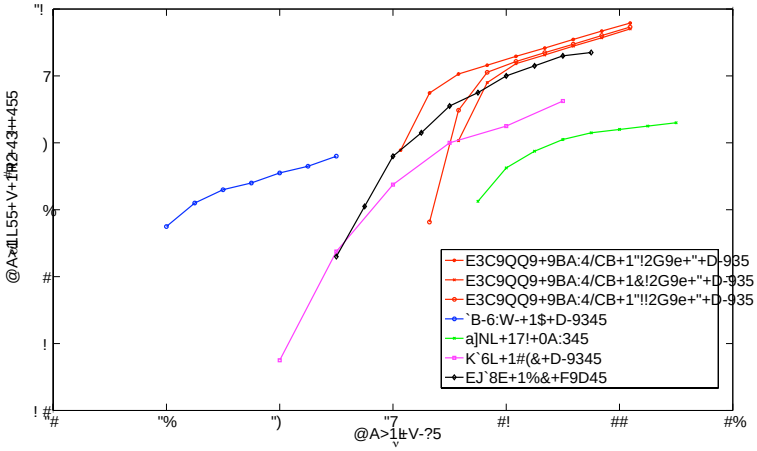
"!
7
)
%
#
!
! #
"#
"%
")
"7
#!
##
#%
E3C9QQ9+9BA:4/CB+1"!2G9e+"+D-935
E3C9QQ9+9BA:4/CB+1&!2G9e+"+D-935
E3C9QQ9+9BA:4/CB+1"!!2G9e+"+D-935
`B-6:W-+1$+D-9345
a]NL+17!+0A:345
K`6L+1#(&+D-9345
EJ`8E+1%&+F9D45

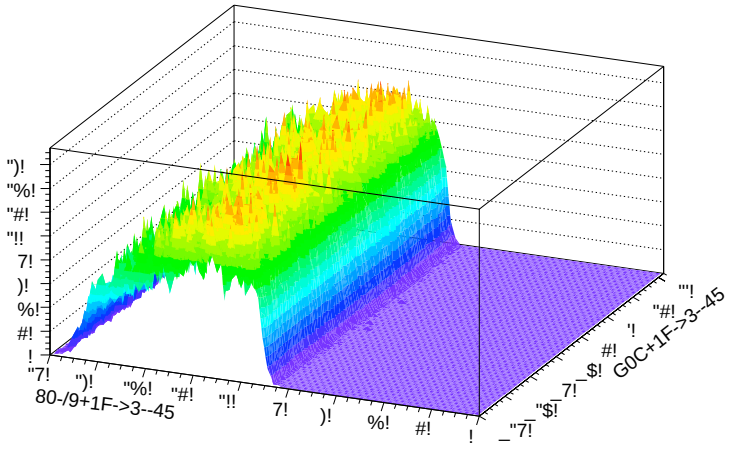
")!
"%!
"#!
"!!
7!
)!
%!
#!
!
"7!
")!
"%!
"#!
"!!
7!
)!
%!
#!
!
80-/9+1F->3--45
_"7!
_"$!
_7!
_$!
#!
'!
"#!
"'!
G0C+1F->3--45

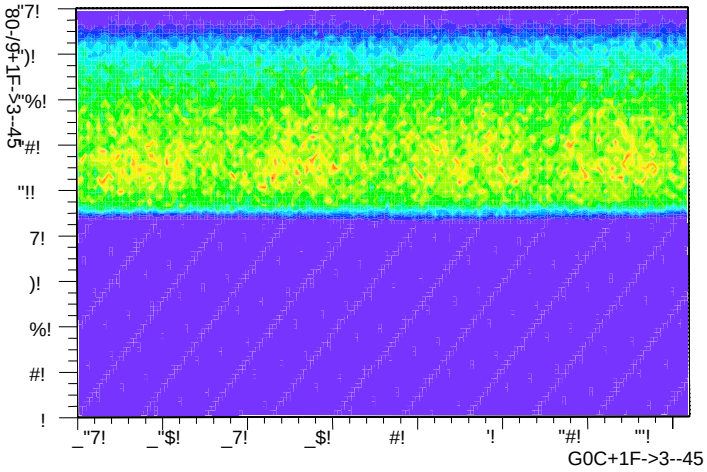
"7!
)!
"%!
#!
"!!
7!
)!
%!
#!
!
80-/9+1F->3--45
_"7!
_"$!
_7!
_$!
#!
'!
"#!
"'!
G0C+1F->3--45

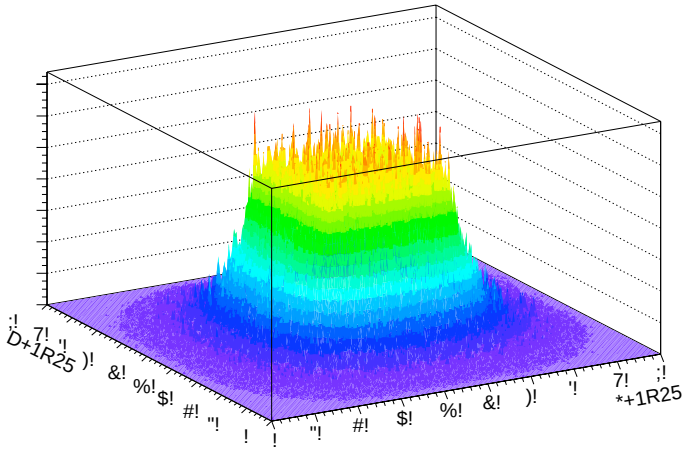

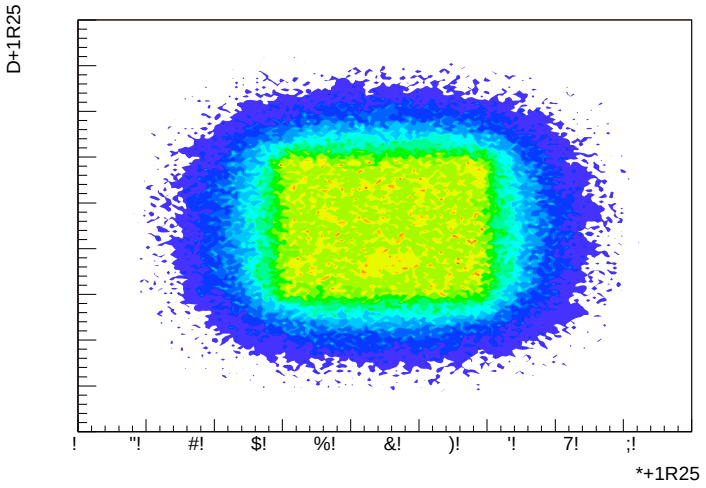

(x, y)

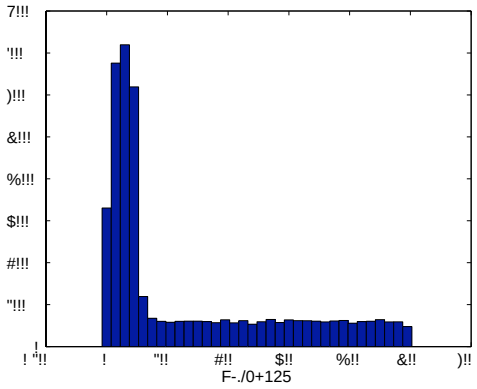
7!!!
'!!!
)!!!
&!!!
%!!!
$!!!
#!!!
"!!!
!
! "!! ! "!! #!! $!! %!! &!!)!!
F-./0+125

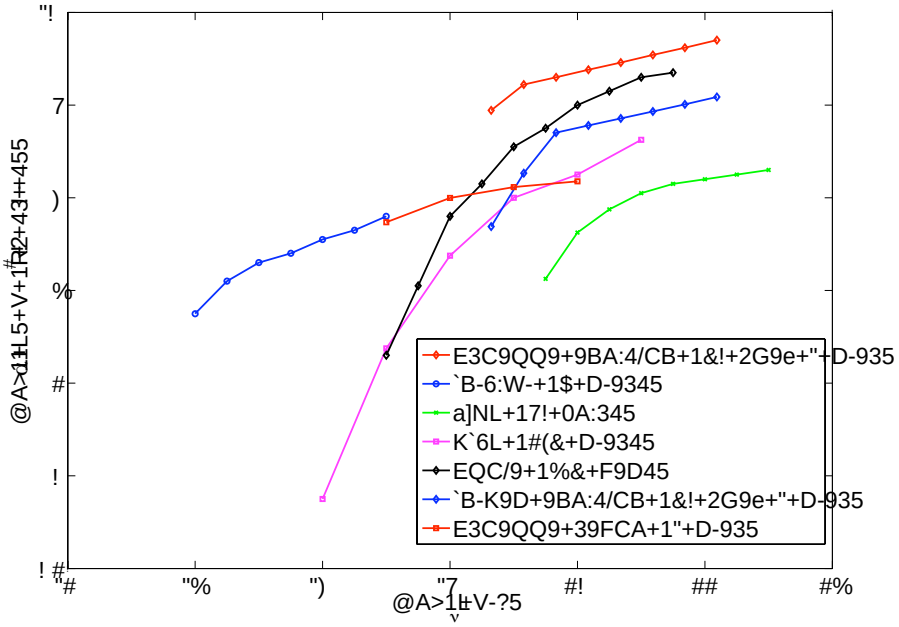
"!
7
)
%
#
!
! #
"# "% ") "7 #! ## #%
@A>1L5+V+1R2+43++455
@A>1L5+V-?5
E3C9QQ9+9BA:4/CB+1&!+2G9e+"+D-935
`B-6:W-+1$+D-9345
a]NL+17!+0A:345
K`6L+1#(&+D-9345
EQC/9+1%&+F9D45
`B-K9D+9BA:4/CB+1&!+2G9e+"+D-935
E3C9QQ9+39FCA+1"+D-935

—

—

21.5 21 20

$\pm$ ^{2}

$\alpha(E)$ $\lambda(E)$

$$\mathcal{L} = \dot{\psi}(i\gamma^\mu \delta_\mu - m)\psi,$$

ψ

$$\psi \rightarrow \psi \ = e^{i\alpha(x)Q}\psi,$$

$$\mathcal{L} = \dot{\psi}(i\gamma^\mu \delta_\mu - m)\psi - e\dot{\psi}\gamma^\mu Q\psi A^\mu - \frac{1}{4}F_{\mu\nu}F^{\mu\nu},$$

A^μ $F_{\mu\nu} = \gamma^\mu A^\nu - \gamma^\nu A^\mu$

ψ A_μ

Q

$\otimes$ $\otimes$

$\otimes$

$$-g\chi_L\gamma_\mu \cdot^\mu \chi_L = g\,\bar{\psi}\gamma_\mu \frac{Y}{2}\psi B^\mu,$$

W$^\mu$ B^μ

T Y

$W^\pm$

$$\chi_L^l = \begin{pmatrix} \nu_{eL} \\ e_L \end{pmatrix} \qquad \chi_L^q = \begin{pmatrix} u_L \\ d_L \end{pmatrix}.$$

e_R u_R d_R

ϕ_i $SU(2)\otimes U(1)$

$$\mathcal{L} = \quad i\sigma_\mu - g \quad \cdot_\mu - g\,\frac{Y}{2}B_\mu \quad \phi^{\,2}.$$

$$V(\phi) = \frac{1}{2}\mu^2\phi^2 + \frac{1}{4}\lambda\phi^4,$$

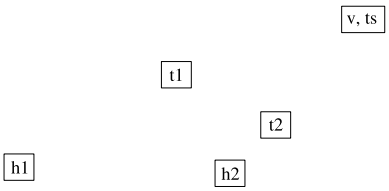

$\mu^2 < 0 \qquad \lambda > 0$

$$\phi = \begin{pmatrix} \phi^+ \\ \phi^0 \end{pmatrix} = \begin{pmatrix} (\phi_1 + i\phi_2)\sqrt{2} \\ (\phi_3 + i\phi_4)\sqrt{2} \end{pmatrix},$$

$$\phi_0 = \frac{1}{\sqrt{2}} \begin{pmatrix} 0 \\ \nu \end{pmatrix},$$

$\nu = \quad \overline{-\mu^2/\lambda}$

B

$W^{\pm} \qquad Z$

$\dot{\boldsymbol{\nu}} = (\nu_x, \nu_y, \nu_z)$

$\dot{\boldsymbol{r}}_i = (x_i, y_i, z_i)$

t_i

t_s

$$\times$$

$$|\dot{\boldsymbol{\nu}} - \dot{\boldsymbol{r}}_i| = c\,(t_i - t_s)\,.$$

$$\begin{aligned}
|\dot{\boldsymbol{\nu}} - \dot{\boldsymbol{r}}_i|^2 &= c^2\,(t_i - t_s)^2 \\
\nu^2 + r_i^2 - 2\dot{\boldsymbol{\nu}} \cdot \dot{\boldsymbol{r}}_i &= c^2\,(t_i - t_s)^2 \\
r_i^2 - r_j^2 \;\; - c^2 \;\; (t_i - t_s)^2 - (t_j - t_s)^2 \;\; &= 2\dot{\boldsymbol{\nu}} \cdot (\dot{\boldsymbol{r}}_i - \dot{\boldsymbol{r}}_j) \\
r_i^2 - r_j^2 \;\; - c^2 \;\; t_i^2 - t_j^2 - 2t_s\,(t_i - t_j) \;\; &= 2\dot{\boldsymbol{\nu}} \cdot (\dot{\boldsymbol{r}}_i - \dot{\boldsymbol{r}}_j) \\
r_i^2 - r_j^2 \;\; - c^2 \;\; t_i^2 - t_j^2 \;\; - 2c^2 t_s\,(t_i - t_j) &= 2\dot{\boldsymbol{\nu}} \cdot (\dot{\boldsymbol{r}}_i - \dot{\boldsymbol{r}}_j)\,.
\end{aligned}$$

$$\dot{\mathbb{R}} + t_s \dot{\boldsymbol{T}} = M \times \dot{\boldsymbol{\nu}},$$

$$\dot{\mathbb{R}} = \{r_i^2 - r_j^2 - c^2 \;\; t_i^2 - t_j^2 \;\}; (i, j = 1, 2; 1, 3; 1, 4)\,,$$

$$\dot{\boldsymbol{T}} = \{2c^2\left(t_i - t_j\right)\}; (i,j = 1,2;1,3;1,4)\,,$$

$$M = 2\begin{pmatrix} dx_{12} & dy_{12} & dz_{12} \\ dx_{13} & dy_{13} & dz_{13} \\ dx_{14} & dy_{14} & dz_{14} \end{pmatrix}.$$

$$\dot{\boldsymbol{y}} = M^{-1} \times \quad \dot{\boldsymbol{R}} + t_s \dot{\boldsymbol{T}}$$
$$\dot{\boldsymbol{y}} = M^{-1}\dot{\boldsymbol{R}} + t_s M^{-1}\dot{\boldsymbol{T}}.$$

$$\dot{\boldsymbol{P}} = M^{-1}\dot{\boldsymbol{R}}$$
$$\dot{\boldsymbol{Q}} = M^{-1}\dot{\boldsymbol{T}},$$

$$\dot{\boldsymbol{y}} = \dot{\boldsymbol{P}} + t_s\dot{\boldsymbol{Q}},$$

s

$\dot{\boldsymbol{y}}$ s

$$|\dot{\boldsymbol{y}} - \dot{\boldsymbol{r}}_i|^2 = c^2\left(t_i - t_s\right)^2 = \left|\dot{\boldsymbol{P}} + t_s\dot{\boldsymbol{Q}} - \dot{\boldsymbol{r}}_i\right|^2$$
$$t_s^2 \;\; c^2 - Q^2 \;\; - 2t_s \;\; c^2 t_i + \dot{\boldsymbol{P}}\cdot\dot{\boldsymbol{Q}} + \dot{\boldsymbol{Q}}\cdot\dot{\boldsymbol{r}}_i \;\; + \;\; c^2 t_i^2 - p^2 - r_i^2 + 2\dot{\boldsymbol{P}}\cdot\dot{\boldsymbol{r}}_i \;\; = 0.$$

$\times$ $\geq$

$$M = ULV^T$$

$$M^{-1} = VL^{-1}U^T,$$

-1

- $\sim$
- $\sim$
- $\sim$
-

χ^2

χ^2 χ^2

χ^2

$$\chi^2 = \left(t_i\left(actual\right) - t_i\left(recon\right)\right)^2 .$$

$$t_i\left(recon\right) = \quad t_{s(\pm)} + \quad h_i - v_{s(\pm)} \quad / c \quad .$$

χ^2

$$\begin{aligned}
\frac{d}{ds} \quad n\frac{dx}{ds} \quad &= \frac{\partial n}{\partial x} \\
\frac{d}{ds} \quad n\frac{dy}{ds} \quad &= \frac{\partial n}{\partial y} \\
\frac{d}{ds} \quad n\frac{dz}{ds} \quad &= \frac{\partial n}{\partial z},
\end{aligned}$$

$n = c_0/c$ c_0 c s

z

$$n = n(z),$$

$$\begin{aligned}
n\frac{dx}{ds} &= constant \\
n\frac{dy}{ds} &= constant \\
\frac{d}{ds} \quad n\frac{dz}{ds} \quad &= \frac{\partial n}{\partial z},
\end{aligned}$$

(x, y)

$$\begin{aligned}
\frac{dx}{ds} &= \cos\theta \\
\frac{dz}{ds} &= \sin\theta.
\end{aligned}$$

c_0

$$\begin{aligned}
n\frac{dx}{ds} &= constant = n\cos\theta \\
\frac{n\cos\theta}{c_0} &= \frac{\cos\theta}{c} = constant,
\end{aligned}$$

$\theta = 0$ c c_n

$$\frac{\cos\theta}{c} = \frac{1}{c_n} = K,$$

$$K = \frac{\cos\theta_0}{c_0} = \frac{\cos\theta_1}{c_1},$$

$\cos\theta_0$ c_0 $\cos\theta_1$ c_1 (x_0, z_0)
(x_1, z_1)

$$n = n(z)$$

$$\begin{aligned}
\frac{dn}{dz} &= \frac{d}{ds}(n\sin\theta) \\
&= n\frac{d\sin\theta}{ds} + \sin\theta\frac{dn}{ds} \\
&= n\cos\theta\frac{d\theta}{ds} + \sin\theta\frac{dn}{ds} \\
&= n\cos\theta\frac{d\theta}{ds} + \sin\theta\frac{dn}{dz}\frac{dz}{ds} \\
&= n\cos\theta\frac{d\theta}{ds} + \sin^2\theta\frac{dn}{dz}.
\end{aligned}$$

$d\theta/ds$

$$\frac{d\theta}{ds} = \frac{\cos\theta}{n}\frac{dn}{dz}$$
$$\frac{d\theta}{ds} = -\frac{\cos\theta}{c}\frac{dc}{dz}$$
$$\frac{d\theta}{ds} = -K\frac{dc}{dz}.$$

$d\theta/ds$

dc/dz

$$\frac{dx}{dz} = \cot\theta,$$

$$x_1 - x_0 = \int_{z_0}^{z_1} \cot\theta dz.$$

$$dt = \frac{ds}{c}$$
$$t_1 - t_0 = \int_{s_0}^{s_1} \frac{ds}{c}$$
$$ds = \frac{dz}{\sin\theta}$$
$$t_1 - t_0 = \int_{z_0}^{z_1} \frac{1}{c}\frac{dz}{\sin\theta},$$

$$s_1 - s_0 = \int_{z_0}^{z_1} \frac{dz}{\sin\theta}.$$

$$c = c_m + gz$$
$$\frac{dc}{dz} = g,$$

$$\frac{d\theta}{ds} = -Kg,$$

$d\theta/ds$

R_c

$$R_c = \frac{1}{d\theta/ds} = \frac{1}{Kg}.$$

$$\begin{aligned} x_1 - x_0 &= \int_{z_0}^{z_1} \cot\theta dz \\ &= \int_{z_0}^{z_1} \frac{\cos\theta}{\sin\theta} dz \\ &= -\int_{\theta_0}^{\theta_1} \frac{\cos\theta d\theta}{Kc}, \end{aligned}$$

$dz/sin\theta \ = \ -d\theta/Kc$

$$\begin{aligned} \cos\theta &= Kc \\ \frac{d\cos\theta}{dz} &= Kc \\ \frac{-\sin\theta d\theta}{dz} &= Kc \\ \frac{dz}{\sin\theta} &= -\frac{d\theta}{Kc}, \end{aligned}$$

$$\begin{aligned} x_1 - x_0 &= \int_{\theta_0}^{\theta_1} \frac{\cos\theta d\theta}{Kc} \\ &= \frac{1}{Kc}[\sin\theta]_{\theta_0}^{\theta_1} \\ &= \frac{1}{Kc}(\sin\theta_0 - \sin\theta_1) \\ c &= g \\ x_1 - x_0 &= \frac{c_0}{g} \quad \frac{\sin\theta_0 - \sin\theta_1}{\cos\theta_0} \quad , \end{aligned}$$

$$t_1 - t_0 = \int_{z_0}^{z_1} \frac{dz}{c\sin\theta}$$

$$= -\int_{\theta_0}^{\theta_1} \frac{d\theta}{g\cos\theta}$$
$$= -\frac{1}{g} ln \quad \frac{\cos\theta_0(1+\sin\theta_1)}{\cos\theta_0(1+\sin\theta_1)} \quad ,$$

$$\int_{\theta_0}^{\theta_1} \frac{d\theta}{g\cos\theta} = \frac{1}{g}\int_{\theta_0}^{\theta_1} \sec\theta d\theta$$
$$= \frac{-1}{g}[ln|sec\theta + \tan\theta|]_{\theta_0}^{\theta_1},$$

$$s_1 - s_0 = \int_{z_0}^{z_1} \frac{dz}{sin\theta}$$
$$= \int_{\theta_0}^{\theta_1} \frac{d\theta}{Kg}$$
$$= \frac{1}{Kg}(\theta_0 - \theta_1)$$
$$= \frac{c_0}{g\cos\theta_0}(\theta_0 - \theta_1).$$

$$z = \frac{c - c_m}{g}.$$

$$z_1 - z_0 = \quad \frac{c_1 - c_m}{g}) - (\frac{c_0 - c_m}{g}$$
$$= \frac{c_1 - c_0}{g}$$
$$= \frac{1}{g} \quad c_0\frac{\cos\theta_1}{\cos\theta_0} - c_0$$
$$= \frac{c_0}{g\cos\theta_0}\left(\cos\theta_1 - \cos\theta_0\right).$$

$$x_1 - x_0 = \frac{c_0}{g} \quad \frac{\sin\theta_0 - \sin\theta_1}{\cos\theta_0}$$
$$t_1 - t_0 = -\frac{1}{g} ln \quad \frac{\cos\theta_0(1+\sin\theta_1)}{\cos\theta_1(1+\sin\theta_0)}$$

$$s_1 - s_0 = \frac{c_0}{g\cos\theta_0}(\theta_0 - \theta_1)$$
$$z_1 - z_0 = \frac{c_0}{g\cos\theta_0}(\cos\theta_1 - \cos\theta_0).$$

θ

ϕ θ_0

(x, y)

x

x

θ ϕ

x, y, z

θ_0

ϕ θ

$\theta \to \pi$ ϕ ϕ θ z

r θ

x y θ y z

$$\begin{pmatrix} x \\ y \\ z \end{pmatrix} = \begin{pmatrix} \cos\theta_0 & 0 & \sin\theta_0 \\ 0 & 1 & 0 \\ -\sin\theta_0 & 0 & \cos\theta_0 \end{pmatrix} \begin{pmatrix} r\cos\theta \\ r\sin\theta \\ 0 \end{pmatrix},$$

$$\begin{pmatrix} x \\ y \\ z \end{pmatrix} = \begin{pmatrix} r\cos\theta\cos\theta_0 \\ r\sin\theta \\ -r\cos\theta\sin\theta_0 \end{pmatrix},$$

x y z ϕ x y z

$$\tan\phi = \frac{\overline{x^2+y^2}}{z}$$

$$\phi = \tan^{-1}\ \frac{\overline{x^2+y^2}}{z}$$

$$\phi = \tan^{-1}\ \frac{\overline{r\cos^2\theta\cos^2\theta_0 + r\sin^2\theta}}{-r\cos\theta\sin\theta_0}$$

$$\phi = \tan^{-1}\ \frac{\overline{\cos^2\theta\cos^2\theta_0 + \sin^2\theta}}{-\cos\theta\sin\theta_0},$$

ϕ θ_0 z

r θ ϕ r θ ϕ

x, y z

$$x = r\cos(\phi)\cos(\theta)$$
$$y = r\cos(\phi)\sin(\theta)$$
$$z = r\sin(\phi).$$

- $\pm$ 1.25 $/2^{15}$ μ
- μ $\times 10^7$ μ

$$\begin{aligned} &= 20\log_{10}\ \frac{[\mu\ /\ ]}{[1\ /\mu\ ]} \\ &= 20\log_{10}\ \frac{S}{S_0} \\ 10^{dB/20} &= \frac{S}{S_0} \\ S &= S_0 \times 10^{140/20} \\ S &= S_0 \times 10^7. \end{aligned}$$

- $\times 10^{-6}\times$ $\times 10^7$ μ μ
-

$$X(f) = \int_{-\infty}^{\infty} x(t) e^{-i2\pi ft} dt,$$

$x(t)$ $X(f)$

$$X(K) = \Sigma_{j=1}^{N} x(j) \omega_N^{(j-1)(k-1)},$$

$\omega = e^{-i2\pi/N}$ N
